OCS Study
MMS 86-0120
Dynalysis Report Number 91

SOUTH ATLANTIC OCS CIRCULATION MODEL
PHASE III

Final Report

L. H. Kantha, H. J. Herring and G. L. Mellor

Prepared for the
Minerals Management Service
U. S. Department of the Interior
Atlantic OCS Region

Under Contract Number
14-12-0001-29203

December 1985

Revised December 1986

Dynalysis of Princeton
219 Wall Street
Princeton, New Jersey 08540
609-924-3911

This report has been reviewed by the Minerals Management Service and approved for publication. Approval does not signify that the contents necessarily reflect the views and policies of the Service, nor does mention of trade names or commercial products constitute endorsement or recommendation for use.

50272-101

REPORT DOCUMENTATION PAGE	1. REPORT NO. MMS 86-0120	2.	3. Recipient's Accession No.

4. Title and Subtitle
SOUTH ATLANTIC BIGHT OCS CIRCULATION MODEL
PHASE III
Final Report

5. Report Date
12/85 Revised 12/86

6.

7. Author(s)
L.H. Kantha, H.J. Herring and G.L. Mellor

8. Performing Organization Rept. No.
Dynalysis Report 91

9. Performing Organization Name and Address
Dynalysis of Princeton
219 Wall Street
Princeton, New Jersey 08540-1512

10. Project/Task/Work Unit No.

11. Contract(C) or Grant(G) No.
(C) 14-12-0001-29203
(G)

12. Sponsoring Organization Name and Address
U. S. Department of the Interior
Minerals Management Service
Atlantic OCS Region
Vienna, Virginia 22180

13. Type of Report & Period Covered
Final Report

14.

15. Supplementary Notes

16. Abstract (Limit: 200 words)

The primary research activity in the present study is to demonstrate that the General Circulation Model, embodies the physics required to produce the observed Gulf Stream variability. The results show that given adequate grid resolution and appropriate boundary conditions the model does produce qualitatively realistic shingles and intrusions along the western boundary of the Gulf Stream. These features are shown to form and propagate with the correct velocity and to have the characteristic thermal signature which is observed in satellite imagery.

Another important component of the study is to provide circulation fields for immediate application to satisfy MMS oil spill modelling requirements. For this purpose recourse is made to the Characteristic Tracing Model, a diagnostic model driven by climatological data. Both the seasonal variations and overall climatological values of the currents and transports are presented.

The model simulations are based upon the extensive hydrographic data sets assembled from both national archives (National Oceanographic Data Center and Fleet Numerical Oceanography Center) and local sources including the observational projects supported by the MMS. Climatological distributions of the various water mass characteristics, wind stresses and heat fluxes have been produced. The domain for which data has been analyzed encompasses the coastal waters of the east coast of the United States from 65°W to 82°W and 23°N to 46°N, excluding a data sparse sector south of 30°N and east of 70°W.

17. Document Analysis a. Descriptors

General Circulation Model
Gulf Stream Frontal Eddies
Prognostic Circulation Model
Diagnostic Circulation Model

b. Identifiers/Open-Ended Terms

Atlantic Coast (U.S.) - Hydrography
Atlantic Coast (U.S.) - Meteorology
Atlantic Coast (U.S.) - Circulation
Atlantic Coast (U.S.) - Climatology

c. COSATI Field/Group

18. Availability Statement:	19. Security Class (This Report) Unclassified	21. No. of Pages
	20. Security Class (This Page) Unclassified	22. Price

(See ANSI-Z39.18) See Instructions on Reverse OPTIONAL FORM 272 (4-77) (Formerly NTIS-35)

EXECUTIVE SUMMARY

An evaluation of the potential impact of offshore oil and gas exploration and production activities is a complex and difficult task. These activities can produce not only surface and sub-surface pollution from accidental spills but also from intentional disposal of drilling by-products such as cuttings and muds. For a proper assessment of the risks involved in the development of the offshore regions, knowledge of ocean current distribution at various depths throughout the water column is needed. It is these currents which provide the transport mechanism for pollutants and might cause spilled material to be transported to beaches and vulnerable natural resource areas.

Building upon the framework established under Phase II of this investigation, the General Circulation Model (GCM) and the Characteristic Tracing Model (CTM) have been refined and applied to the problem of deducing the circulation along the east coast of the United States, including the South Atlantic Bight (SAB). The primary research activity in the present study is to demonstrate that the GCM, proposed during Phase II, embodied the physics required to produce the observed Gulf Stream frontal variability. The results contained in this report show that given adequate grid resolution and appropriate boundary conditions the model does produce qualitatively realistic shingles and intrusions along the western boundary of the Gulf Stream. These features are shown to form and propagate with the correct velocity and to have the characteristic thermal signature which is observed in satellite imagery.

Another important component of the study is to provide circulation fields for immediate application to satisfy MMS oil spill modelling

requirements. For this purpose recourse is made to the CTM, a diagnostic model driven by climatological data.

The CTM, based on geostrophic/Ekman dynamics includes the effect of bottom stresses in the planetary potential vorticity balance. A turbulence mixing model based on second moment techniques of turbulence closure incorporated into the model takes into account the influence of the wind and bottom stresses on the currents. The model is designed to provide a diagnostic means for deducing the transports and currents in the water column from the prescribed hydrographic and surface wind data. This report describes the results of the CTM applied to the east coast of the United States, with primary emphasis on the South Atlantic Bight. Both the seasonal variations and overall climatological values of the currents and transports are presented.

The model simulations are based upon the extensive hydrographic data sets assembled from both national archives (National Oceanographic Data Center and Fleet Numerical Oceanography Center) and local sources including the observational projects supported by the Minerals Management Service of the Department of the Interior. These data, which more than double the data used in Phase II, along with the Surface Marine Observations archived at the National Climatic Center, have been subjected to a comprehensive data analysis procedure to produce climatological distributions of the various water mass characteristics, wind stresses and heat fluxes. The domain for which data has been analyzed encompasses the coastal waters of the east coast of the United States from 65°W to 82°W and 23°N to 46°N, excluding a data sparse sector south of 30°N and east of 70°W.

TABLE OF CONTENTS

	Page
DISCLAIMER	ii
REPORT DOCUMENTATION PAGE	iii
EXECUTIVE SUMMARY	v
TABLE OF CONTENTS	vii
LIST OF FIGURES	ix
LIST OF TABLES	xiii
TABLE OF NOTATION	xv
LEXICON OF ACRONYMS	xvii
LEXICON OF TECHNICAL TERMS	xix
1. INTRODUCTION	1
2. CLIMATOLOGICAL DATA ANALYSIS	5
2.1 Surface Flux	7
2.1.1 Analysis	11
2.1.2 Editing and Interpretation	13
2.1.3 Climatological Distributions	18
2.2 Hydrography	29
2.2.1 Acquisition	31
2.2.2 Reduction	36
2.2.3 Climatological Distributions	39
2.3 Characteristic Tracing Model	64
2.3.1 Model Description	65
2.3.2 Diagnostic Circulation	70
3. GULF STREAM FRONTAL VARIABILITY	85
3.1 Known Characteristics	85
3.2 Previous Studies	87
3.3 General Circulation Model	90
3.4 Results from Numerical Experiments	96
3.4.1 Propagating Wind Stress	97
3.4.2 Modulation of Gulf Stream Intensity	98
3.4.3 Modulation of the Lateral Position of the Gulf Stream	109
4. CONCLUDING REMARKS	139
ACKNOWLEDGEMENTS	145
REFERENCES	147

APPENDICES

		PP
APPENDIX A:	Climatological Data Reduction	
	A.1: Meteorology	90
	A.2: Hydrography	142
APPENDIX B:	Climatological Data Analysis	160

LIST OF FIGURES

		Page
Figure 2.1	Illustration of 1/4° x 1/4° grid used for data reduction.	8
Figure 2.2	A map of the Eastern Continental Shelf showing the bathymetry of the region.	9
Figure 2.1.1	The number of surface Marine Observations whose characteristics were acceptable for use in calculating the annual stress distribution.	19
Figure 2.1.2	Annual average distributions of the climatological wind stress vector for the Eastern Continental Shelf.	20
Figure 2.1.3	Annual average distributions of the climatological average stress magnitude for the Eastern Continental Shelf.	21
Figure 2.1.4	Annual average distribution of the sensible heat flux for the Eastern Continental Shelf.	22
Figure 2.1.5	Annual average distribution of the latent heat flux for the Eastern Continental Shelf.	23
Figure 2.1.6	Annual average distributions of the net surface heat flux for the Eastern Continental Shelf.	24
Figure 2.1.7	Annual average distributions of the net radiant heat flux for the Eastern Continental Shelf.	25
Figure 2.1.8	Annual average distributions of the sea surface temperature for the Eastern Continental Shelf.	26
Figure 2.1.9	Annual average distributions of the air temperature for the Eastern Continental Shelf.	27
Figure 2.2.1	Hydrographic Data Reduction.	30
Figure 2.2.2	Total number of observations of temperature at 0 m depth before editing.	42
Figure 2.2.3	Total number of observations of salinity at 0 m depth before editing.	43
Figure 2.2.4	Total number of observations of temperature at 1000 m depth before editing.	44
Figure 2.2.5	Total number of observations of salinity at 1000 m depth before editing.	45

Page

Figure 2.2.6	Annual temperature distribution at 0 m depth.	48
Figure 2.2.7	Annual temperature distribution at 500 m depth.	49
Figure 2.2.8	Annual temperature distribution at 3000 m depth.	50
Figure 2.2.9	Annual salinity distribution at 0 m depth.	51
Figure 2.2.10	Annual salinity distribution at 500 m depth.	52
Figure 2.2.11	Annual salinity distribution at 3000 m depth.	53
Figure 2.2.12	Annual σ_t distribution at 0 m depth.	54
Figure 2.2.13	Annual σ_t distribution at 500 m depth.	55
Figure 2.2.14	Annual σ_t distribution at 3000 m depth.	56
Figure 2.2.15	0/500 m dynamic height distribution for the annual case.	59
Figure 2.2.16	500/1000 m dynamic height distribution for the annual case.	60
Figure 2.2.17	Depth of 25.8 σ_t surface for the annual case.	61
Figure 2.2.18	Temperature distribution on 25.8 σ_t surface for the annual case.	62
Figure 2.2.19	Salinity distribution on 25.8 σ_t surface for the annual case.	63
Figure 2.3.1	Total transport in the water column for the annual case.	73
Figure 2.3.2	Distribution of stream function for the annual case.	74
Figure 2.3.3	Distribution of sea surface elevation for the annual case.	75
Figure 2.3.4	Distribution of geostrophic velocity at the surface for the annual case.	76
Figure 2.3.5	Total velocity at the surface for the annual case.	77
Figure 2.3.6	Geostrophic velocity at 500 m depth for the annual case.	78
Figure 2.3.7	Geostrophic velocity at 3000 m depth for the annual case.	79

Page

Figure 3.3.1	The computational grid shown schematically off the coast of the Carolinas.	92
Figure 3.3.2	Vertical cross-section of the computational grid shown in Figure 3.3.1.	93
Figure 3.4.1	Calculated fields on day 11 for propagating wind stress experiment.	99
Figure 3.4.2	Calculated fields on day 12 for propagating wind stress experiment.	100
Figure 3.4.3	Calculated fields on day 13 for propagating wind stress experiment.	101
Figure 3.4.4	Calculated fields on day 14 for propagating wind stress experiment.	102
Figure 3.4.5	Calculated fields on day 15 for propagating wind stress experiment.	103
Figure 3.4.6	Calculated fields on day 16 for propagating wind stress experiment.	104
Figure 3.4.7	Calculated fields on day 17 for propagating wind stress experiment.	105
Figure 3.4.8	Calculated fields on day 18 for propagating wind stress experiment.	106
Figure 3.4.9	Calculated fields on day 19 for propagating wind stress experiment.	107
Figure 3.4.10	Calculated fields on day 20 for propagating wind stress experiment.	108
Figure 3.4.11	Calculated fields on day 11 for Gulf Stream intensity modulation experiment.	110
Figure 3.4.12	Calculated fields on day 12 for Gulf Stream intensity modulation experiment.	111
Figure 3.4.13	Calculated fields on day 13 for Gulf Stream intensity modulation experiment.	112
Figure 3.4.14	Calculated fields on day 14 for Gulf Stream intensity modulation experiment.	113
Figure 3.4.15	Calculated fields on day 15 for Gulf Stream intensity modulation experiment.	114
Figure 3.4.16	Calculated fields on day 16 for Gulf Stream intensity modulation experiment.	115

Page

Figure 3.4.17	Calculated fields on day 17 for Gulf Stream intensity modulation experiment.	116
Figure 3.4.18	Calculated fields on day 18 for Gulf Stream intensity modulation experiment.	117
Figure 3.4.19	Calculated fields on day 19 for Gulf Stream intensity modulation experiment.	118
Figure 3.4.20	Calculated fields on day 20 for Gulf Stream intensity modulation experiment.	119
Figure 3.4.21	Calculated surface temperature fields for days 13 to 16 for Gulf Stream lateral position modulation experiment with Δx = 10 km.	123
Figure 3.4.22	Calculated surface temperature fields for days 17 to 20 for Gulf Stream lateral position modulation experiment with Δx = 10 km.	124
Figure 3.4.23	Calculated fields on day 11 for Gulf Stream lateral position modulation experiment with Δx = 25 km.	125
Figure 3.4.24	Calculated fields on day 12 for Gulf Stream lateral position modulation experiment with Δx = 25 km.	126
Figure 3.4.25	Calculated fields on day 13 for Gulf Stream lateral position modulation experiment with Δx = 25 km.	127
Figure 3.4.26	Calculated fields on day 14 for Gulf Stream lateral position modulation experiment with Δx = 25 km.	128
Figure 3.4.27	Calculated fields on day 15 for Gulf Stream lateral position modulation experiment with Δx = 25 km.	129
Figure 3.4.28	Calculated fields on day 16 for Gulf Stream lateral position modulation experiment with Δx = 25 km.	130
Figure 3.4.29	Calculated fields on day 17 for Gulf Stream lateral position modulation experiment with Δx = 25 km.	131
Figure 3.4.30	Calculated fields on day 18 for Gulf Stream lateral position modulation experiment with Δx = 25 km.	132
Figure 3.4.31	Calculated fields on day 19 for Gulf Stream lateral position modulation experiment with Δx = 25 km.	133
Figure 3.4.32	Calculated fields on day 20 for Gulf Stream lateral position modulation experiment with Δx = 25 km.	134
Figure 3.4.33	Calculated surface temperature fields for days 13 to 16 for Gulf Stream lateral position modulation experiment with Δx = 25 km but A_M doubled and A_H halved.	135

Page

Figure 3.4.34 Calculated surface temperature fields for days 17 to 20 for Gulf Stream lateral position modulation experiment with Δx = 25 km but A_M doubled and A_H halved. 136

LIST OF TABLES

Table 1. COMPUTATIONAL GRID DEFINITION. 95

TABLE OF NOTATION

A	$= 5$ dynes/cm^2, constant
A_T	$= 10°C$, constant
a	$= 1.15 \times 10^{-4}$ °C^{-1}, constant
C_D	Drag coefficient
C_E	Mass transfer coefficient
C_H	Heat flux coefficient
D	Depth
E	Mass flux at surface
f	$= 2\Omega \sin \phi$
F_c	Proportion of cloud cover
F_r	Albedo
g	$= 9.801$ m s^{-2}, acceleration due to gravity
H	Sensible heat flux at surface
I,J	Number of grid points in each direction
I_s	Clear sky insolation
k	$= 1.35 \times 10^{-12}$ cal cm^{-2} K^{-4} s^{-1},
M	Climatological mean value at point (i,j)
N	Number of observations
N_t	Total number of observations at all grid points for that season
O	Observed data value at point (i,j)
P_v	Vapor pressure in millibars
q	Specific humidity
s	Standard deviation
T	Temperature
T'	Temperature perturbation as prescribed in Equation (3.7)

T_o	= 4°C, reference temperature
t_p	= 8 days, constant
t_v	= 8 days, constant
$\vec{u}$	Wind velocity vector
u,v	Velocities in the x and y directions, respectively
x	Horizontal coordinate shown in Figure 3.3.1
x_b	$= x - x_f$
x_c	= 135 km, constant
x_f	= 100 km, constant
z	Vertical coordinate shown in Figure 3.3.2
λ	= 30 km, constant
δ	$= 1.25 \times 10^{-5}\ m^{-1}$, constant
ΔT	= 7°C, reference temperature difference
ε	$= 0.65 \times 10^{-3}\ m^{-1}$, constant
ε_m	= .98, relative emissivity
ρ	Air density
σ_t	$= 1000(\rho - 1)$, reduced density
σ_x	= 35 km, constant
σ_z	= 200 m, constant
$\vec{\tau}$	Wind stress vector at surface
(τ_{ox}, τ_{oy})	x and y components of the wind stress
ϕ	Latitude
Ω	$= 0.73 \times 10^{-4}\ s^{-1}$, earth's rotational frequency

LEXICON OF ACRONYMS

AXBT	Aircraft Expendable Bathythermograph
CTD	Conductivity, temperature, depth instrument
CTM	Characteristic Tracing Model
DOE	Department of Energy
DOI	Department of the Interior
ECS	Eastern Continental Shelf
FACTS	Florida Atlantic Coast Transport Study
FNOC	Fleet Numerical Oceanography Center
GABEX	Georgia Bight Experiment
GCM	General Circulation Model
GOM	Gulf of Maine
MAB	Middle Atlantic Bight
MASAR	Mid-Atlantic Slope and Rise program
MBDS	Minerals Management Service, Bureau of Land Management, Department of Energy, Skidaway Institute of Oceanography Data Sets
MMS	Minerals Management Service
MOODS	Master Oceanographic Observation Data Set
NASACS	North Atlantic Slope and Canyon Study
NCDC	National Climatic Data Center
NOAA	National Oceanographic and Atmospheric Administration
NODC	National Oceanographic Data Center
ONR	Office of Naval Research
OSRA	Oil Spill Risk Analysis
SAB	South Atlantic Bight
SAPOS	South Atlantic Physical Oceanography Study
SEEP	Shelf Edge Exchange Processes study

STACS	Subtropical Atlantic Climate Study
STD	Salinity, temperature, depth instrument
SYNBAPS	Synthetic Bathymetric Profiling System

LEXICON OF TECHNICAL TERMS

Advection
: The process of transport of an oceanic property solely by the motion of the fluid particles.

Baroclinic
: A state in a fluid in which the lines of constant density and pressure do not cross one another.

Barotropic
: A state in the fluid in which surfaces of constant density are parallel to surfaces of constant pressure, a situation which occurs in a homogeneous nonstratified fluid.

Bathythermograph
: A device for obtaining a record of temperature versus depth in the ocean from a ship under way. Salinity measurements are not possible with this device.

Bousinesq approximation
: An assumption used in fluid dynamics which neglects small differences in density except when the differences are multiplied by gravity in various governing equations.

Cartesian coordinate system
: A system of orthogonal coordinates with three space variables convenient for many types of problems. In this system the coordinate lines are always straight and never exhibit any curvature.

Connective process
: A process which is accomplished by virtue of the transport of a property with a flowing fluid.

Coriolis force
: An apparent (fictitious) force acting on a moving particle resulting from the earth's rotation. This force causes particles in the northern hemisphere to be deflected to the right of the motion.

Eddy diffusivity
: A coefficient which is a measure of a turbulent transfer of fluid properties.

Eddy viscosity
: A coefficient which is a measure of a turbulent transfer of momentum.

Ekman currents
: The currents induced in the upper layers of the ocean by a shear stress at the surface. The currents deviate farther from the direction of the wind at greater depths from the surface due to the effect of earth's rotation.

Finite difference method

A common numerical integration procedure in which the derivatives in the differential equations of motion are replaced by finite difference approximations at a discrete set of points.

Geostrophic balance

A situation in fluid dynamics in which there is an exact balance between the horizontal pressure gradient and the Coriolis force.

Hydrography

The measurement and description of the physical features of the ocean, such as temperature, salinity, turbidity and chemical constituents.

Hydrostatic assumption

A situation in which one assumes that the vertical pressure gradient force exactly balances the gravity force.

Latent heat flux

Apparent removal of latent heat of vaporization from the surface layer in proportion to the change in phase of water from a liquid to a gas.

Latent heat of vaporization

The quantity of heat required to change the phase of water from a liquid to a gas (590 cal gm^{-1}).

Mesoscale

A length scale approximately between 10 and 150 km used in oceanography to characterize various circulation features which appear, for example, eddies, fronts, jets and meanders.

Mode splitting technique

A procedure which permits the calculation of the free surface elevation in a numerical model with little sacrifice in computational time by solving for the volume transport separately from the vertical velocity shear.

Net heat flux

Net heat absorbed into the sea surface representing the algebraic sum of the radiant heat flux, the sensible heat flux and the latent heat flux.

Net longwave radiation

The longwave radiation (>4μm) absorbed into the ocean, representing the algebraic sum of the incident and emitted longwave radiation.

Net shortwave radiation

The shortwave radiation (>4μm) absorbed into the ocean, representing the difference between the insolation and the reflected shortwave radiation.

Objective analysis scheme

Technique used objectively and systematically to fill in data gaps that inevitably exist in an observed field.

Orthogonal
: Perpendicular.

Radiant heat flux
: Net radiant heat flux absorbed into the ocean representing the algebraic sum of the long wave and short wave heat fluxes.

Reynolds stresses and fluxes
: Mathematical terms which arise in fluid dynamical equations that represent scales of motion smaller than those resolved explicitly. Much of the theory of turbulence is concerned with the approximation of these Reynolds terms.

Sensible heat flux
: The transfer of heat from one material to another without the associated transfer of mass.

STD/CTD cast
: Information obtained from devices which allow for the measurement of temperature and salinity of the water column at continuous depths throughout the vertical.

Synoptic
: An instantaneous realization (snap shot).

Thermocline
: A region in the ocean where there is a more rapid change in temperature than above or below it in the water column.

Turbulence closure
: The process of parameterizing, usually in an empirical fashion, the effects of turbulent motions on the mean flow.

Turbulence macroscale
: A length scale which represents the distance over which a turbulent eddy acts.

Vorticity, absolute (or planetary)
: Sum of the relative vorticity and the Coriolis parameter which represents the vorticity in a coordinate system fixed in space.

Vorticity, planetary potential
: In the vertically integrated equations of motion, the planetary potential vorticity is the ratio of the Coriolis parameter to the depth of the fluid. The Characteristic Tracing Model is based on the assumption that this quantity is conserved along a fluid stream column.

Vorticity, relative
: The curl of the velocity field evaluated in a coordinate system rotating with the earth.

1. INTRODUCTION

Responsible management of the development of offshore oil and gas resources is best achieved through an understanding of both production and environmental issues. The need to study the marine environment, and in particular the factors which drive the ocean circulation, is clear. It is the oceanic currents which transport pollutants such as spilled oil at the surface, or drill cuttings and mud at depth. These pollutants may impact beaches and vulnerable natural resource regions, like seabird habitats.

The investigation reported here is part of an on-going effort to assist the Minerals Management Service (MMS) of the Department of the Interior (DOI) in evaluating the impact of offshore drilling and production activities on the East Coast of the United States including the South Atlantic Bight (SAB). There are two primary objectives of the study described herein. The first is to quantify existing knowledge regarding the physical oceanography of the Eastern Continental Shelf (ECS) for use by the Minerals Management Service (MMS) in writing environmental impact statements for offshore oil leasing activities. The second is to provide rational estimates of the circulation in this region at the surface, mid-depth and bottom for input to the MMS Oil Spill Risk Analysis (OSRA) model.

The research program has been designed to meet these objectives in an expedient manner and yet maintain a high level of scientific credibility. This is accomplished by inferring climatological circulation for immediate input to the oil spill modelling effort and at the same time performing testing and evaluation of the General Circulation Model (GCM) in order to be prepared to produce more comprehensive results at a later date as they are required.

There is a relatively large volume of observational data for the Eastern Continental Shelf that is available from a variety of sources (see Kantha, Blumberg, Herring and Mellor, 1983). This data is necessary to provide boundary conditions for the numerical models but it also contains much information which contributes directly to the understanding of the Shelf circulation. In the aggregate the observational data set yields considerably more insight, particularly with respect to climatology, than the constituents do to the individual investigators. Therefore an important task in the research program is the assembly, quality control and analysis of the data to provide an atlas of all available information.

The diagnostic climatological circulation may be viewed as either a derived data product or a modelling product. The Characteristic Tracing Model (CTM) employed here is driven by climatological density fields from the analysis of historical hydrographic data, and climatological wind fields from historical marine sea surface data, but includes effect of bottom roughness as well. Besides providing additional insight concerning the observational data, the diagnostic circulation, based on the conservation of planetary potential vorticity, represents the first estimate of the distribution of currents at all depths throughout the region. As such it has been used as input to the oil spill risk assessment model. The climatological velocity also represents a physically realistic and dynamically consistent lateral boundary condition specification to drive the GCM.

Evidently low frequency spatial and temporal variability is of considerable importance on the outer shelf in the SAB. This variability is influenced by the western front of the Gulf Stream and requires the complete physics of the GCM. Consequently the other major component of the research program involves GCM calculations both to investigate the

parameters governing the variability and to demonstrate the ability of the GCM to reproduce this behavior.

Earlier calculations of the Gulf Stream with the General Circulation Model [Blumberg and Mellor, 1983], did not produce the observed Gulf Stream frontal variability. Insufficient horizontal grid resolution in the model is thought to be the primary cause. Instabilities in the Gulf Stream boundaries of the critical scales were not resolved and therefore could not form.

As a test of this hypothesis, high resolution calculations representing the western boundary of the Gulf Stream were performed using the full three-dimensional General Circulation Model. The grid is orthogonal rectilinear with variable spacing to conserve computer time. A cross-shore spacing of 5 km in the vicinity of the Gulf Stream front provides an adequate resolution of shear layer instabilities. The grid then expands on either side to place the boundaries farther from the region of interest.

For these exploratory calculations the boundary conditions and topography are specified as proposed by Luther and Bane [1985] for their slope instability studies. Besides representing a reasonable specification of the domain, these conditions also allow for direct comparison of the calculations with the analytical calculations of the authors.

In a series of numerical experiments to simulate Gulf Stream frontal activity, several different types of external forcing have been explored. The results of these calculations indicate that cold dome meanders of the Gulf Stream can be produced by modulation of the lateral position of the Gulf Stream. They shed light on Gulf Stream frontal variability and establish confidence in the ability of the model to predict them.

2. CLIMATOLOGICAL DATA ANALYSIS

Observational data and synthesis of that data play an essential role in the understanding and the prediction of ocean circulation processes. The data alone describe the existing conditions and provide information which gives insight into the driving mechanisms. They are also an essential component of numerical models that provides boundary conditions and initial conditions for computational domains which are limited in time and space. They are indispensable for diagnostic models of ocean circulation such as the CTM. Both wind stress and density fields are needed as input to the model and must be derived from observations.

Historical data archives such as the National Oceanographic Data Center (NODC), Fleet Numerical Oceanography Center (FNOC), and the National Climatic Data Center (NCDC) are the main sources of the climatological data used in this report. However all available hydrographic data from a variety of sources have been gathered from their originators and included in the data base. These sources include the South Atlantic Bight Physical Oceanography Program of the Minerals Management Service. Because of the relatively small amounts of data available, it is important to assemble as much data as is practical, and then extract as much information as is possible. At the same time, it is essential to exclude erroneous data values and alleviate data biases so as to obtain meaningful, climatologically representative distributions.

The primary domain of interest to the present study is the South Atlantic Bight (SAB), the region of the coastal ocean to the south of 36°N latitude. The northern boundary of the modelled domain was placed at this latitude during Phase II of the modelling effort [Kantha, Blumberg,

Herring and Mellor, 1981]. From that study it became obvious that the northern boundary near Cape Hatteras was not located properly from a dynamical point of view. The boundary cut across the most dynamically active and interesting features of the Eastern Continental Shelf (ECS) circulation. It is at this latitude that the northward flowing Gulf Stream is joined by the southward current from the Middle Atlantic Bight (MAB) and the combined currents make their dramatic departure from the coast into the Atlantic Ocean. Clearly, placing the domain boundary in this region, although appropriate for the traditional demarcation of the South and Middle Atlantic Bights, did not respect the dynamics of the flow. It made interpretation of climatological data and circulation difficult and prescribing satisfactory boundary conditions for the GCM nearly impossible.

During deliberations concerning the optimal location of the northern boundary of the modelling domain of the CTM 83, it became clear that an ideal opportunity existed for modelling the entire Eastern Continental Shelf of the United States, and also that modelling the entire ECS would provide a greater insight into the dynamics of the region around Cape Hatteras. The larger domain would therefore improve the understanding, depiction and interpretation of the circulation in the South Atlantic Bight.

Climatological data reduction and analysis, and CTM 83 calculations for this ECS region were done in two stages. As reported in an earlier version of this report, the calculations were done for the domain north of 26.5°N, bounded to the east by 65°N, during year 1 of Phase III. During year 2, the domain was extended southward to 22.75°N and instead of repeating needlessly the calculations over the larger domain, both hydrographic and surface flux data analyses and CTM calculations were done

over only the southern extension of the domain with some overlap with the northern domain. This southern domain extends therefore from 22.75°N to 26.75°N and 81.75°W to 74°W. The region to the east of 74°W and south of 26.75°N was omitted mainly because the focus of interest is the Straits of Florida and not the region east of the Bahamas, but also because of sparsity of data and complexity of topography. The results for the two domains were melded together with a linear interpolation in the overlap region. As the resulting fields attest, the technique has been successful and cost effective, and the needless expense of performing the calculations over the entire enlarged domain has been avoided.

The domain selected for processing of the climatological data (and modelling of the circulation by CTM 83) is shown in Figure 2.1. The region is bounded on the east side by 65°W longitude and on the south by 22.75°N latitude. Hydrographic data has been processed on the ¼° x ¼° grid shown, whereas the Surface Marine Observations have been binned on ½° x ½° grid, and interpolated and smoothed on the ¼° x ¼° grid shown using the Herring Poisson technique described in Kantha et al. [1981] and Blumberg, Herring, Kantha and Mellor [1983]. The CTM also utilizes the same grid. The southeast corner of the domain has been masked primarily because the coverage there is so sparse that both the climatological properties and diagnostic calculations there are unreliable. Besides, that region is outside the focus of interest. Therefore hereafter the region will be omitted both from display and discussion. Figure 2.2 depicts the bottom topography of the region derived from high resolution bathymetry.

2.1 Surface Flux

The air-sea interface is the most variable and also frequently the most important boundary of an oceanic region. Accurate knowledge of the

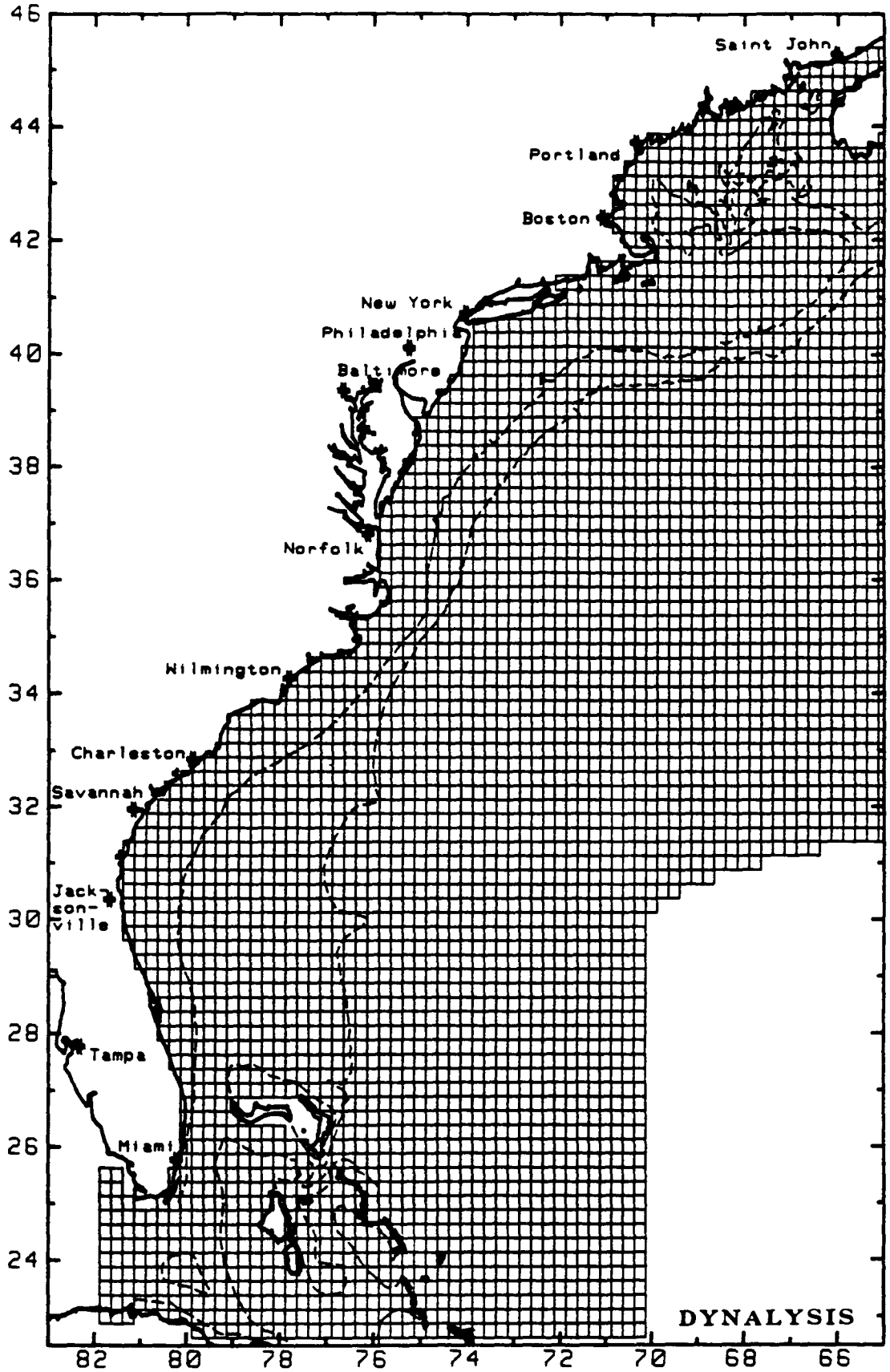

Figure 2.1 Illustration of 1/4° x 1/4° grid used for data reduction.

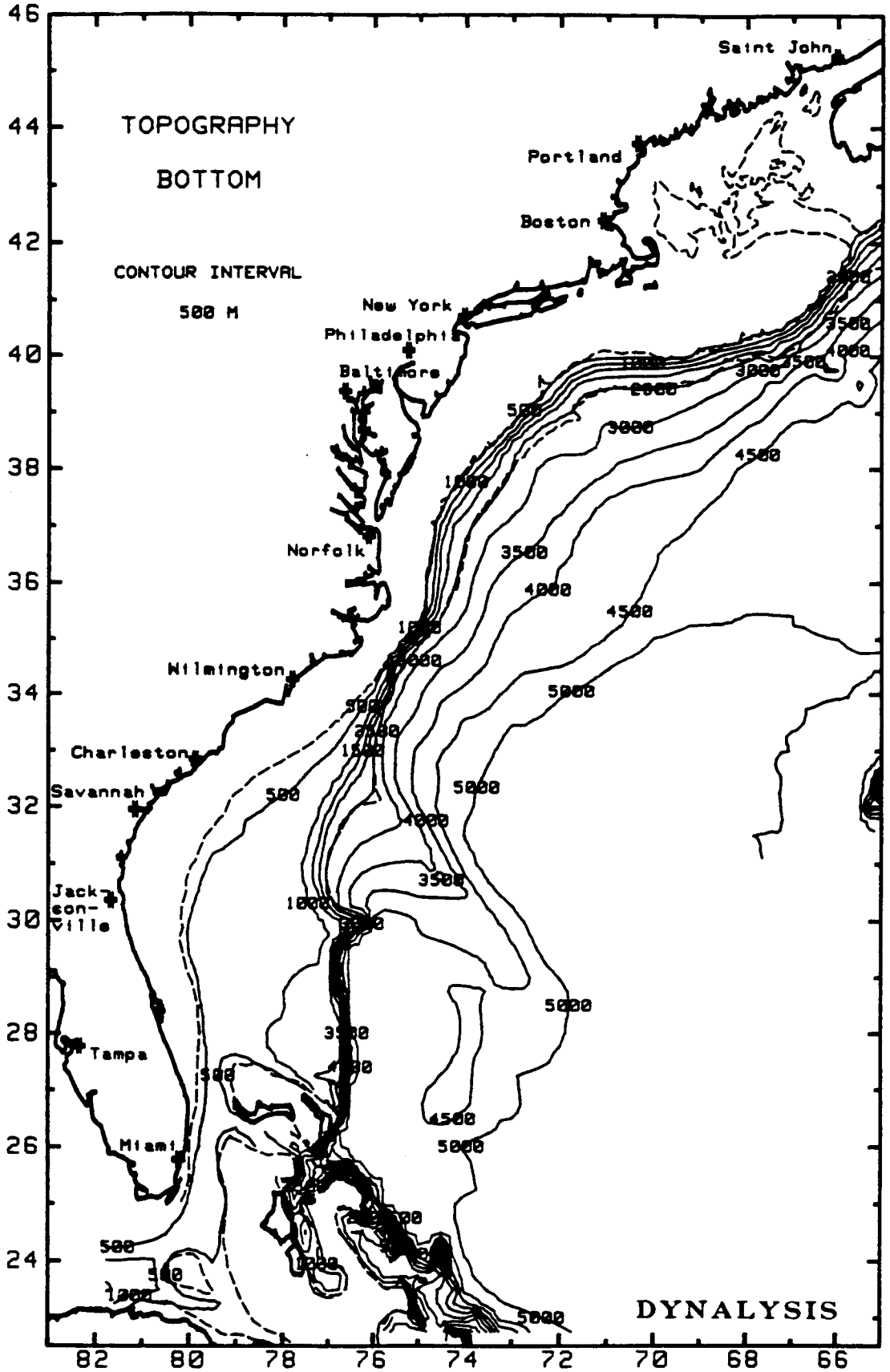

Figure 2.2 A map of the Eastern Continental Shelf showing the bathymetry of the region.

surface fluxes is therefore of paramount interest in determining the climatology of a region. While direct measurements of surface fluxes have been made for research purposes, their coverage in time and space does not begin to be sufficient.

Fortunately there exists a large data set of observations of surface conditions at the air-sea interface, which , although it does not include direct flux measurements, can be used to infer fluxes. The data, from ship logs of the world's merchant and naval fleets, are archived by the National Climatic Data Center under the name Marine Surface Observations. The data is comprised of basic measurements routinely taken at the change of the watch. The parameters include wind speed and direction, air, sea and wet bulb temperatures and cloud cover. While not of uniformly high accuracy and containing some inevitable bias, the data, nevertheless, represents a unique and valuable resource. The records extend back over more than a century, are relatively uniformly distributed over the months of the year and cover the world oceans in direct proportion to the shipping activity.

For these reasons the data have been carefully studied by a number of investigators to glean from it the maximum possible information. In terms of spatial coverage and records processed, the two most monumental achievements are those of Bunker, who, after refining the empirical content of the flux relations, calculated surface fluxes [Bunker, 1976] and their recent trends [Bunker, 1979] for the entire North Atlantic Ocean, and Hastenrath and Lamb who computed climatological conditions [1977] and heat budget [1978] for the tropical Atlantic and Eastern Pacific Oceans. Other researchers have examined the remaining United States coastal waters. A regional analysis of the Gulf of Mexico has been performed by Etter [1975]. Nelson [1977] has examined the wind stress and

the heat flux [Nelson and Husby, 1983] of the Eastern Pacific California current region.

To date the Western Atlantic and the United States eastern continental shelf have not received sufficient attention. Seasonal wind stress in the northern portion of the continental shelf has been obtained by Saunders [1977]. Weber and Blanton [1980] have determined monthly winds for the near shore region in the South Atlantic Bight but the complete complement of climatological variables is not available in sufficient detail to establish a coastal climatology or produce boundary conditions for a numerical model. The results presented here have been prepared in response to those needs.

The technique of obtaining the sea surface climatology and surface flux from the Marine Surface Observations involves both science and art. The scientific aspect of the problem is the development and verification of increasingly more precise analytical or semi-empirical relationships between those meteorological variables contained in the Surface Marine Observation data and the surface fluxes of primary concern. There are two major areas of research; the turbulent flux of momentum, energy and mass through the surface layer and the radiant heat transfer at the surface.

2.1.1 Analysis

The turbulent flux problem has been studied both in the laboratory by Nikuradse [1933], Moore [1951], Seban and Shimazki [1951], and in the field by Wu [1967; 1968], Pond et al. [1971] and Holland [1972]. The results have been analyzed and correlated by Prandtl and Schlichting [1934], Millikan [1938], Clauser [1954], Charnock [1953], Sheppard [1958] and Kader and Yaglom [1972] to produce remarkably general semi-empirical relations for turbulent flux of momentum, energy and mass.

For computational purposes the fluxes are usually expressed in the form of bulk aerodynamic functions of the quantities reported in the Surface Marine Observation data set. The most common forms are:

$$\vec{\tau} = C_H |U_{10}| \, U_{10}, \tag{2.1}$$

$$H = C_E |U_{10}| \, (T_{10} - T_0), \tag{2.2}$$

and

$$E = C_D |U_{10}| \, (q_{10} - q_0), \tag{2.3}$$

where $\vec{\tau}$, H and E are the stress vector, sensible heat flux and mass flux at the surface. The quantities ρ, T and q are the air density, temperature and specific humidity respectively and $\vec{U}$ is the wind velocity vector. The subscripts 10 and 0 refer to the arbitrary 10 meter bridge height and the sea surface respectively.

The empiricism is concentrated in the coefficients, C_D, C_H and C_E, which in general are functions of the observed variables. The relations for the coefficients used to obtain the present results are tabulated and their derivation is described in Kantha, et al. [1981].

Sea surface radiation has been studied intensively over a period of many years. Angstrom [1924], Kimball [1928], Tabata [1964] and Reed [1976] quantified the solar radiation. Measurements of the reflected solar radiation were performed by Neuman and Hollman [1961] and Payne [1972] to determine net insolation. Finally Angstrom [1924], Brent [1939], Sverdrup, Johnson and Fleming [1942], Anderson [1954] and Reed and Halpern [1975] established the empirical dependence of the longwave radiation.

The specific relations used here are:

$$R_s = I_s(1 - 0.71F_c)(1 - F_r), \tag{2.4}$$

and

$$R_1 = \varepsilon_m k \left[T_{10}^4 \, (0.39 - 0.05 \, P_{v10}^{\frac{1}{2}}) \, (1 - 0.9 \, F_c) - (T_{10}^4 - T_0^4) \right] , \qquad (2.5)$$

for the net shortwave and net longwave radiation respectively as given in Price, Mooers and Van Leer [1978], where I_s is the clear sky insolation, ε_m the emissivity, k the Boltzmann constant, F_c the proportion of cloud cover, F_r the albedo and P_v is vapor pressure in millibars.

Unfortunately the fluxes obtained from these correlations are not necessarily as accurate as one might expect considering the sophistication of the equations and the accuracy of the data used to determine the constants. In fact, the Surface Marine Observations viewed individually are a very imperfect data set. What saves the data set as a whole from oblivion is that it contains a statistically meaningful quantity of data. In order to use these data therefore, one must adopt the psychology that any, and perhaps many, records are expendable in the quest for accuracy. This is the stage at which judgment becomes important as described in the sections which follow.

2.1.2 Editing and Interpretation

Many of the specific shortcomings of the data have been discussed by previous users. Bunker [1975] and Nelson [1977] each, provide detailed discussions of the problems uncovered and the solutions employed.

Most of the outright errors are easily found. They represent data which are read incorrectly or entered in the wrong units by an inexperienced seaman. Simple tests to establish reasonable bounds on all data values are essential when using these data. The most unequivocal solution

for these errors is to ignore the entire observation. In the present data reduction effort each record eliminated is printed out and in all cases the decision has proved correct.

The bounds for this first pass are set broad to eliminate data that are actually wrong. For climatological purposes it is also desirable to eliminate data which are unrepresentative by virtue of some anomalous oceanographic or meteorological event such as a hurricane. A two step process is used to accomplish this. First of all in a data set spanning forty years, multiple records from the same ship during a short period of time attach an artificial weight to those observed conditions. This is overcome by averaging any number of observations in a given grid box during any one week period and considering them as equivalent to a single observation.

Secondly, more refined bounds are placed on data acceptance. When all data have been reduced, in a given grid box the mean and standard deviation are calculated. Using these values any data which differs from the mean by more than 3 times the standard deviation is rejected and the final value of the mean and standard deviation is recalculated. This process eliminates data which are climatological outliers for any reason not otherwise recognized or easily quantified.

There are certain biases in the data acquisition which are more insidious, however. Records containing these biases are either too pervasive to ignore or too difficult to identify to eliminate effectively as described in the following examples. The wind data are assumed to be recorded at a position 10 meters above the surface regardless of the type of ship. While the hull and superstructure of the ship certainly distort the airflow, this effect is difficult to assess because of the wide variety of ships involved. Finally there is a widespread use of the engine inlet temperature as sea surface temperature even though it is

likely to be drawn at a depth considerably below the surface and be heated in the ship's plumbing before it reaches the engine inlet. There appears to be little that can be done, after the fact, to remedy these problems and their recognition merely serves as a caution in interpreting the results.

Another frustrating acquisitional bias is the brutal quantization which characterizes most of the earlier international data. Nelson [1977] observed that most of the earlier data was obviously recorded using the 16 points of the compass and the Beaufort scale (and undoubtedly estimated at that). These same data sets contain the ship location only to the nearest whole degree of latitude and longitude. As a result, Weber and Blanton [1980] eliminated any data record reporting the location as even degrees but this would seem rather drastic. Here the most attractive solution was to eliminate the data from source decks 184 though 197 and 281 which are the worst offenders on both of these counts. While these data sets represent only 4% of the total data set, they contain virtually all of the early historic data. Therefore the resulting data set only spans the four decades from the forties through the seventies and of that the last two decades decidedly have the best coverage.

Aliasing of the solar radiation could result from the quantization of the times the observations were made. Although in theory the observations could be made at any time, in practice the vast majority appear to have been made at six hourly intervals which presumably correspond to the changing of the watch. These times, 0600, 1200, 1800 and 2400 hours, are described in the National Climatic Data Center manual as representing Greenwich Mean Time. However, regardless of the time zone of the record the major hours are the same and it is most likely that they actually represent local time. In either case, the average of the instantaneous insolation for these times would not accurately reflect the average

insolation through the day. For climatological purposes, then, the hour of the observation is ignored and the average daily insolation for the appropriate month and latitude is taken from Budyko [1963], assuming all other observed conditions to be constant throughout the day.

Fair weather bias describes the predilection of seamen to navigate to avoid storms and to take advantage of favorable winds and currents. Of course, the data does not include a record of the intentions of the navigator and in any case there would be no way to introduce the effects of the storm during the data analysis phase. Therefore, the most obvious implication of the fair weather bias, the underestimation of storm activity, must be accepted as unavoidable.

A more subtle manifestation of the bias, the implications of the subjective assessment of present weather conditions on rainfall, has been studied in some detail by Tucker [1961] and Dorfman and Bourke [1978]. The result is a correlation between actual precipitation data and the judgments by seamen as expressed by the present weather code in the Surface Marine Observation data. This technique might reasonably be expected to bypass the subjectivity in the data and therefore is employed in obtaining the present results.

The navigator's affinity for favorable winds and currents should pose no particular difficulty if the data on wind magnitude and direction is as represented by the National Climatic Data Center personnel. The wind data is said to give the absolute direction and speed of the wind, corrected for compass deviation, ship velocity and current velocity. That the data is corrected for compass deviation is likely since the ship's navigator would presumably be concerned with the true course. Whether the seaman recording the data would take the trouble to determine the ship's heading and speed and perform the vector operation to compensate the wind measurements is problematical and on the balance must be judged unlikely. The National

Climatic Center does not have the information available to do so and therefore regardless of the intention, the data is probably not compensated for ship speed. Whether or not this conjecture is true, there is virtually no chance that the data has been compensated for effects of currents, which in most cases are not well known.

The inescapable conclusion then is that any single data value may have a significant error in the wind record. What has obscured this fact is that wind velocities tend to be very large compared to those of the currents in most places. With regard to the ship velocity, one would expect that with a large data set such as this, the ship velocities would average out to produce a fairly representative mean wind field albeit with an unnecessarily large standard deviation.

In the present data set there are two important differences. First, the Gulf Stream currents are not negligible compared to the wind speed and second, seamen have known this fact for a long time and always seek the Gulf Stream when going north and avoid it going south. Therefore the ship velocities and currents in this case are well correlated in space. The result is an anomaly in the wind velocity over the Gulf Stream and again less obviously in the southern shipping route to the east of the Gulf Stream. This anomaly in the results of Kantha et al. [1981] was observed and noted by Brown [1981]. The optimum solution to this problem is presently under investigation.

All things being considered, the obvious vagaries of the data acquisition technique discussed above provide some perspective in interpreting the results. They also serve to suggest that there is a practical limit to the sophistication of the scientific aspect of the data analysis without a corresponding improvement in the art with which the records are selected and interpreted.

2.1.3 Climatological Distributions

The data analyzed in this study consist of the full TD9760 file, which was once designated TDF-11 and includes all data from 1800 until 1969, and the TD1129 file including all data from the 1970's decade. The data analysis process is performed on each record individually and the derived distribution of each output variable is averaged separately to maintain the influence of nonlinearities. The monthly, seasonal and annual distributions of the climatological mean and standard deviation have been calculated for a number of quantities including the wind velocity, wind stress and mean stress magnitude, the latent, sensible, radiant and net heat flux, evaporation and precipitation and the air, sea surface and wet bulb temperatures. As an example, some of the annual distributions are shown in Figures 2.1.1 through 2.1.9. For completeness the monthly distributions of wind stress and net heat flux are given in Appendix A.1.

Figure 2.1.1 is the distribution of the total number of observations which contained sufficient information to infer the convective fluxes. The distribution of observations is remarkably uniformly divided over the months of the year except possibly during the winter months in the northernmost portion. While the shipping lanes are clearly defined, there are statistically meaningful numbers of observations at virtually all points.

The annual average wind stress distribution is shown in Figure 2.1.2. The stress field is the result of predominantly westerly winds along the northern portion of the coast and offshore and predominantly northerlies in the near shore South Atlantic Bight region. These results compare well with the near shore coarse grid results of Saunders [1977] in the northern portion. The best comparison with the monthly wind stress distributions

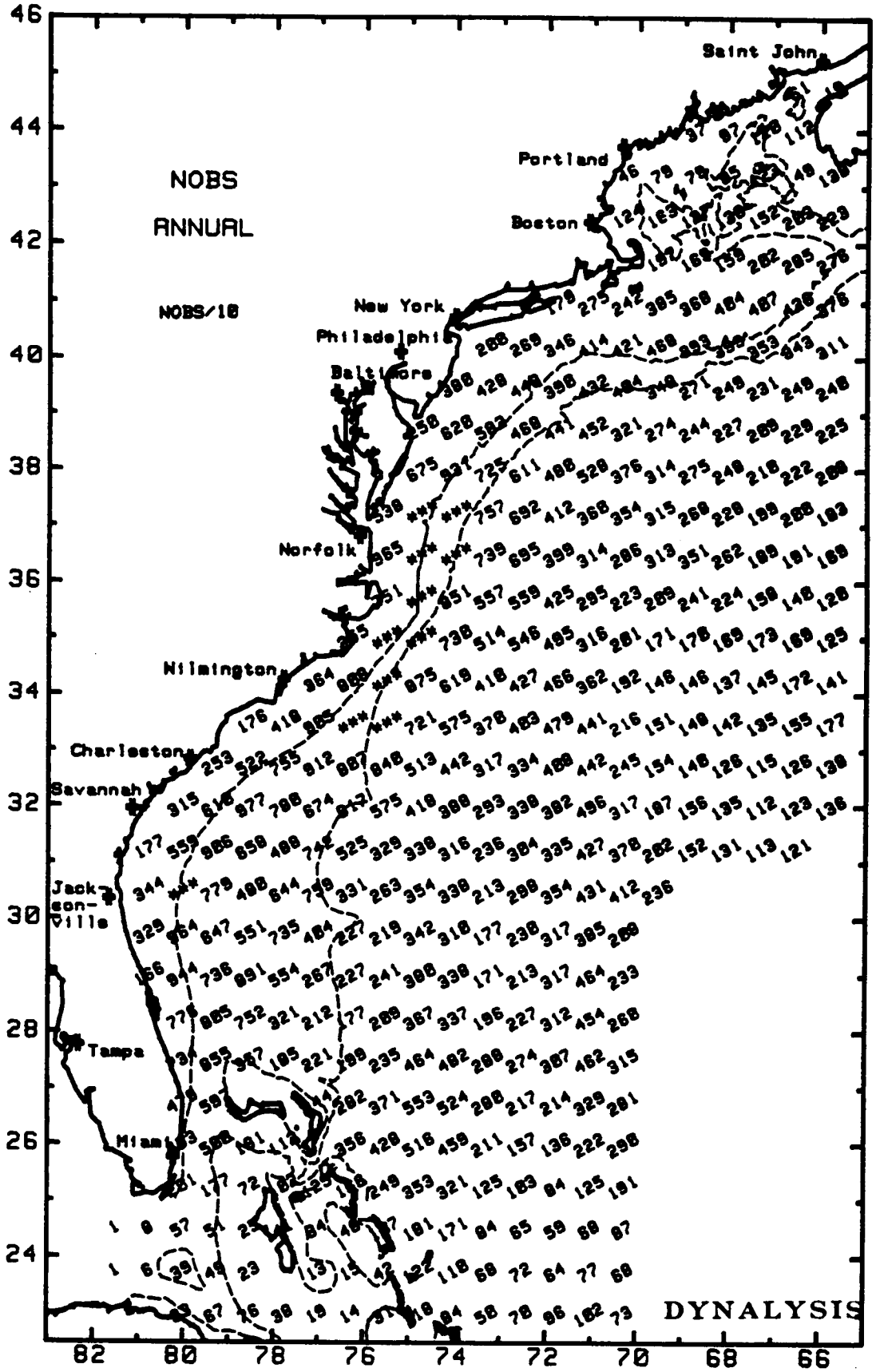

Figure 2.1.1 The number of surface Marine Observations whose characteristics were acceptable for use in calculating the annual stress distribution.

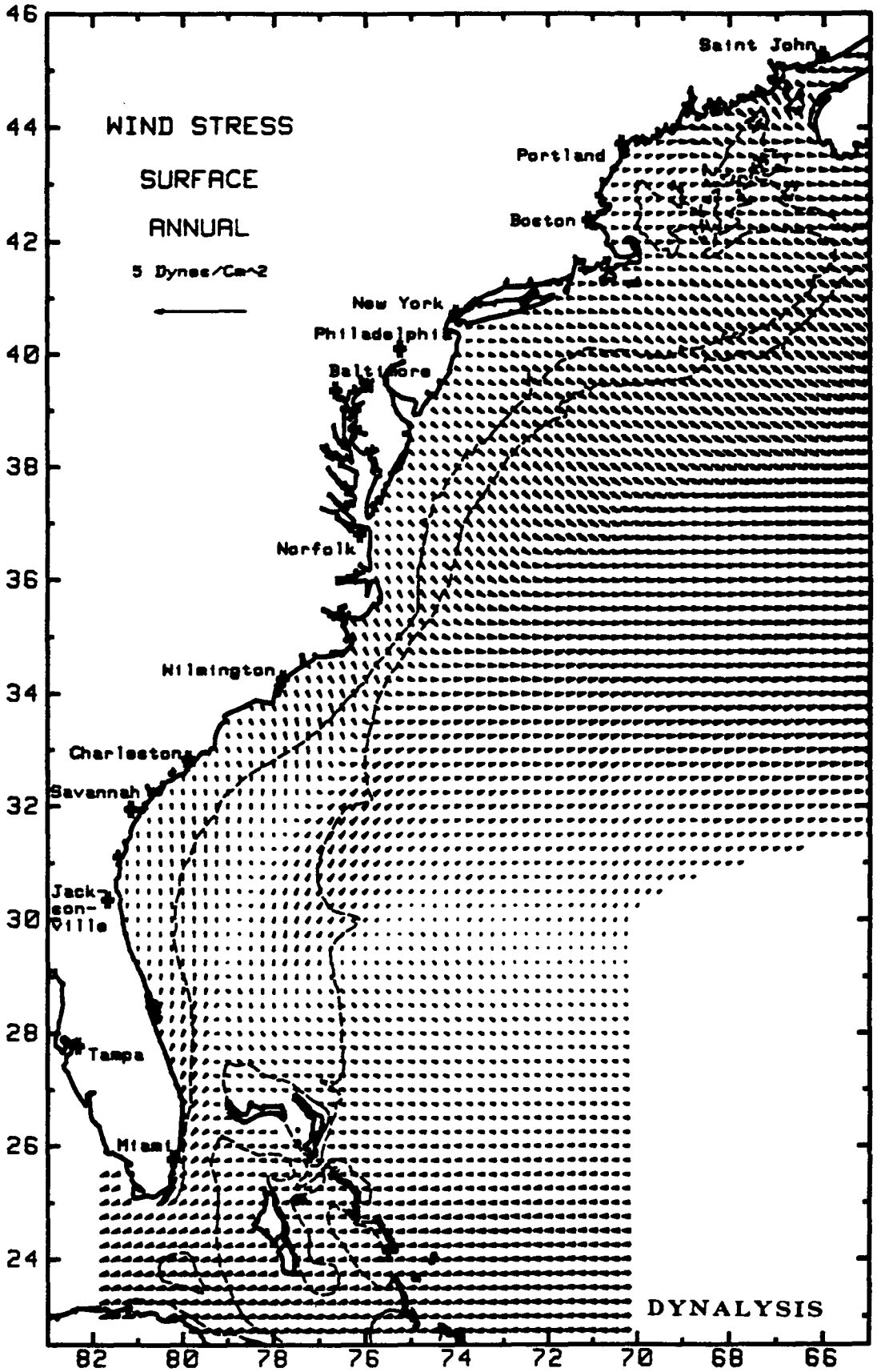

Figure 2.1.2 Annual average distributions of the climatological wind stress vector for the Eastern Continental Shelf.

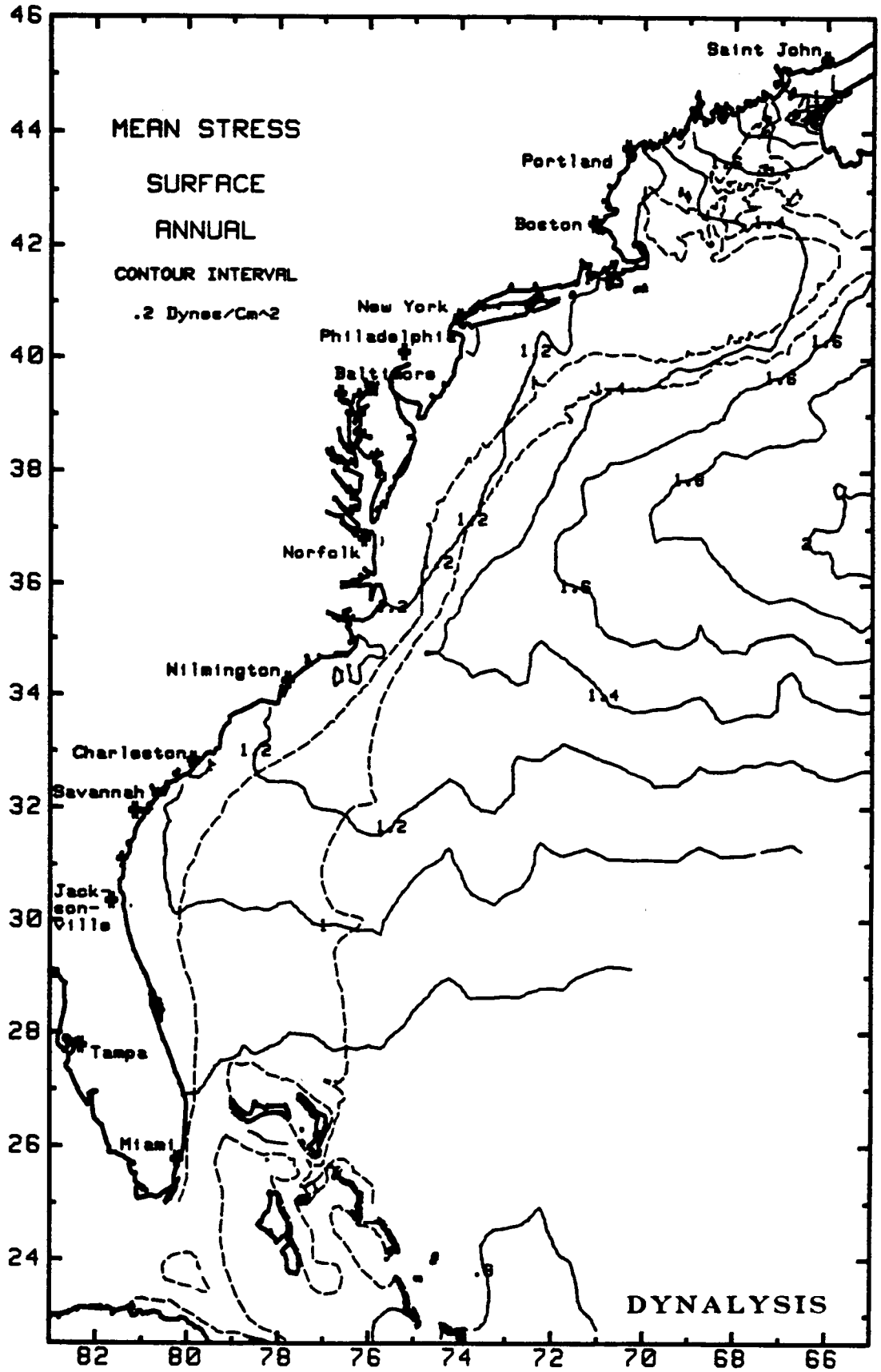

Figure 2.1.3 Annual average distributions of the climatological average stress magnitude for the Eastern Continental Shelf.

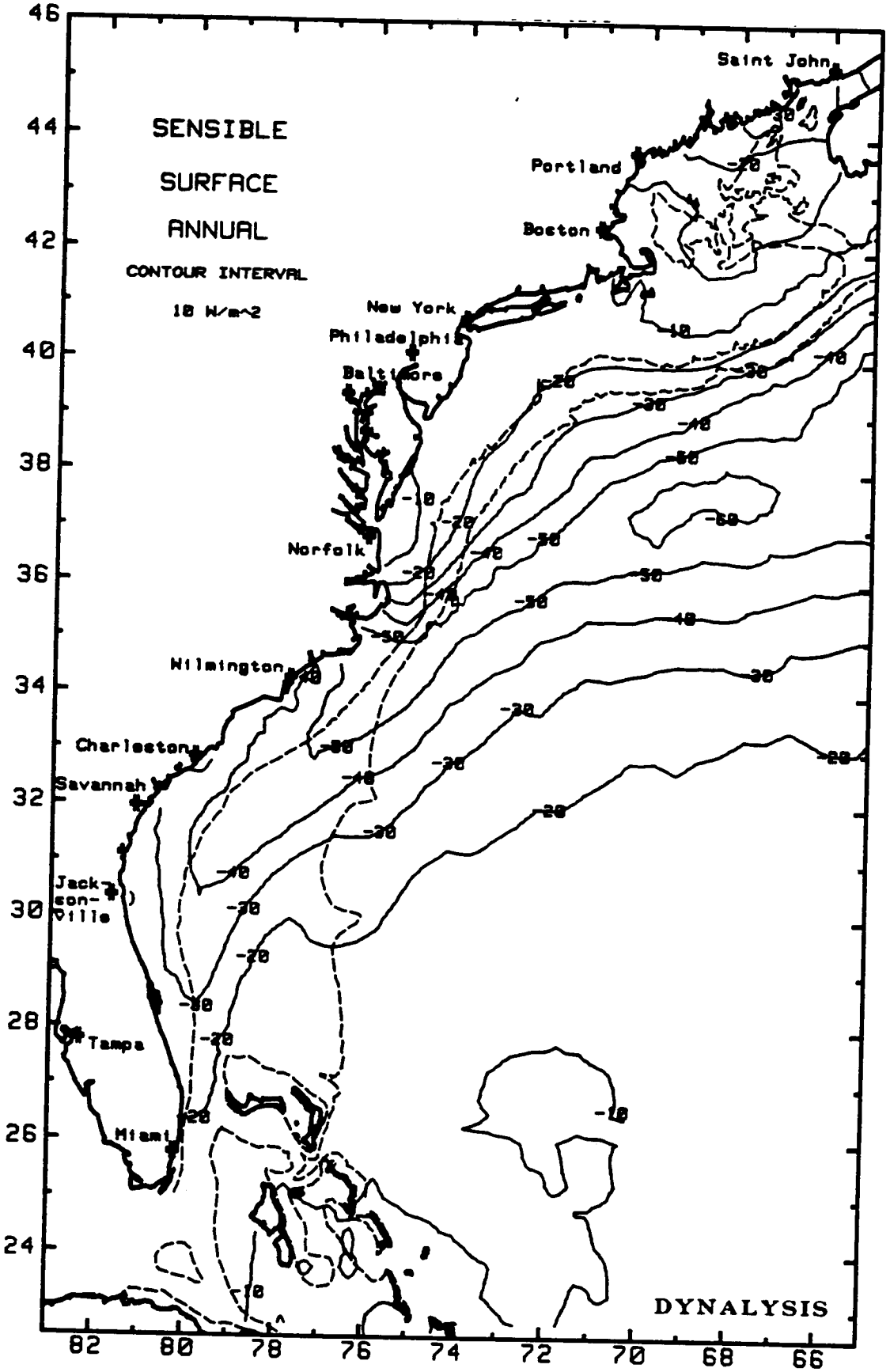

Figure 2.1.4 Annual average distribution of the sensible heat flux for the Eastern Continental Shelf.

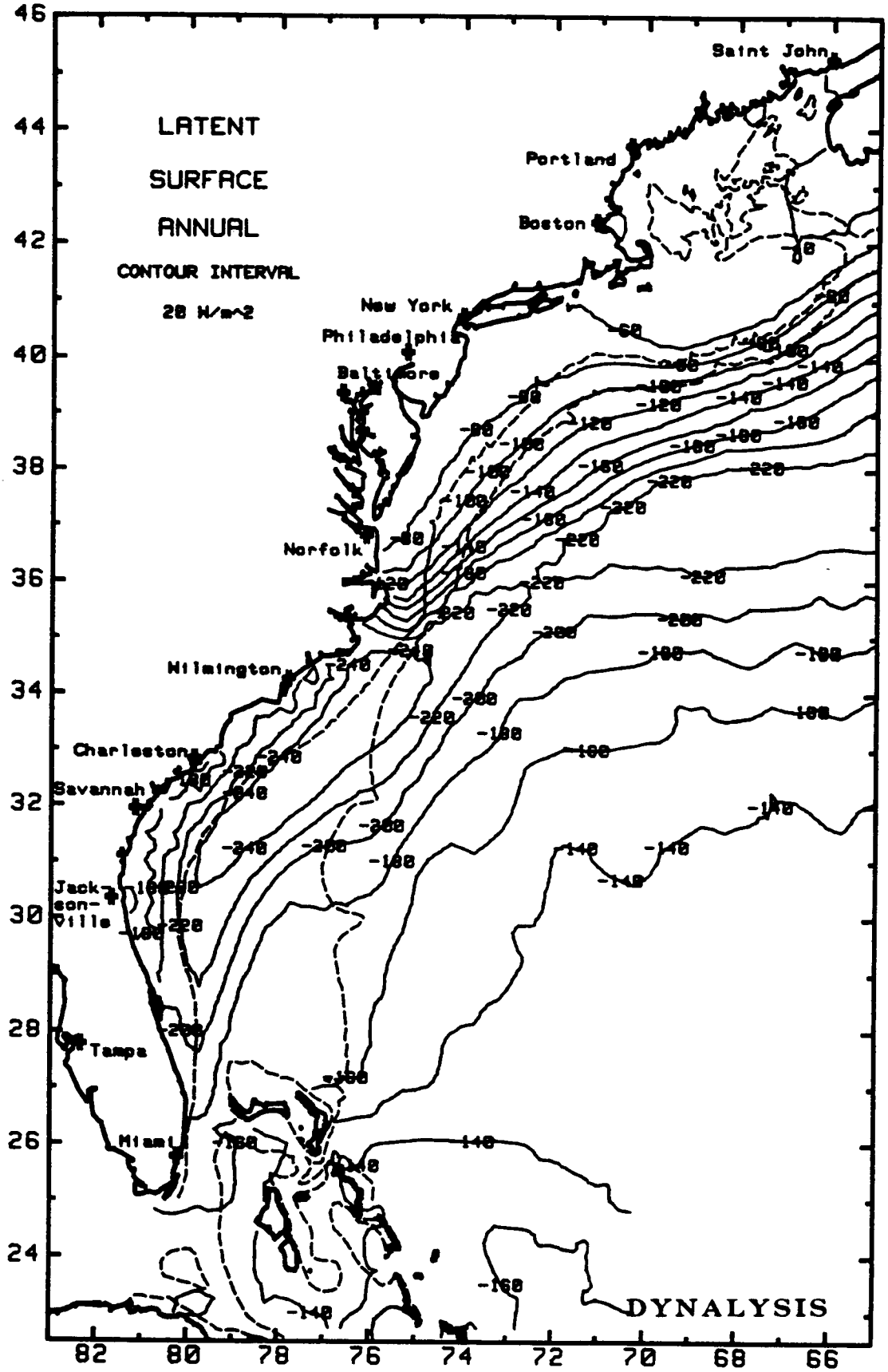

Figure 2.1.5 Annual average distribution of the latent heat flux for the Eastern Continental Shelf.

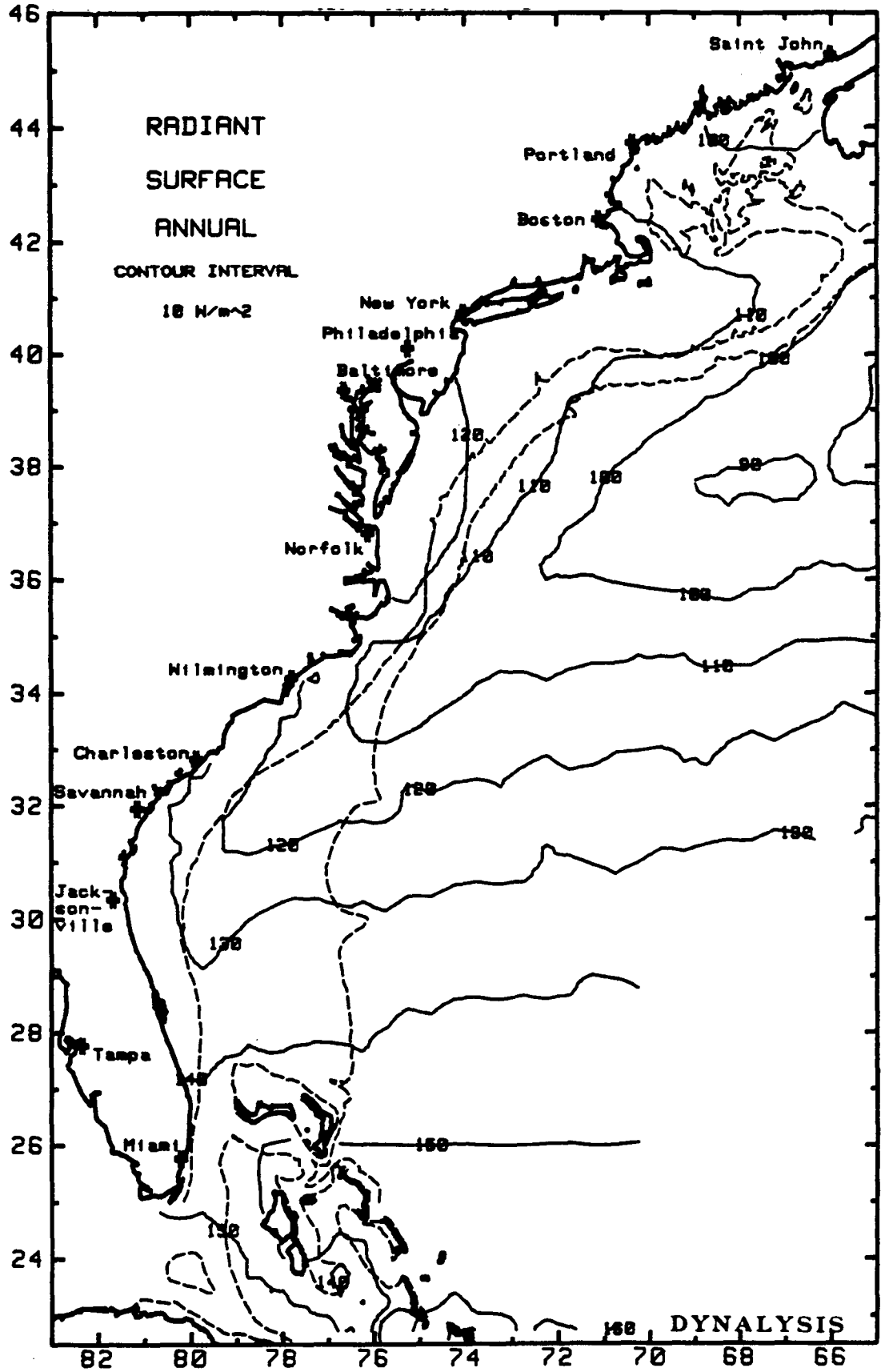

Figure 2.1.6 Annual average distributions of the net surface heat flux for the Eastern Continental Shelf.

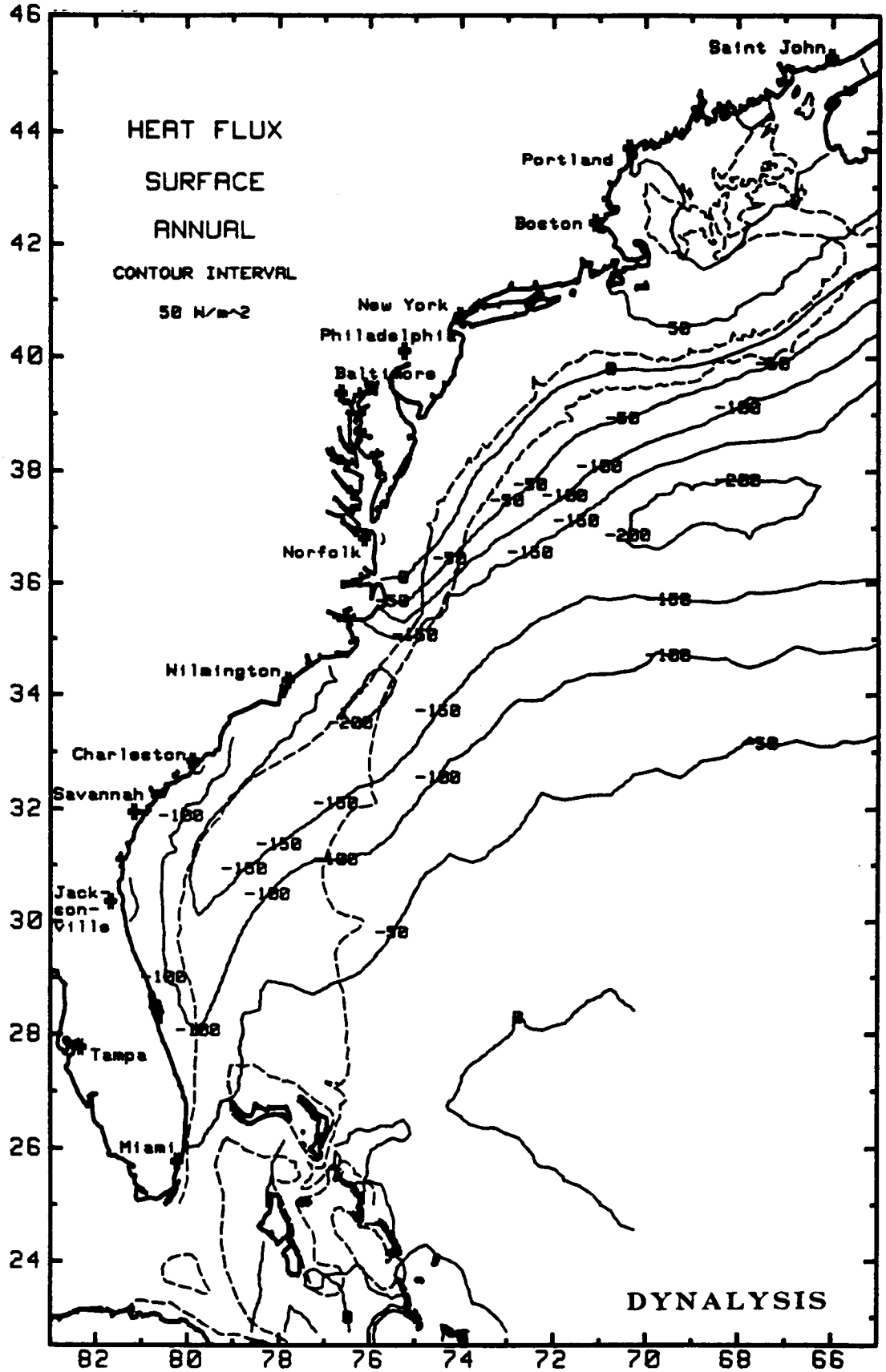

Figure 2.1.7 Annual average distributions of the net radiant heat flux for the Eastern Continental Shelf.

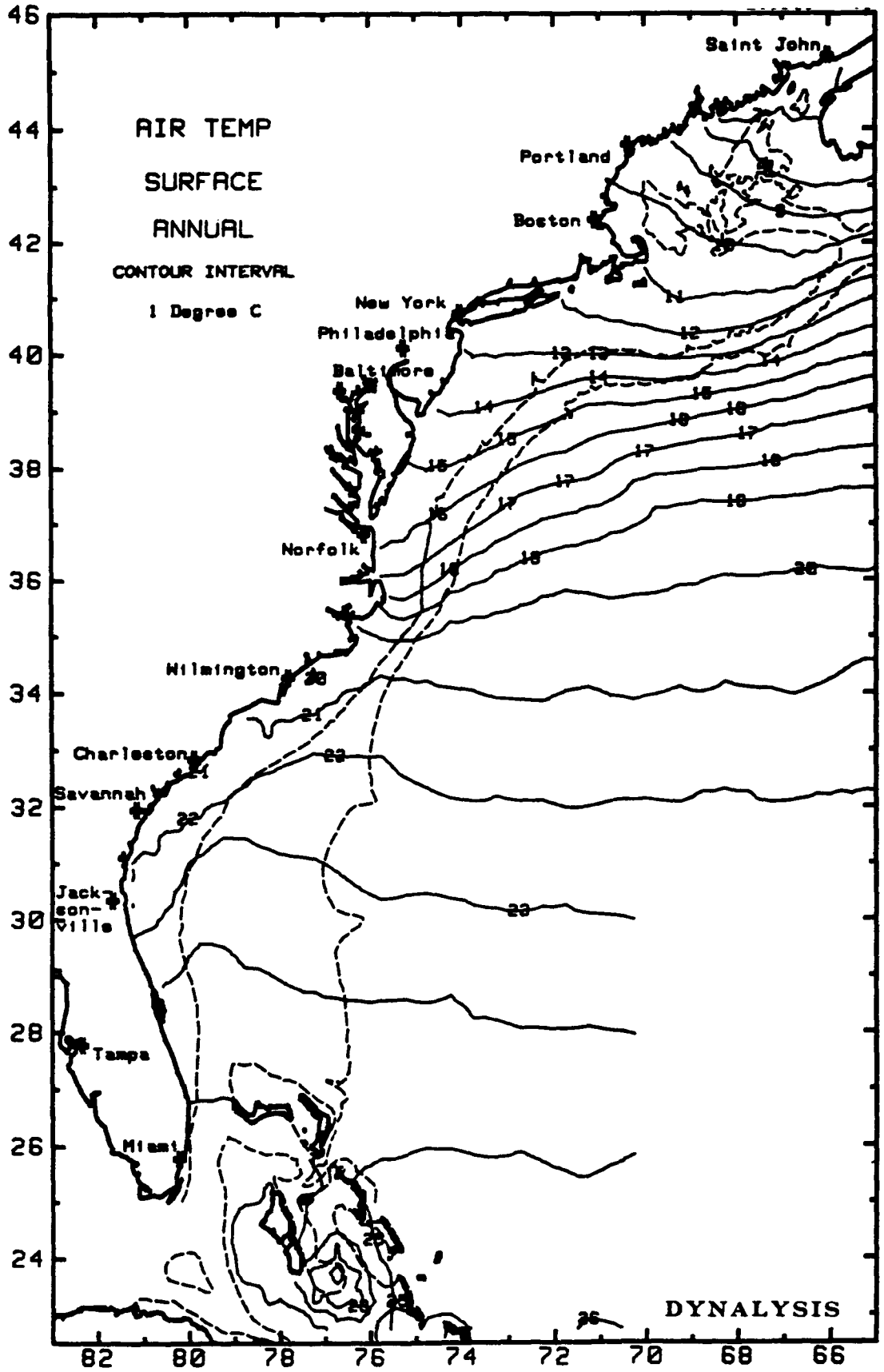

Figure 2.1.8 Annual average distributions of the sea surface temperature for the Eastern Continental Shelf.

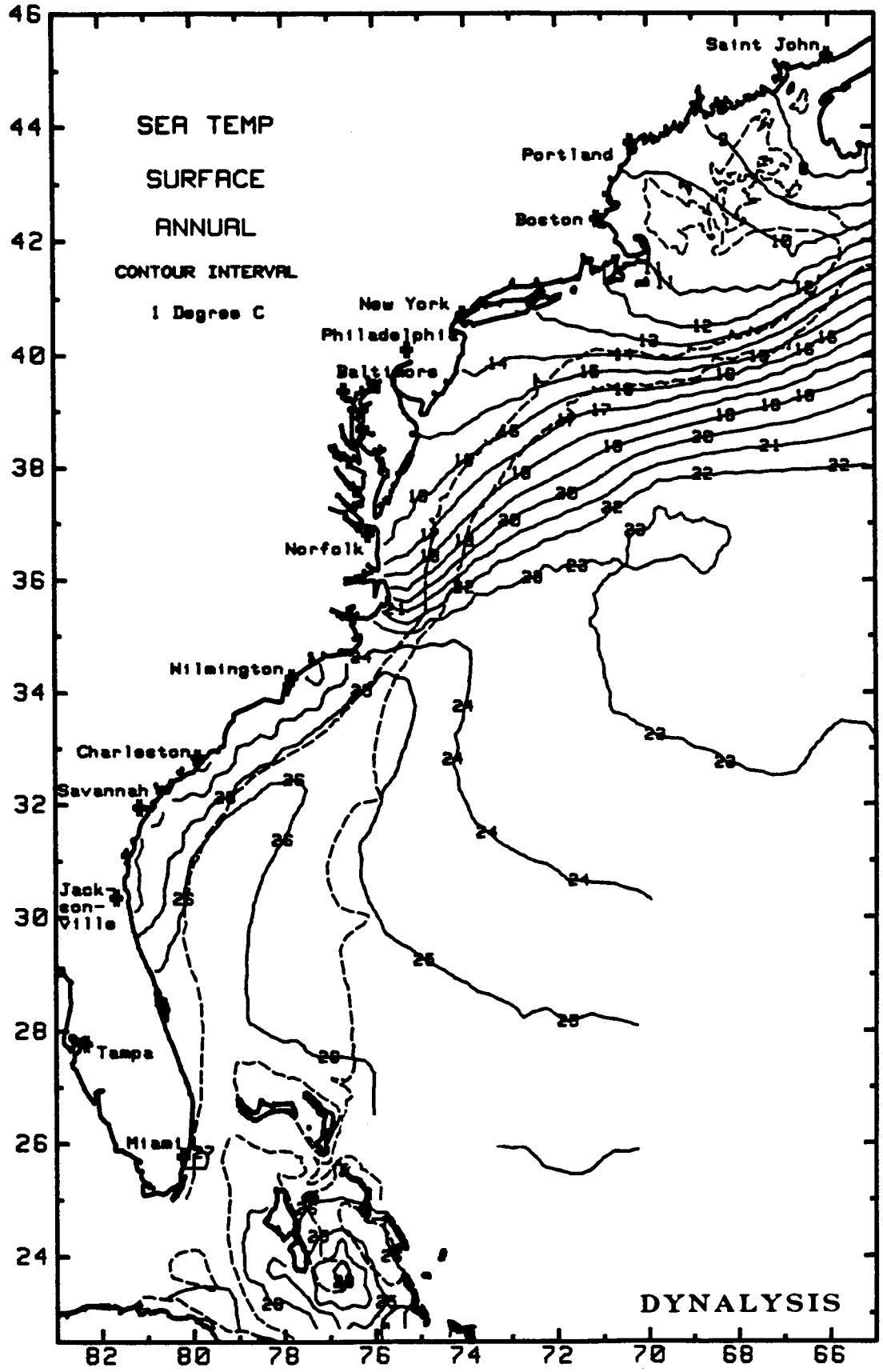

Figure 2.1.9 Annual average distributions of the air temperature for the Eastern Continental Shelf.

in Appendix A.1 is the coastal wind velocity distributions of Weber and Blanton [1980]. In this case, although a visual comparison of magnitudes is difficult due to the distinction between wind speed and stress, the correspondence between the distribution of wind directions is remarkable for all months. The mean stress contours in Figure 2.1.3 exhibit a strengthening in the northerly and offshore regions which is consistent with the behaviour of the vector stress.

The net heat flux distribution and its constituents in Figures 2.1.4 through 2.1.7 taken in conjunction with the air and sea-surface temperature fields provide insights into the heat balance of the region. As a result of the similarity in their transport mechanism, the distributions of latent and sensible heat flux have the same appearance. Of course the latent heat flux is nearly a factor of four greater due to the importance of the heat of vaporization. Both are enhanced and show the strong signature of the Gulf Stream where, as may be seen from comparison between air and sea temperatures in Figures 2.1.8 and 2.1.9 respectively, the air-sea temperature difference is the largest. In contrast they are noticeably reduced in response to the relatively cold water mass extending down the Northern and Mid-Atlantic Bights to Cape Hatteras which is evident in the sea-surface temperature.

Along the northern coast they are balanced by the net radiant heating. Inland of the shelf break there is a moderate radiant surplus and beyond, the convective process prevails. In the South Atlantic Bight, although the radiant heating increases with decreasing latitude, it is no match for the warm Gulf Stream water and the combined sensible and latent fluxes out are twice as large as radiant energy in. Of course the radiant flux is itself comprised of two components, the net insolation or short wave radiation from the sun minus the long wave, Stefan-Boltzmann,

radiation back from the water. The back radiation, which is also enhanced by the warm Gulf Stream water causes the contours of net radiation in Figure 2.1.6 to dip southward over the Gulf Stream.

The comparison of these heat transfer results with those presented by Bunker [1976] is satisfactory. Bunker's results are on a coarse grid and are illustrated with large contour intervals. The net heat flux appears very similar in distribution but has a 25 W/m^2 higher maximum over the Gulf Stream. Along the northern coast the comparison is within the accuracy of the plots. The sensible heat flux obtained by Bunker has a maximum offshore which, again, is 25 W/m^2 higher than the maximum found here, but the distributions in nearshore compare very closely.

Perhaps the most interesting data are the monthly distributions in Appendix A.1. Since each month is analyzed separately, the evolution of the numerous features is a reassuring conformation of at least the self consistency of the data set. Finally the distributions compare well with experience along the east coast including the findings of Weber and Blanton [1980], Saunders [1977], Bunker [1976] and Hastenrath and Lamb [1977 and 1978].

2.2 Hydrography

Climatological distributions of the oceanic properties such as temperature, salinity and σ_t have been obtained from historical hydrographic data. These data are then used as input to diagnostic models for deducing the currents in the water column and also for initializing the General Circulation Model. The process of data analysis consists of two phases, the acquisition phase and the reduction phase, which by themselves involve several steps as illustrated in Figure 2.2.1. The objective of the acquisition phase is to prepare, using data from various data sources, a single comprehensive data base which contain observations virtually free

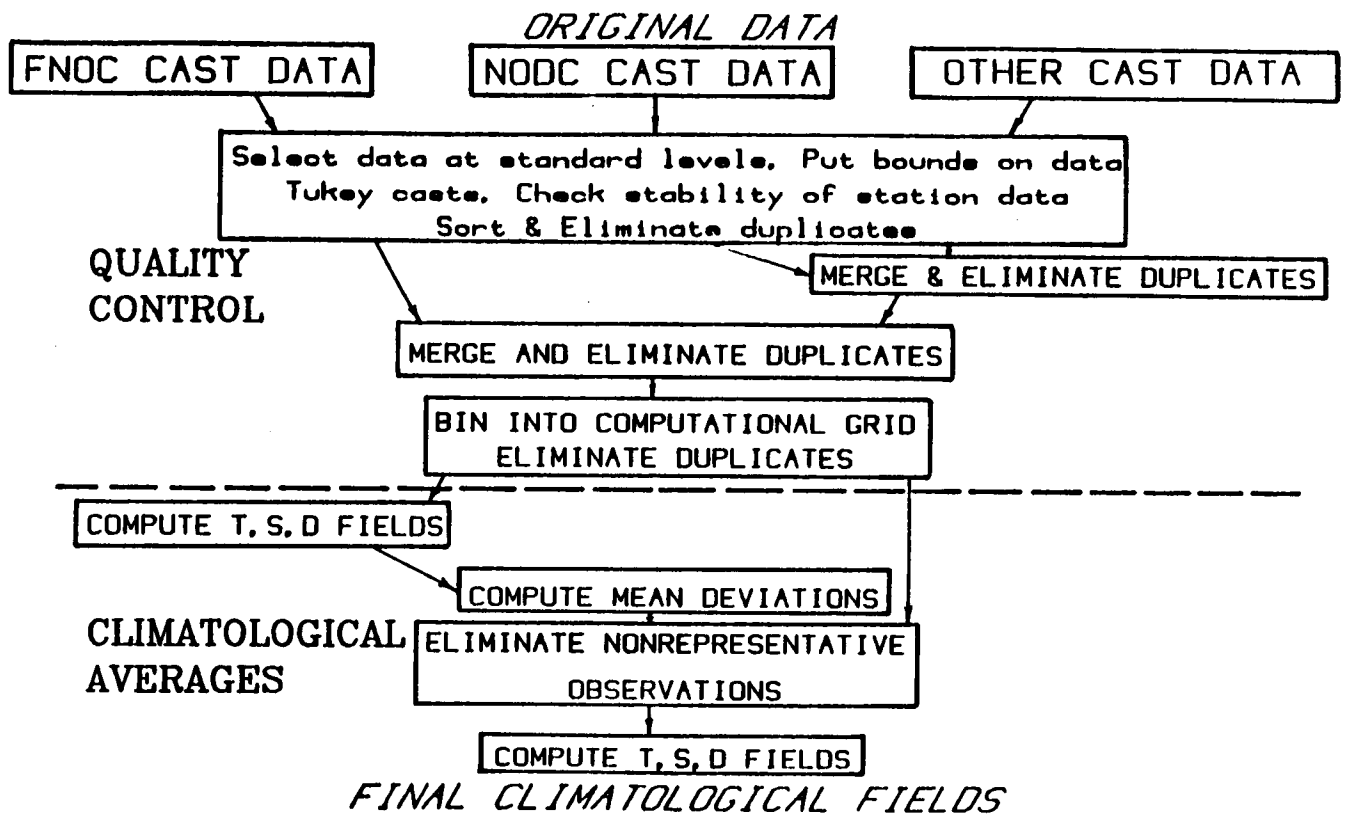

Figure 2.2.1 Hydrographic Data Reduction

from errors and duplication. The reduction phase consists of using this data base to obtain meaningful, representative climatological distributions of various properties in the ocean.

2.2.1 Acquisition

The major sources of historical oceanographic data for the coastal waters off the East Coast are the National Oceanographic Data Center (NODC) historical data archives and the Fleet Numerical Oceanography Center (FNOC) data files. In the South Atlantic Bight itself, data is available from other sources; observational programs such as the Georgia Bight Experiment (GABEX I & II) sponsored by the Department of Energy/MMS, cruises conducted by Skidaway Institute of Oceanography (from 1975 to 1979), mainly over the continental shelf off the Carolinas, and observational programs in the South Atlantic Bight sponsored by the Bureau of Land Management (BLM) and the Minerals Management Service (MMS/SAPOS program). Most of the data were not available from national archives and had to be gathered from original sources. Data sets from all these sources contain both temperature and salinity data, from expendable bathythermographs (XBT), mechanical bathythermographs (MBT) as well as hydrographic STD and Nansen casts. FNOC data is current to 1980 and include most but not all NODC data. NODC files contain many deep station casts. NODC data were acquired at the beginning of 1983 and are the most up-to-date set available. The station data are from '78A' file, the same as the data source used by Levitus [1982], whereas the XBT and MBT data are from '80 combined' file of more recent origin. Both NODC and FNOC data sets were acquired from the original sources, the latter as the result of the efforts of Mr. Sigurd E. Larson of the Pacific Outer Continental Shelf office of the Minerals Management Service.

The objective of the data acquisition phase of the effort is to assemble a comprehensive data base by merging the data from various sources after subjecting each observation to a systematic quality control procedure. Since archival procedures often cannot keep track of the duplicate nature of 'new' data that is incorporated into the archives, there can and often do exist multiple records of the same observation. In order to avoid biasing towards multiple records, it is essential to identify and eliminate all duplicates in the data base. Finally, it is necessary to identify and discard erroneous data in each record. All these steps are necessary to ensure that the climatological distribution of various properties such as temperature, salinity and σ_t derived from the historical data base are as accurate and error free as possible.

To identify and eliminate duplicates in a given data set, it is necessary to sort the records in the set in a logical order so that multiple records are adjacent to one another. Efficient sort and merge routines are therefore an indispensable part of the data acquisition phase. The procedure adopted is to sort all the records in a data set by position and time of observation and to check each record with two previous records in the sequence to see whether the position and time of observation are identical. If so, the data in the records are examined to check whether they are identical, to within a specified accuracy (if T, S and σ_t are all within ± 0.04 units, the record is regarded as a duplicate), to those of the two previous records. If the record satisfies these requirements, it is regarded as a duplicate and discarded. Otherwise it is retained and used to check the next record in the sequence. This procedure involving serial processing of all the records in the data set appears to be quite efficient in identification and elimination of a majority of the duplicate records. Occasionally, a duplicate record might

end up displaced by two or more records from its twin and would not be identified and discarded by this procedure but such occasions are few.

As mentioned earlier, FNOC archives include most data from NODC. However, the data obtained from NODC is more complete and the most recently updated. FNOC data on the other hand, contains Navy-originated records of ocean properties, mostly temperature observations reported routinely by Naval vessels, that are not part of the NODC data base. In addition, there are also small amounts of data from various other sources in the FNOC archives. So it was decided that the NODC and other data sets (these will be referred to as MMS/BLM/DOE/SKIDAWAY sets, MBDS for short) be merged with the FNOC set but only after all NODC data in the latter were identified and discarded.

For the purpose of determining the spatial distributions of oceanic properties and providing input to the various models, especially the diagnostic CTM, only data at selected levels in the vertical are of interest. These levels have been chosen to be the NODC standard depths. FNOC and MBDS data sets, on the other hand, contain data at observed depths only and it was therefore necessary to interpolate the data to standard depths. Also, the FNOC data set is in a packed format with the data compressed to save storage space. An unpacking routine supplied by Mr. Craig Nelson of the National Marine Fisheries Service (National Oceanic and Atmospheric Administration), with some modifications to the driver program, was used to extract data, other than NODC-originated, from the FNOC data set.

Data obtained from NODC for the northern domain consisted of a total of about 233,000 casts in the region to the west of 65°W longitude and to the north of 26.5°N latitude. Out of these, 29,850 were station casts (both temperature & salinity observations) or roughly 13.4%, and 72,280 were XBTs and 120,870 were MBTs (only temperature observations) or roughly

86.6%. FNOC data in the domain, after the exclusion of NODC data consisted of a total of 107,300 casts, mostly temperature observations. MBDS data consisted of about 3,100 casts, both XBT and station casts. For the southern domain extending from 22.75°N to 26.75°N and 81.75°W to 70.75°W, NODC data consisted of about 25000 casts, with about 7615 XBT, 14075 MBT and 3310 station casts. FNOC data in the domain consisted of about 14650 casts, mostly temperature observations. Thus a total of about 335,000 casts are available in the northern domain and 39650 casts in the southern domain.

The data acquisition procedure employed in processing these data sets was as follows: from each data set, only data at selected levels within the domain of interest were extracted, gross bounds were imposed so as to eliminate erroneous data and each cast was rewritten with a standard header format to facilitate merging and sorting of data from different sources. The same precision was retained in header and data information in all data sets to facilitate elimination of duplicates.

All data from a given source, such as for example NODC, were merged together, sorted and subjected to a duplicate elimination process. The FNOC data set contains MBT and station casts in no particular order and is presorted by months. The various processing tasks could all be done in a single step: selecting data in the domain, rejecting data not within the data bounds, extracting standard level data and eliminating duplicate records. The data from various sources were then merged together and again sorted and stripped of duplicates. All data were of course decimated to standard levels before subjecting them to this process. Each time data from a new source (or more data from the same source) are merged into the data base, the records are sorted and stripped of duplicates. This repetitive procedure is essential for eliminating data biases.

The resulting data base was subjected to further quality control by subjecting each cast to a one-dimensional three-point Tukey filter. This filter chooses the median of the data and the adjacent data values, and is a non-linear filter with very useful properties: it removes only sharp spikes in the record but leaves the rest of the record virtually unchanged including more gradual changes. It has been used in speech processing with excellent results [Rabiner, Sambur and Schmidt, 1975]. Subjecting each cast to a Tukey filter eliminates erroneous data points in that cast. Station casts consisting of a T, S, and σ_t information at various levels were also subjected to a gross 'stability' check. If σ_t at any level was less than that immediately above by more than +0.01, the entire T, S, and σ_t data for that level were discarded. The resulting data base consisted of a total of 331,130 casts for the northern domain and 39616 for the southern domain with less than 10% of simultaneous T and S observations.

Finally, the data set was readied for the data reduction phase by binning the casts onto the computational grid (i.e., grouping the casts in each grid box together, irrespective of the hour of observation), and subjecting the reordered set to another duplication elimination procedure with a more stringent definition of duplicate of data. The latter step assumes that in any particular grid box, if the day of observation and the data in two casts were identical, then one of the records should be treated as a duplicate even if the longitude and latitude are not exactly identical. This assumption is of course valid only for small enough grid sizes. In this case, ¼° grid size used was deemed small enough to undertake this additional step. This step resulted in discarding of an additional 3,242 records in the northern and 432 in the southern domain so that the final data base comprised of 327,888 casts for the northern domain and 39184 records in the southern. The duplicates remaining in this are few if any. It should also be remarked that the process of

deducing the distributions of various properties from these data during the data reduction phase is relatively insensitive to a few remaining duplicates.

It should be pointed out that despite the apparently large amount of historical data, the data coverage in this region of the coastal ocean is sparse, especially as far as salinity is concerned. Although FNOC Navy-originated data is roughly 30% of the data base, its impact is considerably less. Almost all Navy data are observations of temperature only, many just at the surface. Thus although it is of great help in deducing temperature distributions in the ocean, it makes very little contribution in deducing the density structure which is the basis of the diagnostic CTM calculations. Finally, the majority of the casts in the entire data base are shallow casts. Only NODC and MBDS data contain some deep casts that go beyond 1000 m. In any case, less than 10% of the total, roughly 30,000 casts are T,S observations for the northern domain and 3000 for the southern domain.

2.2.2 Reduction

Historical data, by its very nature, is not the optimum climatological data set. It contains sampling biases in both time and space. Certain regions, such as around Woods Hole Oceanographic Institution tend to be well-sampled whereas others, such as the deep ocean regions, are comparatively under-sampled. The regions closer to the shore are better-sampled than those far off-shore. Shipping routes are better sampled than most other regions. In addition to this spatial bias, sampling also tends to be biased towards fair weather seasons. In any case, historical data represents imperfectly sampled climatology. The use of objective analysis schemes to derive long-term climatological averages from historical data is, therefore, unavoidable and care must be exercised to obtain represen-

tative results. It is the objective of the data reduction phase to obtain long term (for example, seasonal) averages of ocean properties such as temperature, salinity, and σ_t from the quality-controlled data set obtained during the data acquisition phase; hopefully, they are a good estimate of the true climatological average.

Objective analysis schemes are an invaluable tool in many areas, such as weather prediction, which involve derivation of distributions of a property over the domain of interests from data, observed or otherwise, at isolated points. The most frequently used objective analysis scheme is of the iterative difference-correction type developed by Cressman [Cressman, 1959; see also Levitus, 1982]. Here the domain of interest is overlaid by a grid, an initial value is guessed at each grid point and the final value is arrived at, taking into account the influence of all observed data points within a radius of influence of the grid point in an iterative manner. The objective analysis scheme used in this report is not that of Cressman but one that is more versatile. The scheme was developed by H. James Herring and for a brief description of the scheme and comparison with the Cressman scheme, the reader is referred to Appendix A of Blumberg et al. [1983]. It takes into account the reliability of the data point in terms of the relative abundance of observations at the point. The degree of smoothness of the field and conversely the ability of the field to lock onto the data values can be prescribed a priori.

Simple straightforward application of an objective analysis scheme to a data set is not enough to obtain climatologically representative distributions. As an illustration of an extreme case, assume that an annual (overall average) temperature distribution at the sea surface is needed. Inevitably at some grid points, the data is biased toward one season or other. For example, at one grid point all data might have been taken in winter. There is nothing wrong with this data, but when it is

used to derive the annual averages of temperature, the resulting field is pulled at this point toward the winter value whereas a few grid points away, it might be towards a summer value. The outcome is a highly noisy temperature field, not because the data itself is inaccurate but simply because it is 'nonrepresentative' of the climatology desired. No amount of smoothing will remove the problem entirely. What is needed is a means of identifying and discarding such 'nonrepresentative' data points that constitute a part of the data set at the grid point in question.

The strategy used is as follows: using the data set comprised of individual casts obtained from the acquisition phase, at a given level, all data that fall, within the grid box under question and within the season being considered, are averaged to provide the climatological mean desired at the grid point. This mean and the number of observations that went into deriving it are used as input into the Herring objective analysis scheme to derive the first guess climatological mean field over the entire domain. This field will contain biases of the type mentioned earlier. In order to eliminate 'nonrepresentative' observations at a given grid point, one needs a measure of the representativeness of the data set as a whole. Using the original data set comprised of individual observations, the mean standard deviation of all observed data from the climatological mean field is calculated according to;

$$s = \left[\sum_{I,J} \sum_{N} (O_{ijn} - M_{ij})^2 / N_t \right] \tag{2.6}$$

where I, J are the number of grid points in each direction; N is the number of observations; and O and M the observed data value and the climatological mean value at point (i,j); N_t is the total number of observations at all grid points for that 'season'; s is a measure of the

"representativeness" of the observations in producing a climatologically meaningful field. Then going back to the original data set, all observations not within 1.5s of the first guess field are discarded and the reduced set is used to derive the final climatological mean field desired.

The procedure has been found to yield acceptable climatological distributions. The extent of discarded data depends entirely on the variability in the data set. Near the surface where large variability exists, especially in temperature observations, relatively larger number of observations are discarded as nonrepresentative while in the deep ocean, and where variability is small, very few are. In most cases not more than 10-25% of the observations are discarded. Below 1000 m, almost none are. Naturally a less stringent criterion for identifying 'nonrepresentative' data would result in fewer number of discarded data but 1.5s appears to be a reasonable compromise between the percentage of discarded data and representativeness of the resulting field.

2.2.3 Climatological Distributions

Data processing techniques described above have been applied to derive the mean T,S and σ_t distributions at various levels for each of the four oceanic seasons, the seasons defined conventionally:

Winter -- January to March

Spring -- April to June

Summer -- July to September

Fall -- October to December

In addition overall annual averages, averages of the entire data set, have also been derived. The grid resolution is ¼° x ¼° in the longitudinal and latitudinal directions and the domain of interest is shown in Figure 2.1. It should be noted that during Phase II of the South Atlantic Bight modelling effort, hydrographic data was binned on 1° x 1° grid and inter-

polated to ¼° x ¼° grid by objective analysis. Binning directly in ¼° grid boxes enables a better determination of the horizontal gradients and hence a better definition of baroclinicity in the region. In this section, we will present only a few annual climatological distributions. The complete seasonal and annual distributions can be found in Appendix A.2.

The extent of smoothing to be employed in deriving spatial climatological distributions of water mass properties from noisy, statistically imperfect historical archives, necessarily requires compromises. For example, the selection of grid resolution that plays a role in this, is not as trivial as it may appear. The finest grid is not necessarily the best. The reason is related to the available data density. Too fine a grid would imply correspondingly fewer data in each grid, which might mean that such an ensemble might be a poor representative of the desired climatology on the desired time scale. Too coarse a grid would sacrifice spatial resolution for better representation of the desired climatological average. Thus the grid resolution to be selected is dictated by an optimum compromise between spatial and temporal resolution. One is reminded of a loose analogy to the Heisenberg uncertainty principle in quantum mechanics. A simultaneously fine spatial and temporal resolution is difficult and the degree of this difficulty depends on the available data coverage and hence is a function of the region(s) under study.

Similarly the amount of smoothing to be employed is a compromise. Too much suppresses the small scales of importance particularly on the Shelf. Too little leads to "noisy" fields that do not represent the average well. The smoothing chosen in this study, while admittedly large in some regions, is certainly inadequate in many others. The perceived "leakage" from the Gulf Stream off Cape Hatteras to the Shelf regions is

unfortunate, but given the difficulties alluded to above, is unavoidable though undesirable.

When dealing with an historical data base, especially an hydrographic data base, it is essential to understand the sample size and data variability as well as their distribution in both space and time. One hopes that the sample size in each space and time interval chosen is adequate to derive meaningful averages over those intervals, but in hydrography, this hope is not always fulfilled. Since there is no recourse but to use whatever is available to derive the averages sought, it is essential that the distributions of the mean fields so derived be accompanied by indications of the sample size as well as the data variability. Number of observations in each three-dimensional grid box, for the period considered, provides the former, whereas the distributions of standard deviations of the property provide the latter. Unfortunately the sheer magnitude of the data analysis procedure prevented archiving of the standard deviation fields but the sample sizes are available and will be presented next.

Figures 2.2.2 to 2.2.5 present the distributions of the overall number of observations available in the data base (before the data reduction process) of temperature and salinity at 0 and 1000m depths in the ECS waters. As far as is possible to ascertain, these represent all data that is already available to-date. Asterisks denote observations larger than 999 per $\frac{3}{4}°$ square. The great disparity in sampling of the temperature and salinity is immediately obvious. As far as temperature is concerned, the nearshore regions of the ECS appear to be sampled well. The regions of the Middle Atlantic Bight (MAB) and Gulf of Maine (GOM) are better sampled than the South Atlantic Bight (SAB). The Gulf Stream is well-sampled presumably because it is the route that northbound mariners prefer. The extent of salinity observations are considerably smaller

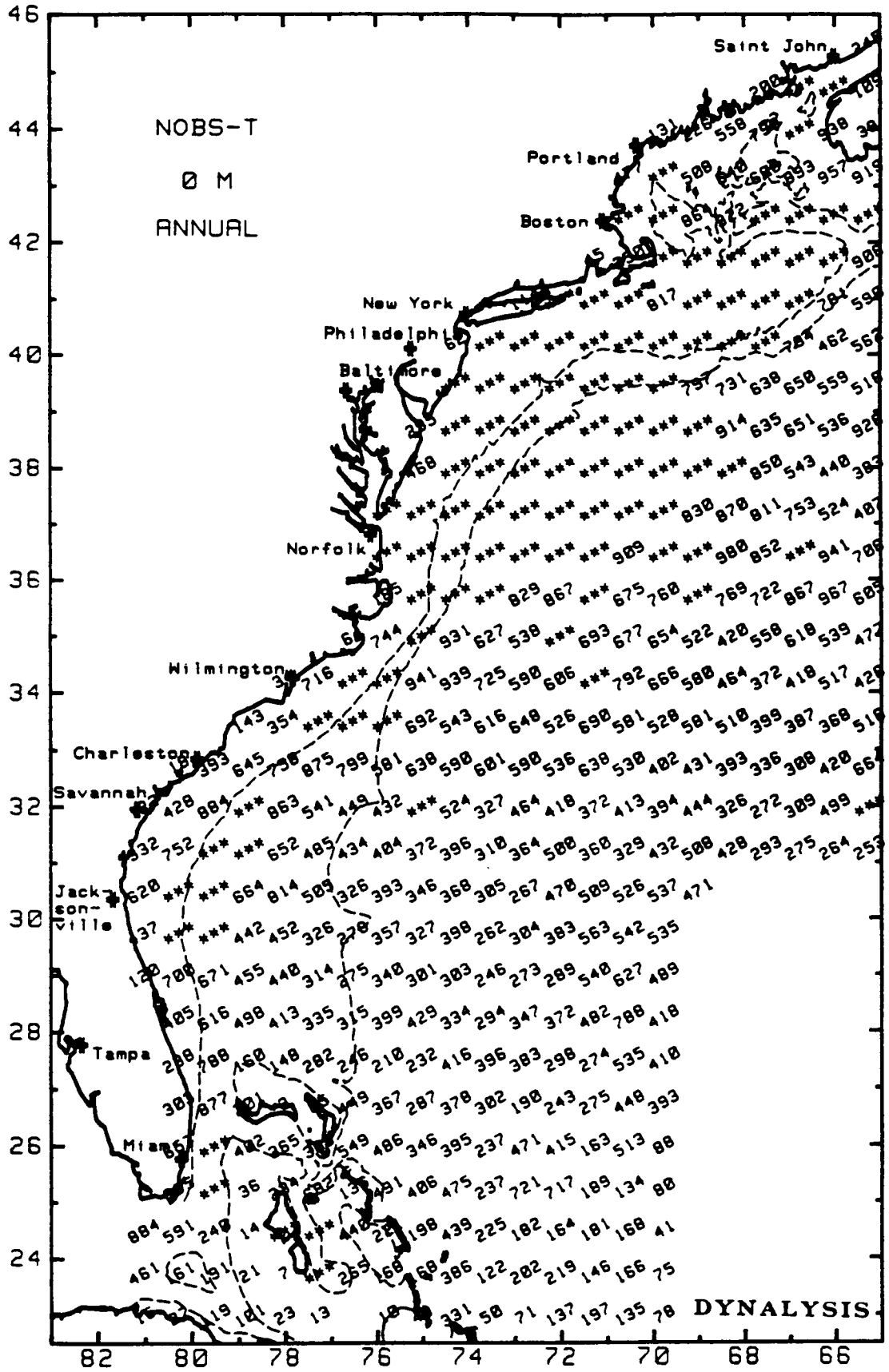

Figure 2.2.2 Total number of observations of temperature at 0 m depth before editing.

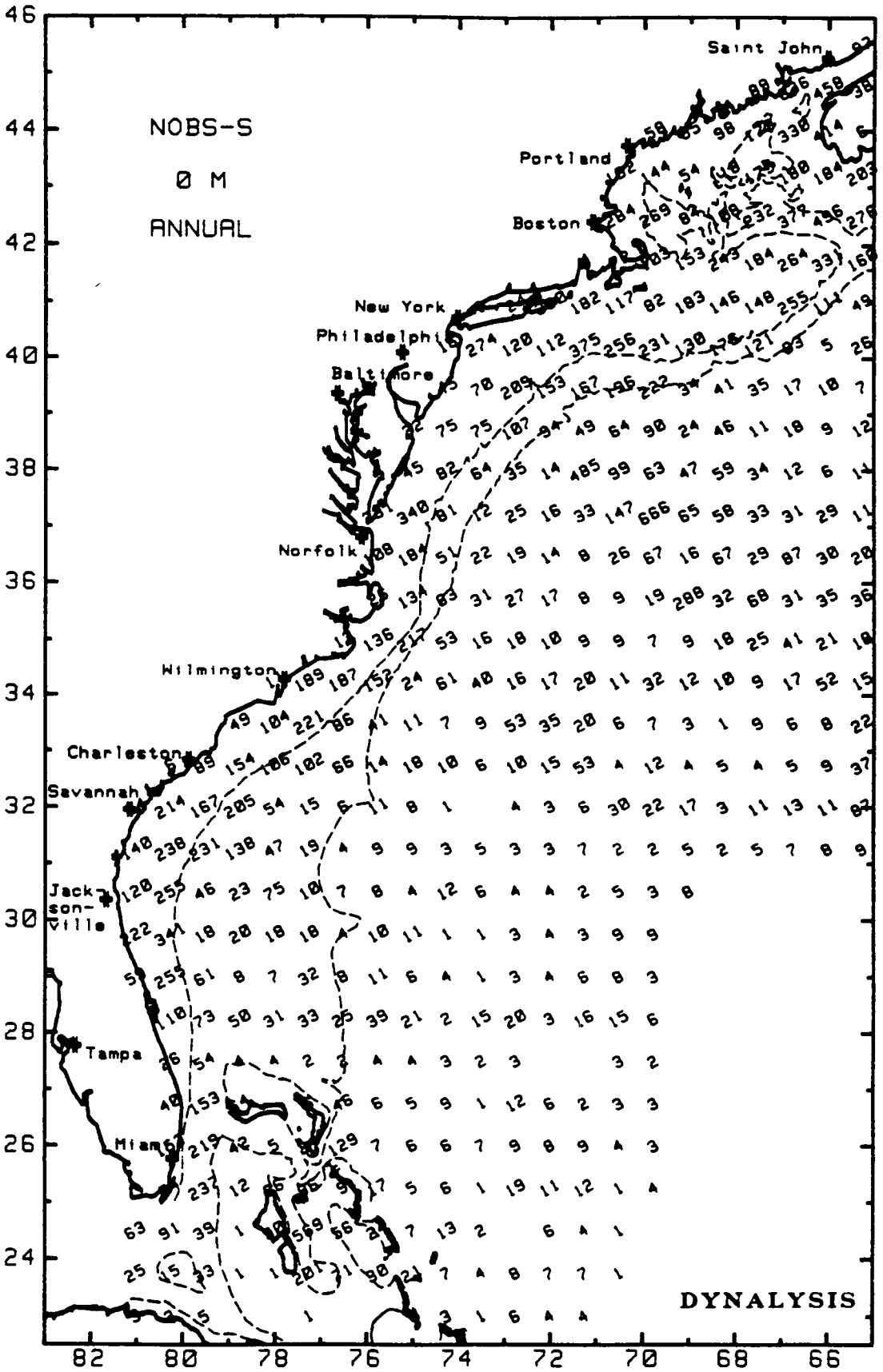

Figure 2.2.3 Total number of observations of salinity at 0 m depth before editing.

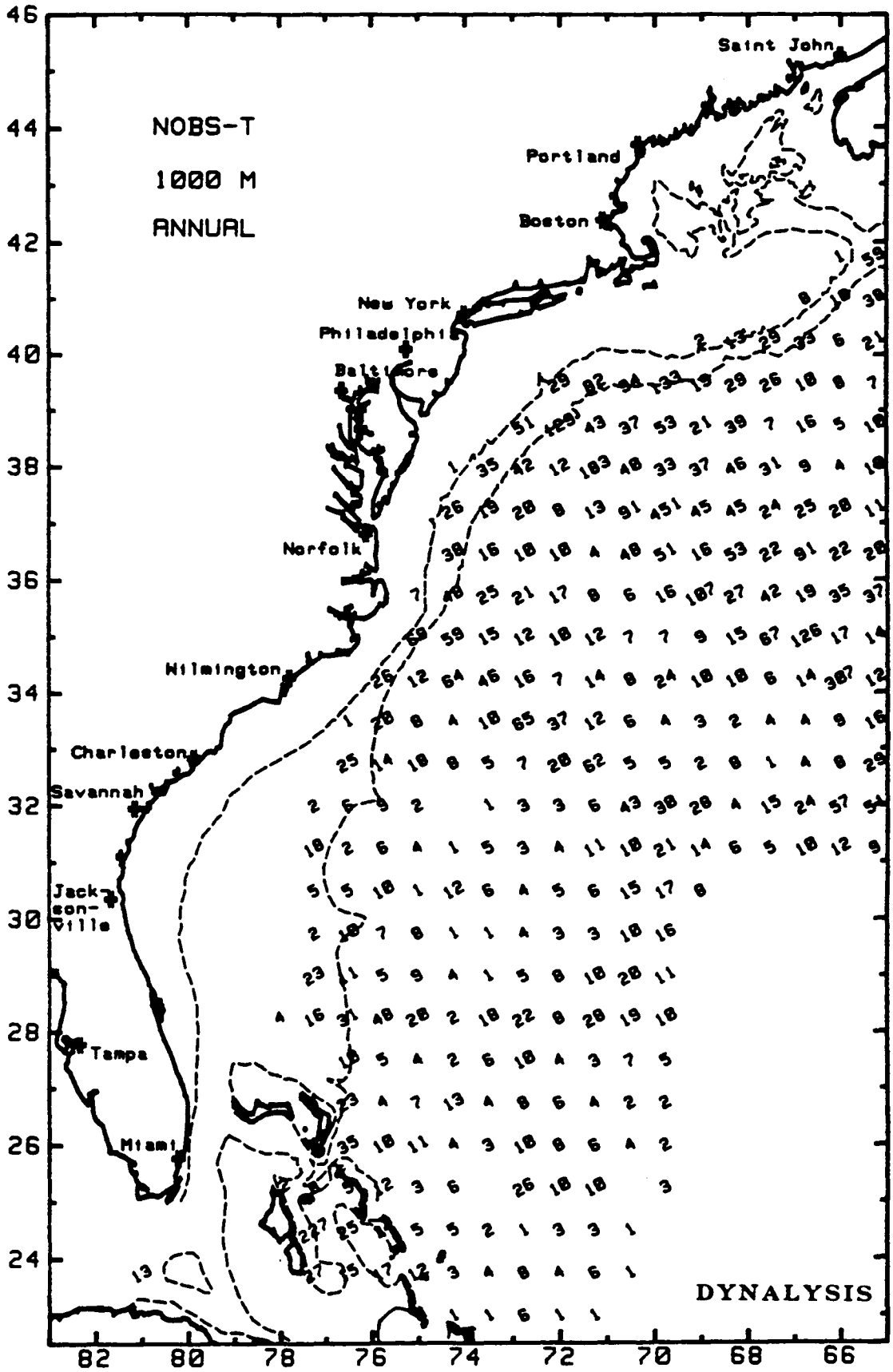

Figure 2.2.4 Total number of observations of temperature at 1000 m depth before editing.

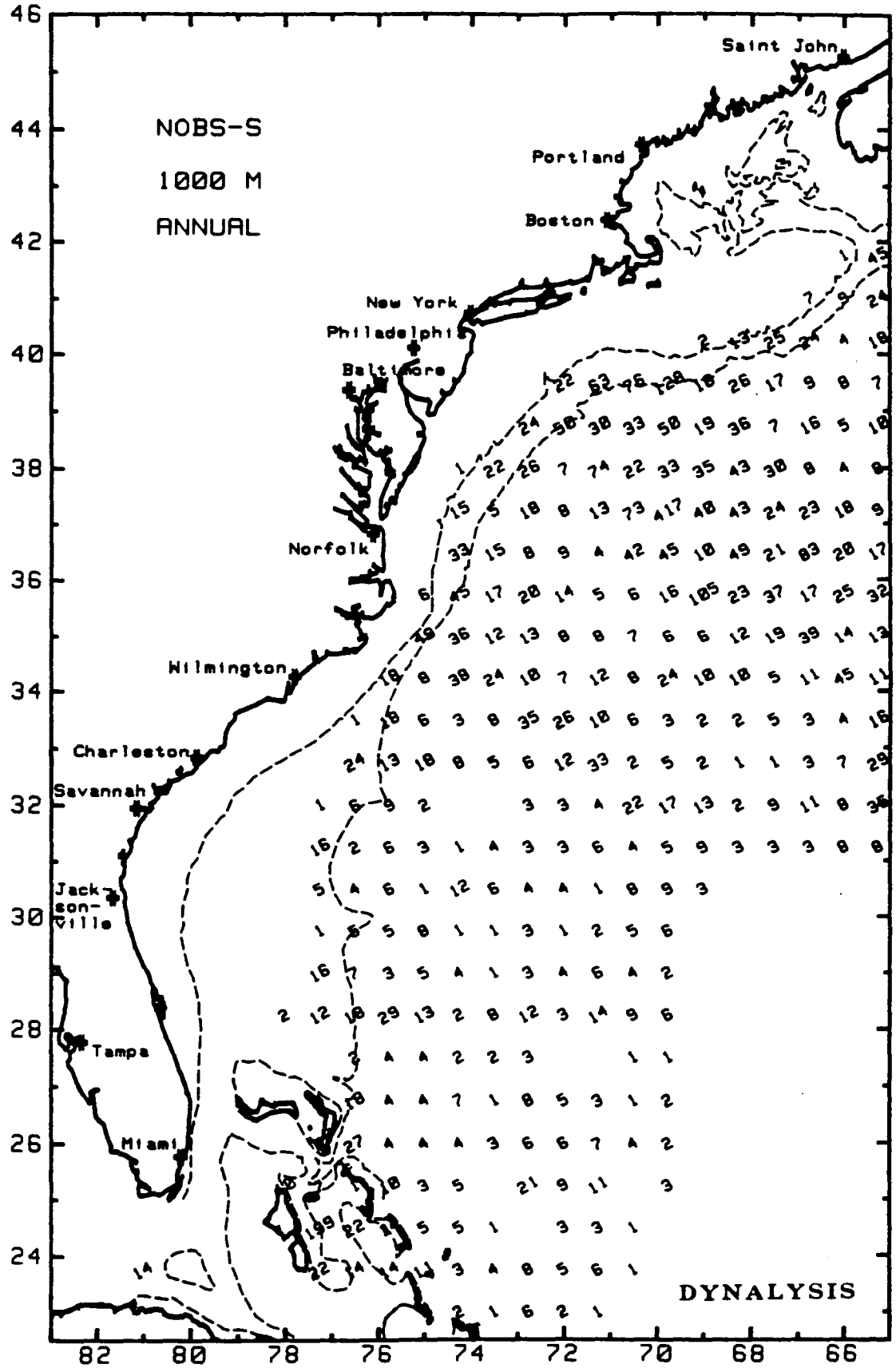

Figure 2.2.5 Total number of observations of salinity at 1000 m depth before editing.

even over the regions of the MAB that have been the objects of intensive oceanographic scrutiny. In the SAB, there are obvious holes beyond the Blake Plateau. But for the MMS sponsored cruises, the coverage would have been even more sparse.

The number of observations of temperature decreases rapidly with depth, mainly because most voluminous temperature observations are either from shallow XBT casts or just surface temperature measurements. FNOC data set contains quite a few of the latter. Formerly MBTs were the backbone of temperature measurements and MBT casts were, in a substantial number of observations, deep casts, but these are seldom used in recent times. Instead, the XBTs have become the main observational means, and most often, deep XBT casts are not made. In any case, the sampling in terms of temperature shows a large drop below 250m or so and again below about 1000m.

Observations of salinity, on the other hand, are done with STD and CTD meters and deep CTD casts are not unusual. But the ship time and expense involved in making CTD casts implies lesser coverage of the ocean by these instruments in general and most of these observations are by research vessels rather than merchant ships. Naturally the number of joint T and S observations is much smaller than that of T observations alone in any space or time interval.

Since most often, the observations in deep water below 1000m are with CTDs, the number of observations of temperature and salinity are roughly similar in depths below 1000m. Also, since for diagnostic modelling it is the joint T and S observations that are important, the number of observations of salinity provides a good indication of the extent of the data base relied upon.

Clearly the observational coverage is sparser in the SAB than in the northern regions in general and in the deeper waters than nearsurface

waters everywhere. Surprisingly the data shows no great disparity in coverage for different seasons at least as far as nearshore and near-surface observations are concerned. However, a matter of concern is that the number of measurements in waters below 1000m is exceedingly small on a seasonal basis so that the derivation of meaningful seasonal distributions of temperature and salinity is nearly impossible. The best recourse is therefore to use the entire data set in deep waters to derive annual distributions and use these as input to the diagnostic model. This procedure is justifiable to some extent because of the lesser "seasonal" variability of the deep ocean. However, the sample size is, more often than not, too small to prevent data biases. These biases would definitely impact the model results because the model uses the entire water column to arrive at the overall circulation. It is these data biases that lead to spurious eddy-like features in oceanic regions with depths exceeding 1000-2000m. The reader should keep this in mind when interpreting the model results.

Figures 2.2.6 to 2.2.14 present the overall (annual) averages of temperature, salinity and σ_t at 0m, 500m and 3000m levels. The northern regions of the ECS can be clearly seen to exhibit larger gradients of T and S than the SAB. For example, the temperature at the surface in the SAB is 20-26°C, whereas even on an annual basis, the temperatures in the MAB and GOM vary from 6°-23°C. The contrast is even larger during winter (see Appendix A). The temperature contours in the southern portion of the MAB and northern portion of the SAB, reflect the presence of the Gulf Stream up to depths of about 1000m. For example, strong temperature fronts are readily discernible in distributions at 100m and 500m depths. Salinities at the surface and nearshore exhibit the influence of estuarine and river water (see Figure 2.2.9), for example at the mouths of Chesapeake Bay, Savannah River and Long Island Sound. The MAB exhibits

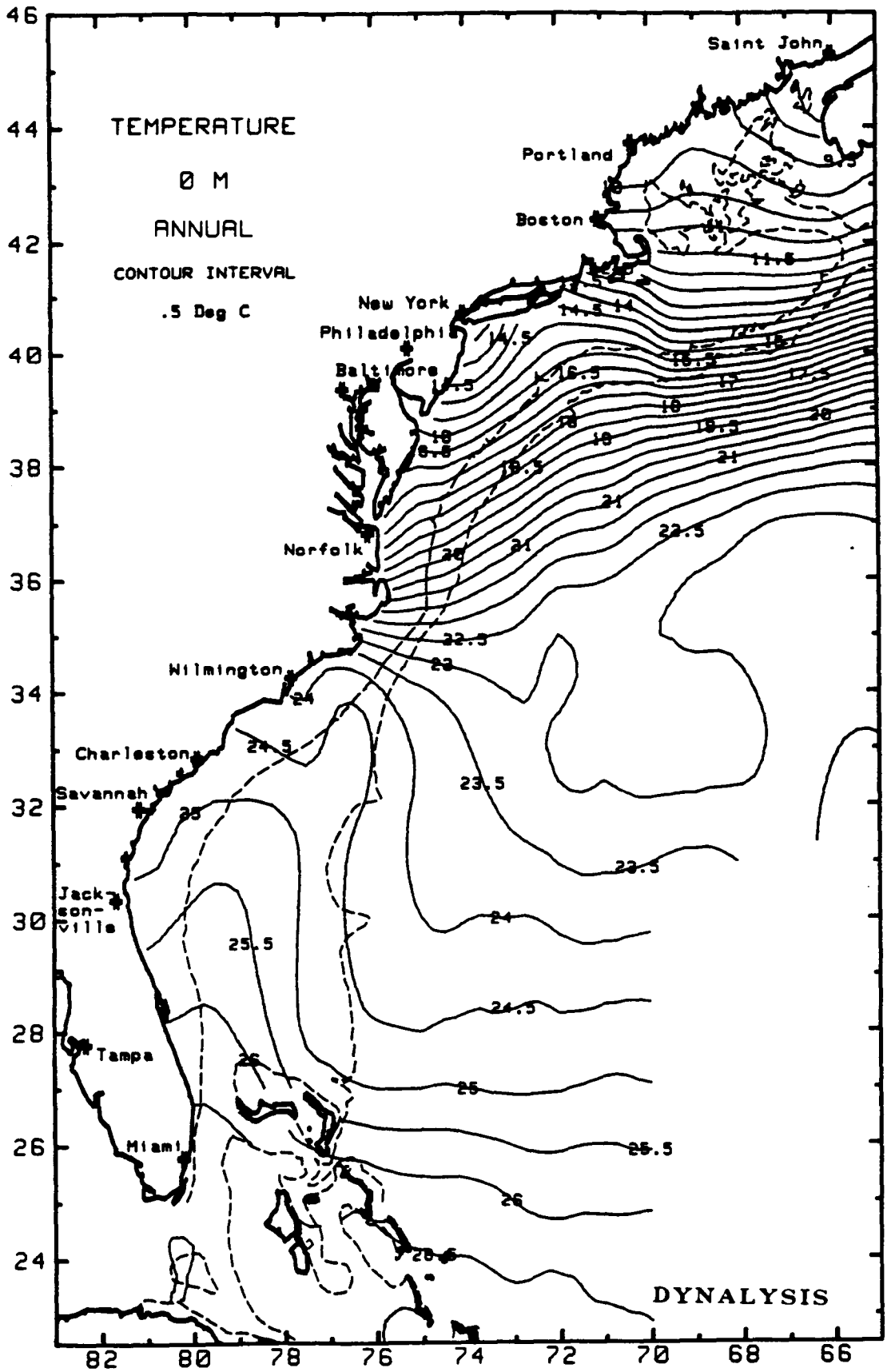

Figure 2.2.6 Annual temperature distribution at 0 m depth.

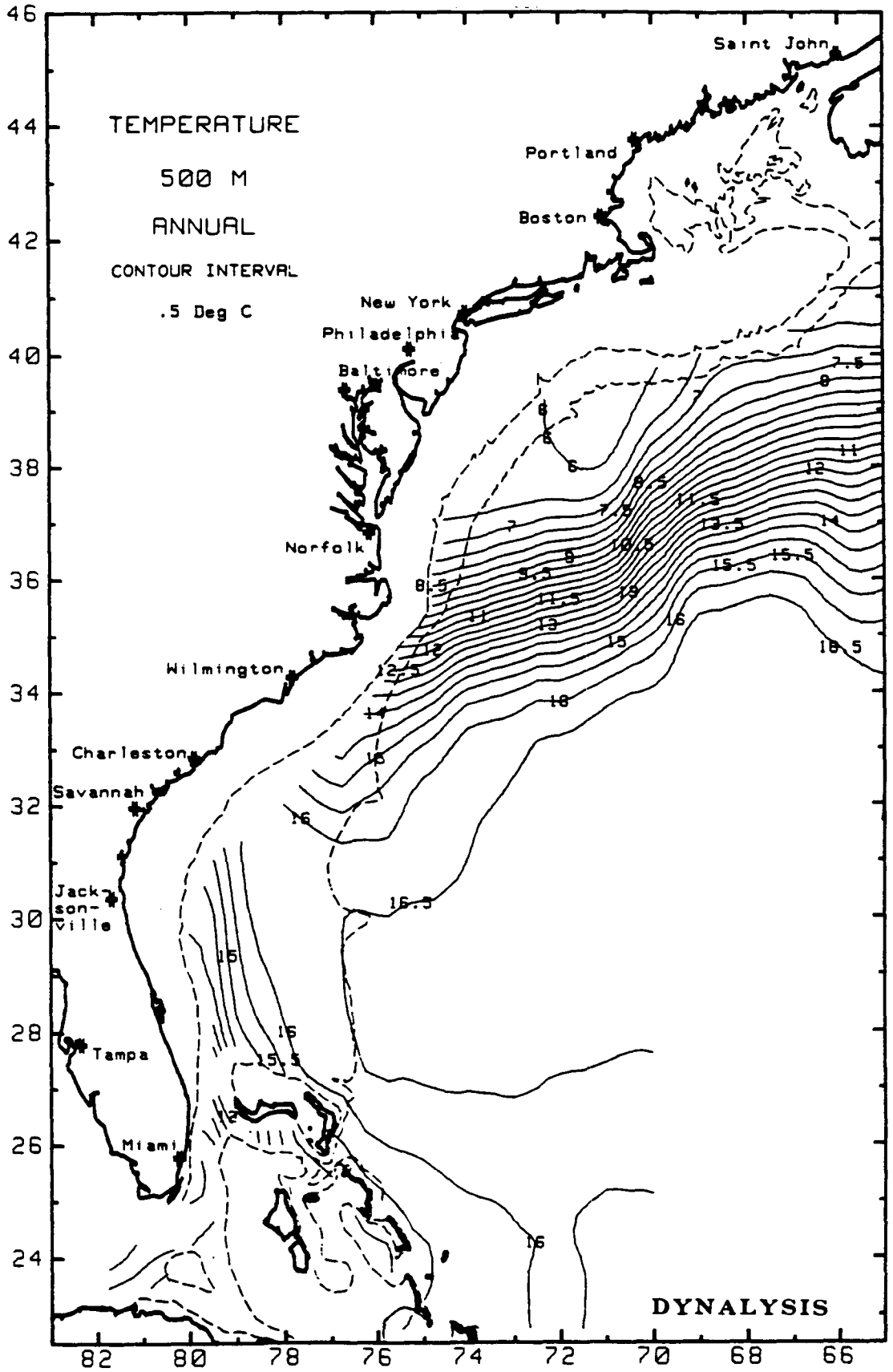

Figure 2.2.7 Annual temperature distribution at 500 m depth.

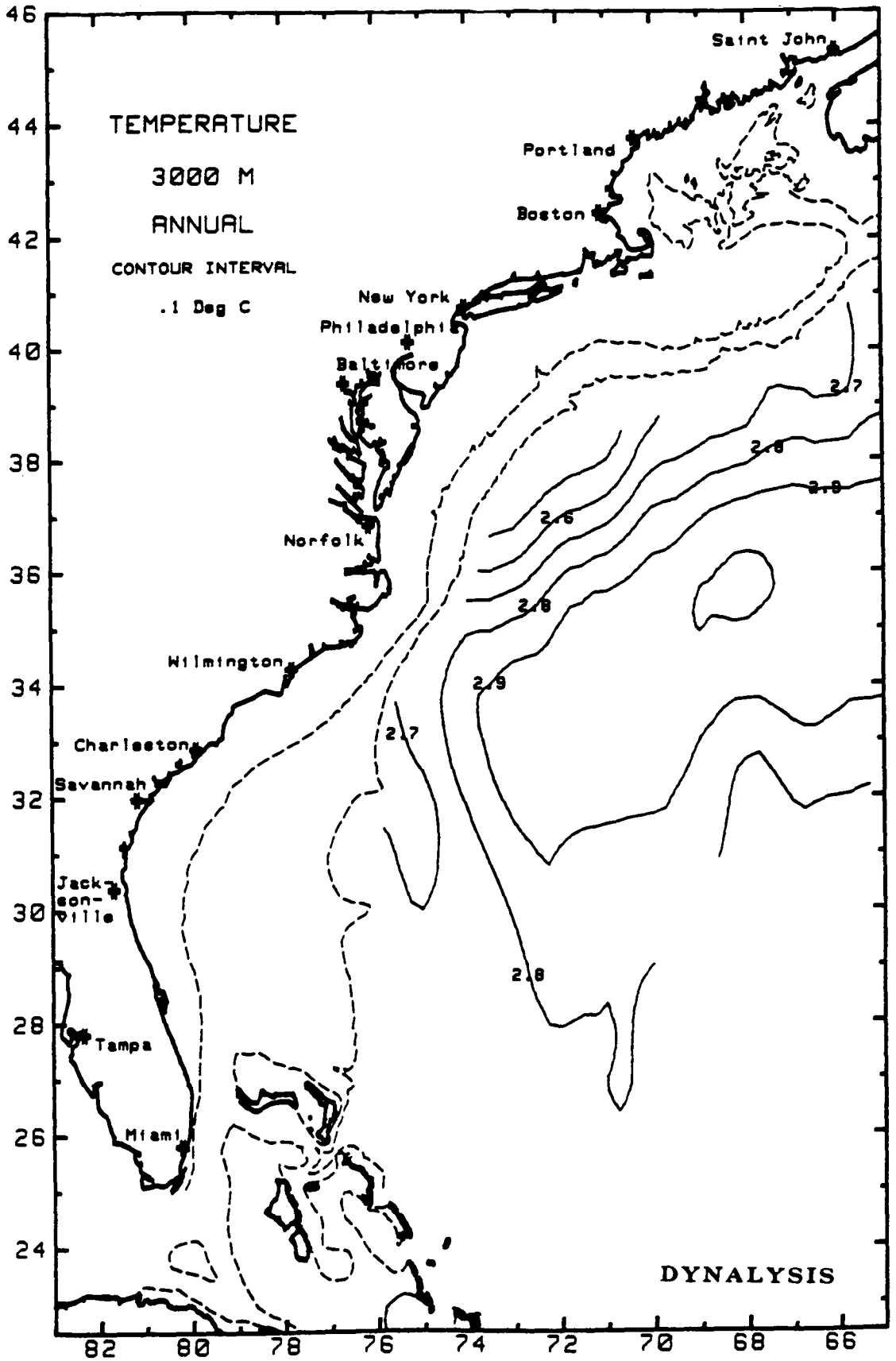

Figure 2.2.8 Annual temperature distribution at 3000 m depth.

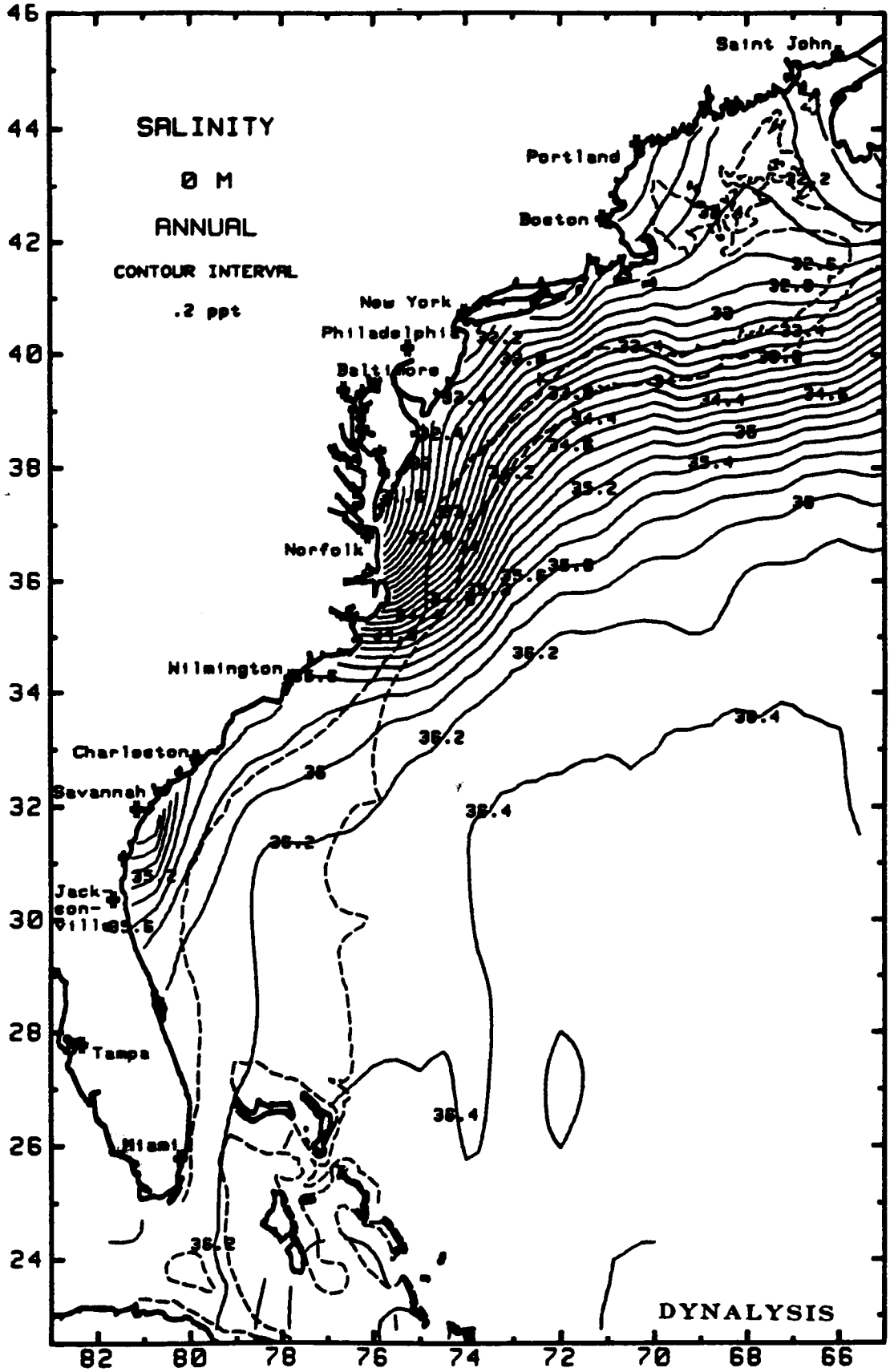

Figure 2.2.9 Annual salinity distribution at 0 m depth.

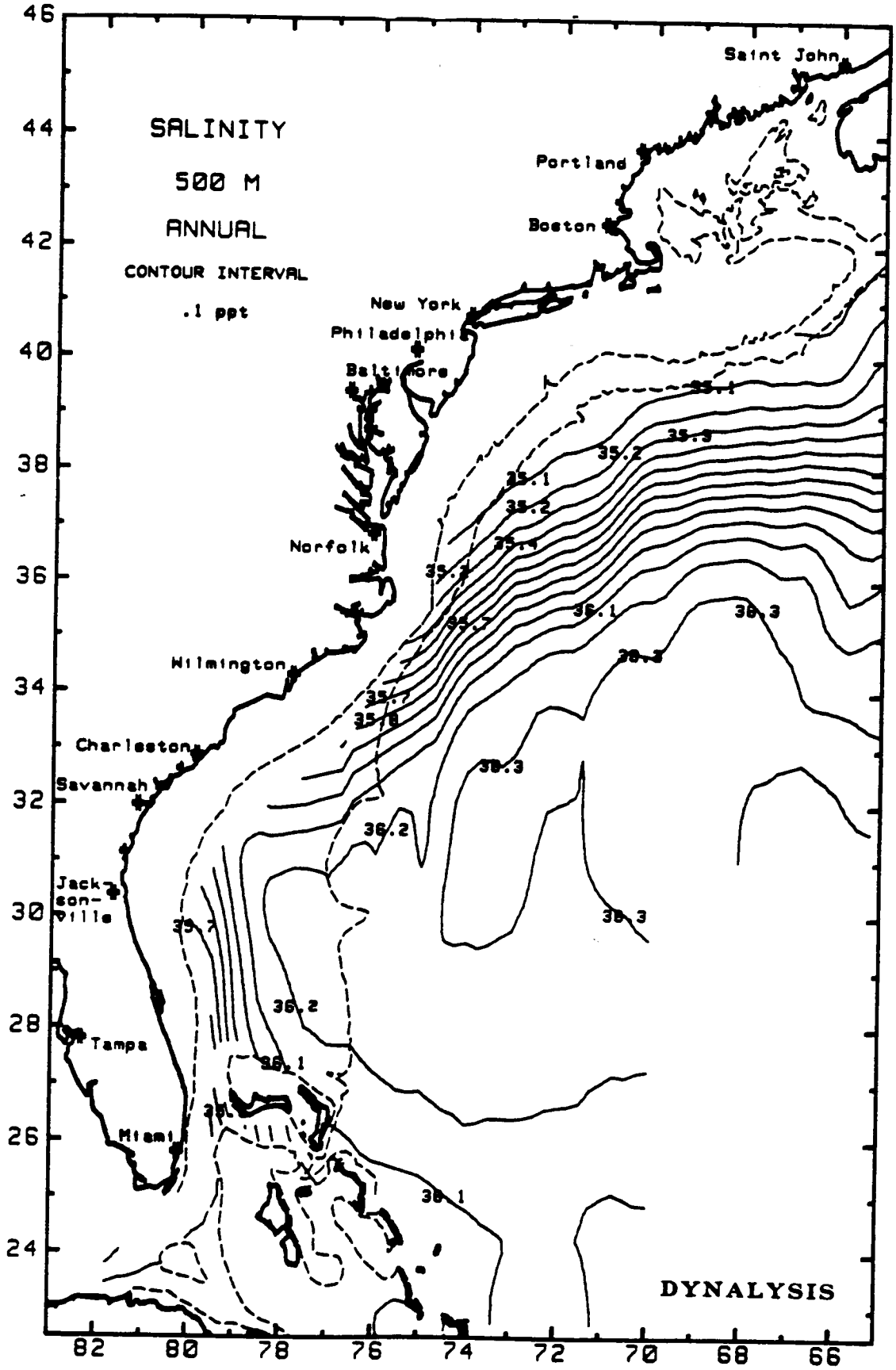

Figure 2.2.10 Annual salinity distribution at 500 m depth.

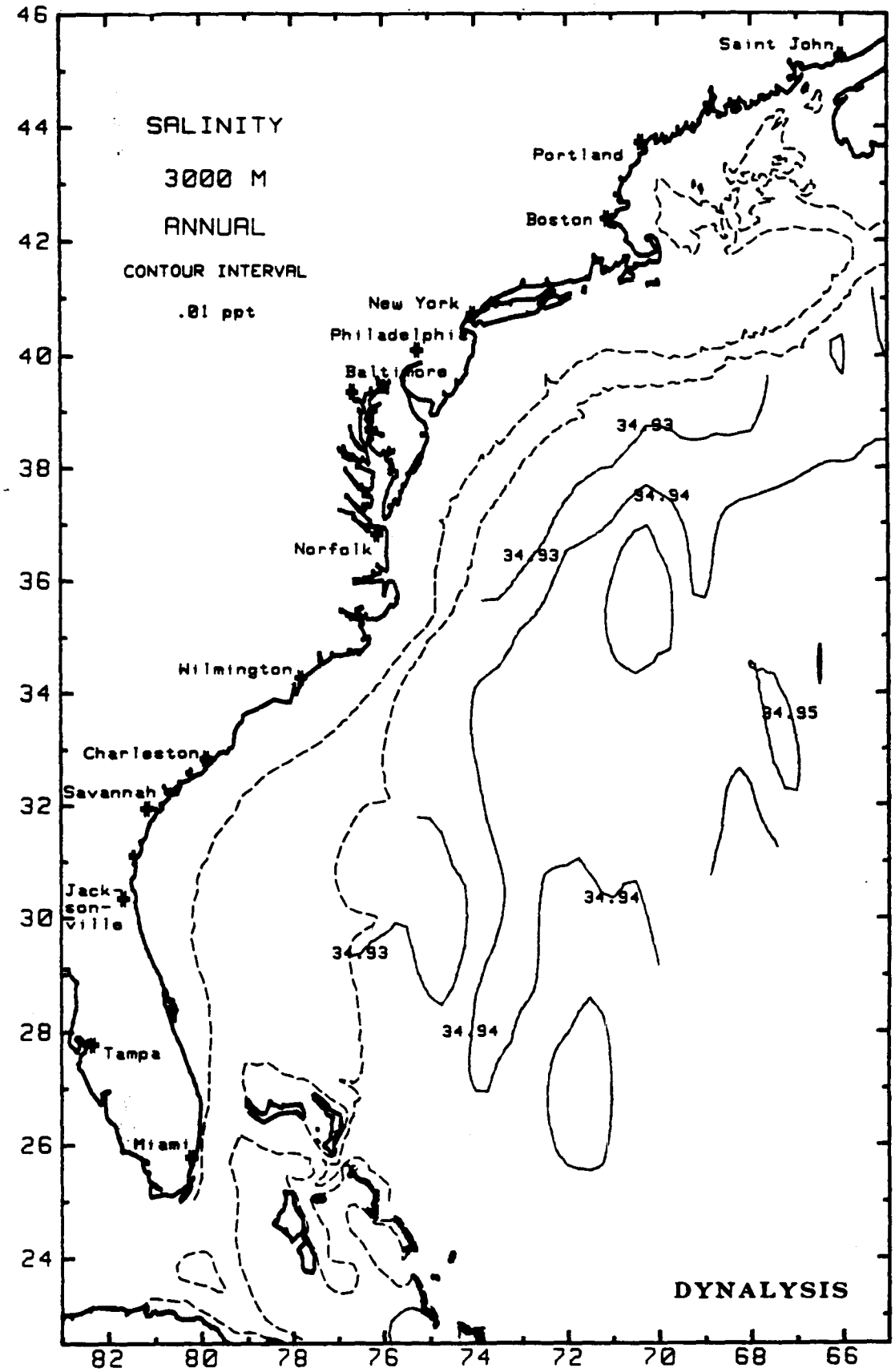

Figure 2.2.11 Annual salinity distribution at 3000 m depth.

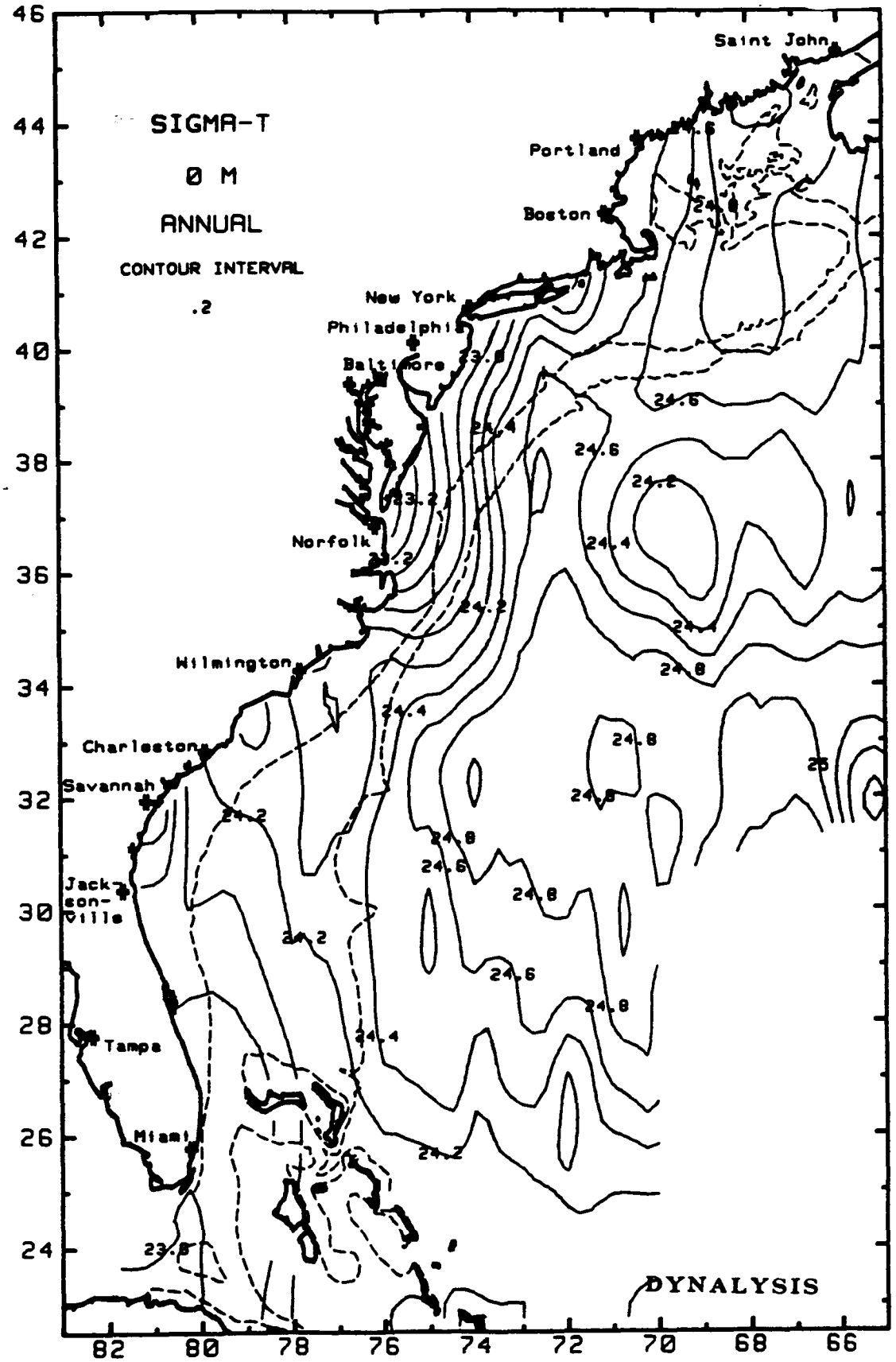

Figure 2.2.12 Annual σ_t distribution at 0 m depth.

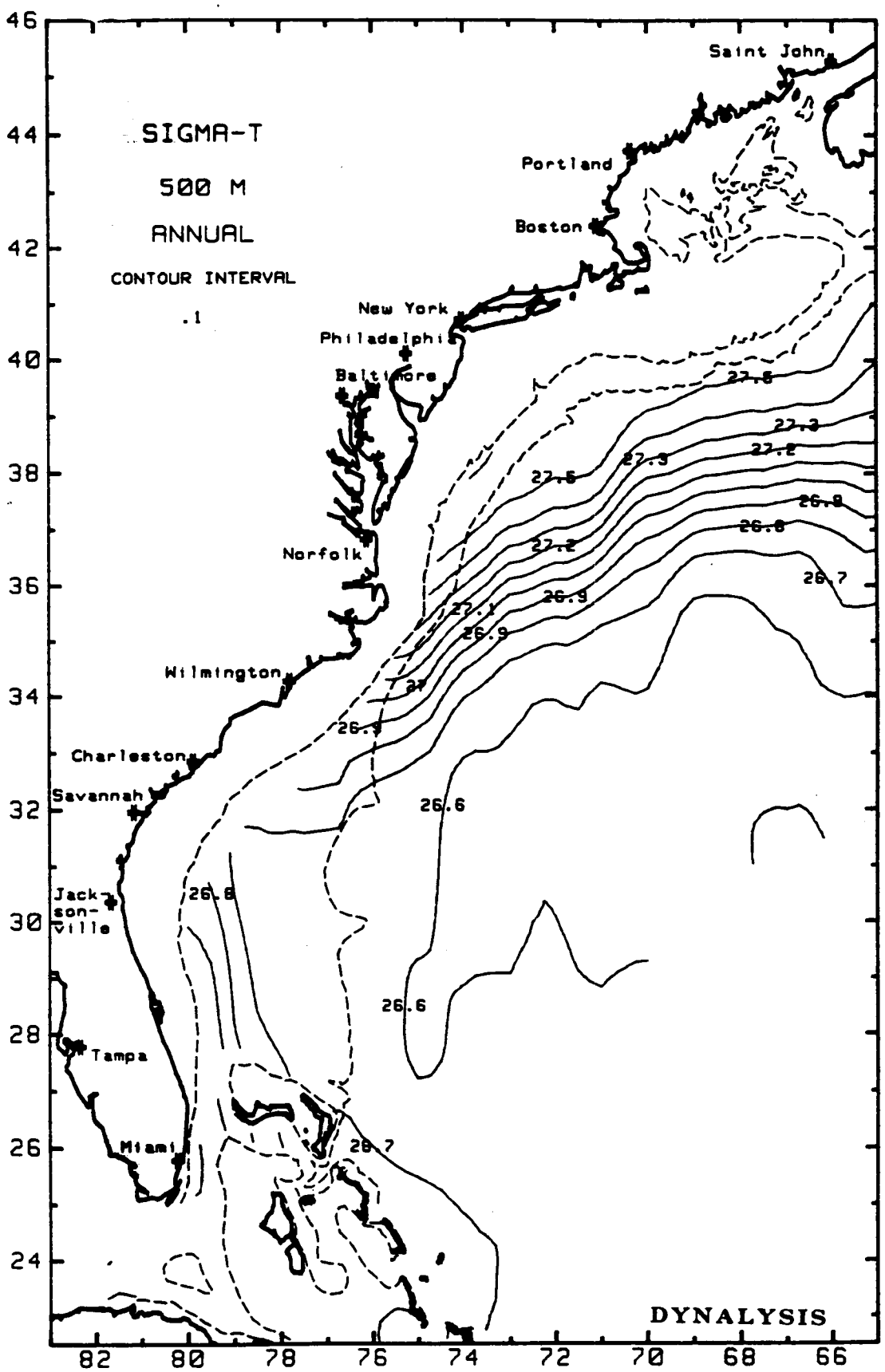

Figure 2.2.13 Annual σ_t distribution at 500 m depth.

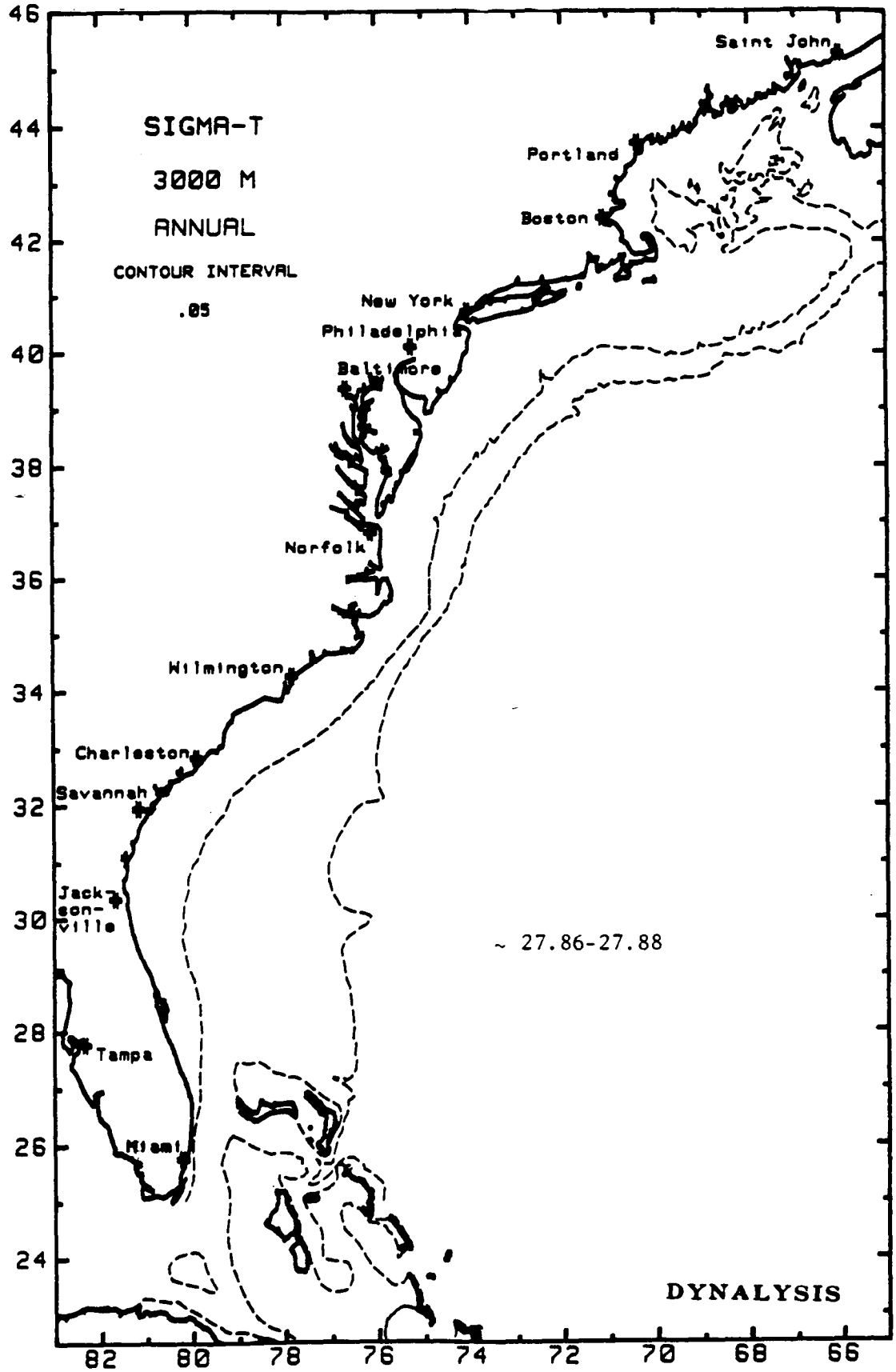

Figure 2.2.14 Annual σ_t distribution at 3000 m depth.

larger salinity variations than the SAB, mainly because of the source of water masses in each region. In the SAB, the Gulf Stream transports equatorial water masses through the region whereas in the MAB, both these water masses and low salinity colder water masses from the north are present. Interestingly enough, the salinities at 3000m are similar in both regions and less than at 1000m, which in turn are considerably less than at 100m, reflecting once again the different water masses resident at different levels in the water column.

At the surface, σ_t distributions (Figure 2.2.13) show estuarine influences nearshore but exhibit no discernible patterns otherwise; whereas the deeper waters (Figure 2.2.13) reflect definitely the influence of the Gulf Stream front in both the MAB and the SAB.

The distributions are in general consistent with those presented by Kantha, Blumberg, Herring and Mellor [1981] for the SAB and Blumberg, Mellor and Levitus [1977] for the MAB. It is difficult to make comprehensive comparison of these results with those of Levitus [1982] because of his coarse 1° x 1° resolution, but the distributions appear to be consistent with his results. The only difference is the amount of "smoothness"; his distributions are smoother. Blumberg et al. [1977] do not present seasonal distributions so that detailed comparisons are not feasible. However they do present the annual distributions at 3000m and these agree with the results presented in this report. Their monthly distributions are consistent at least qualitatively with the current results. The results for the SAB are also consistent with those of Atkinson, Lee, Blanton and Chandler [1983], who presented the distributions of the various properties only on the shelf.

Seasonal and annual distributions of T, S and σ_t are presented in Appendix A.2. and properties at all NODC standard levels for all seasons and the annual case are available on magnetic tape. Examination of the

seasonal distributions reveals certain well-known aspects of the ECS. For example, the near surface horizontal gradients in temperature are much larger in winter especially in the MAB and GOM, because of the winter-time cooling of shelf waters, while the Gulf Stream waters remain relatively warm. The Gulf Stream front is much sharper on a seasonal basis than an annual one because less variability is averaged in the derivation of the mean distributions.

Large river and estuarine flows during summer and spring are reflected in the salinity and σ_t distributions at the surface which show larger gradients at the mouths of these flows than at any other time during the year. The larger seasonal variations of surface temperature in the GOM and the MAB shelf when compared to that of the waters on the Carolina coasts are evident from the seasonal distributions. Sampling biases in terms of eddy-like features in deep oceanic regions, in the Hatteras Abyssal plain for example, can be seen in distributions at 1000m depths. The nearsurface distributions of T and S are in general much smoother than in deeper waters both in SAB and MAB, a reflection, no doubt, of good sampling sizes.

Appendix B contains climatological distributions of properties derived from hydrography, such as dynamic heights and properties on various σ_t surfaces. Here we will present just a few sample fields for the annual case. Figures 2.2.15 and 2.2.16 show the 0/500 m and 500/1000 m dynamic heights. The strong temperature front on the western side of the Gulf Stream is strongly represented in these distributions. Figure 2.2.17 shows the depth of the 25.8 σ_t surface for the annual case. This surface lies closer to the surface in the Georges Bank - Gulf of Maine area than over the Blake Plateau, because of the colder and therefore denser waters in the former region. Figures 2.2.18 and 2.2.19 show

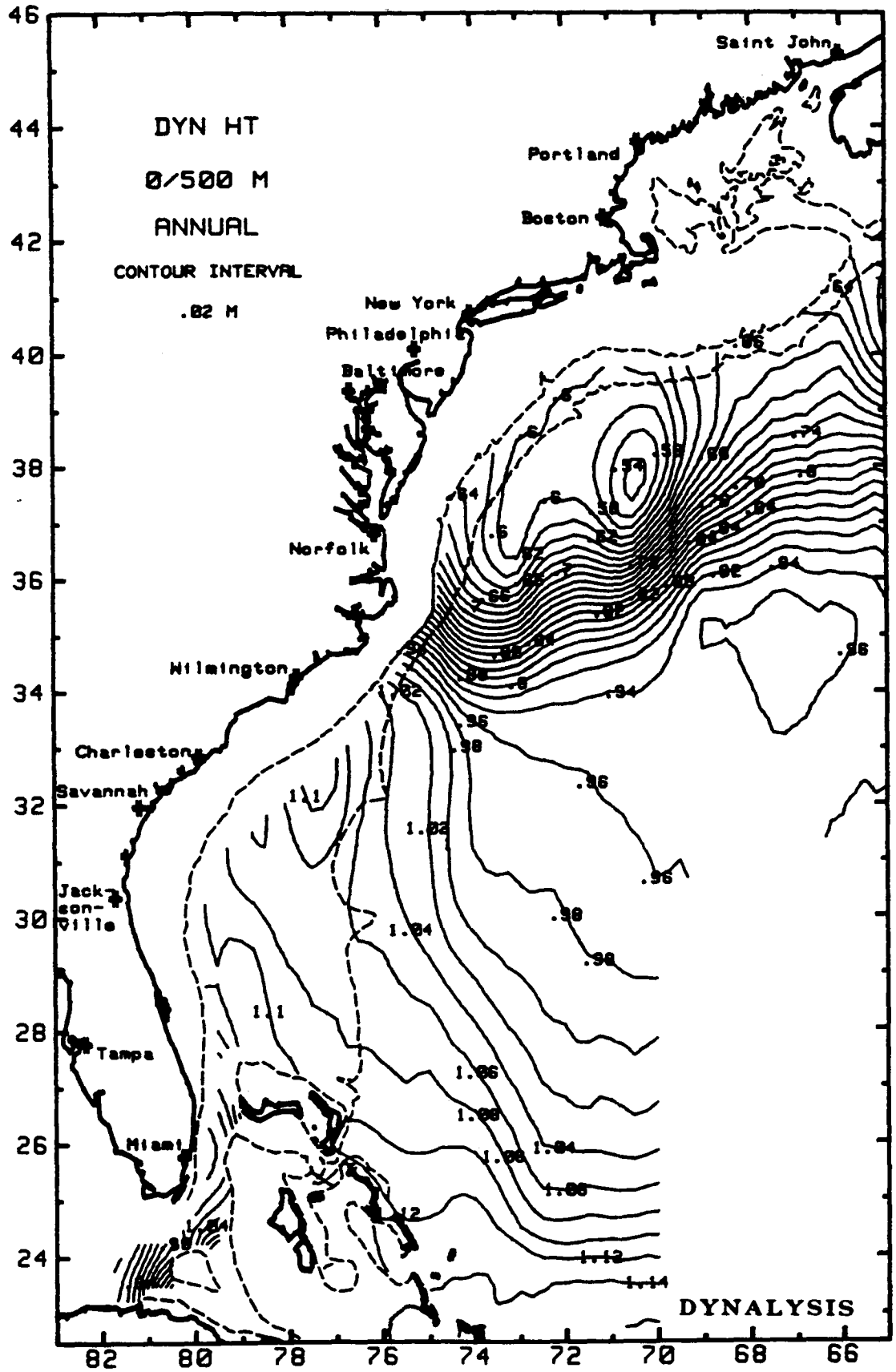

Figure 2.2.15 0/500 m dynamic height distribution for the annual case.

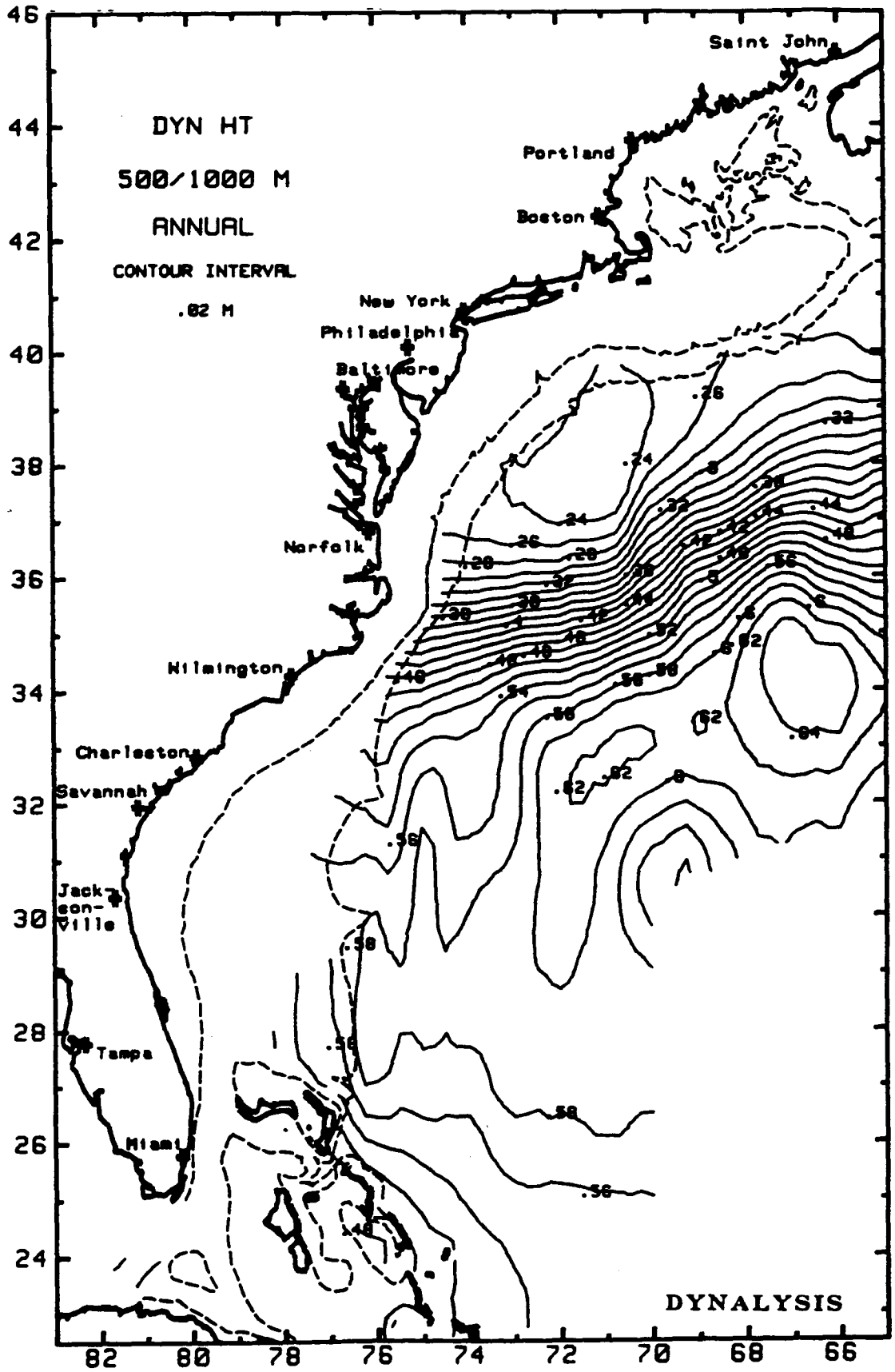

Figure 2.2.16 500/1000 m dynamic height distribution for the annual case.

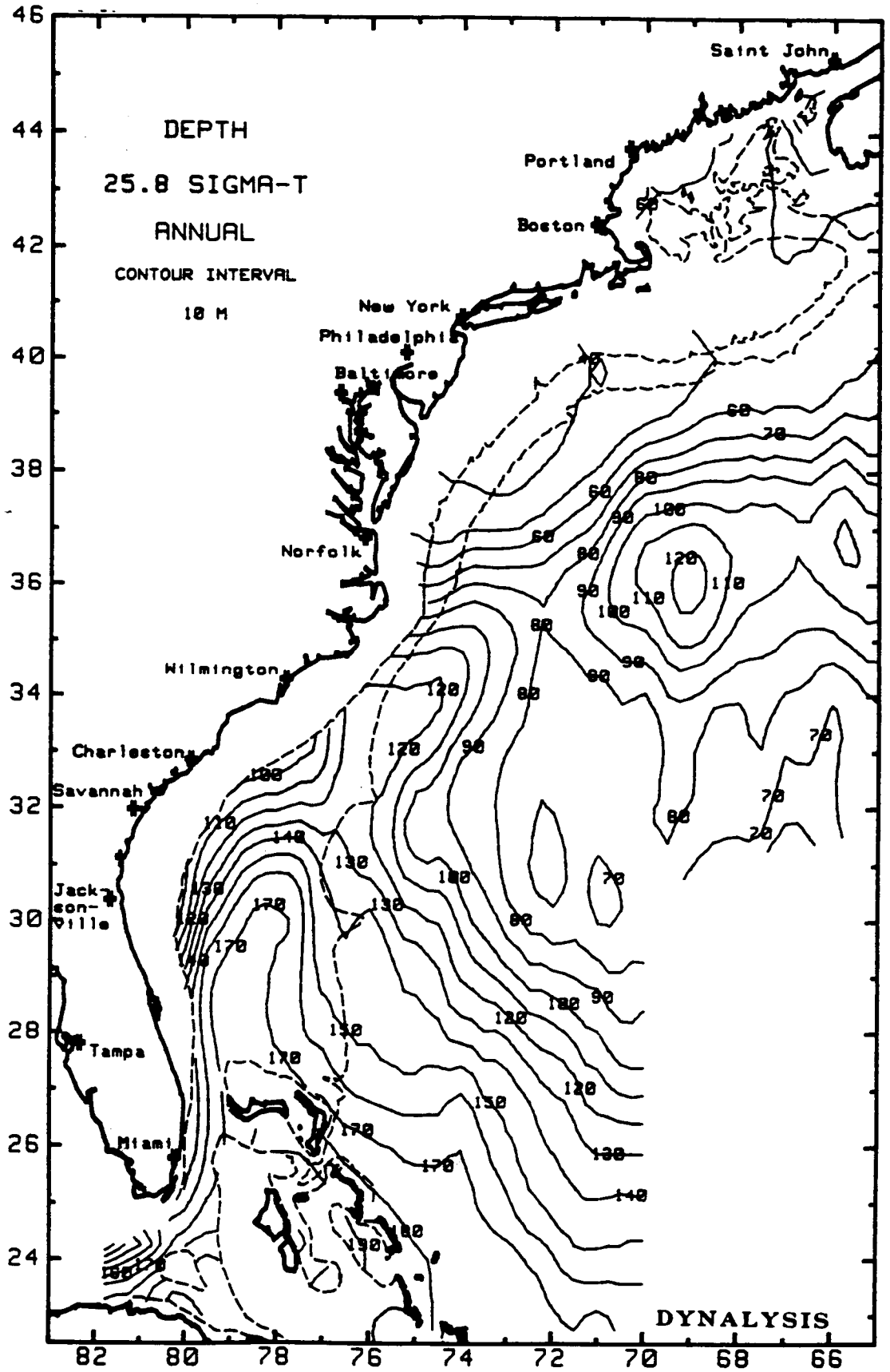

Figure 2.2.17 Depth of 25.8 σ_t surface for the annual case.

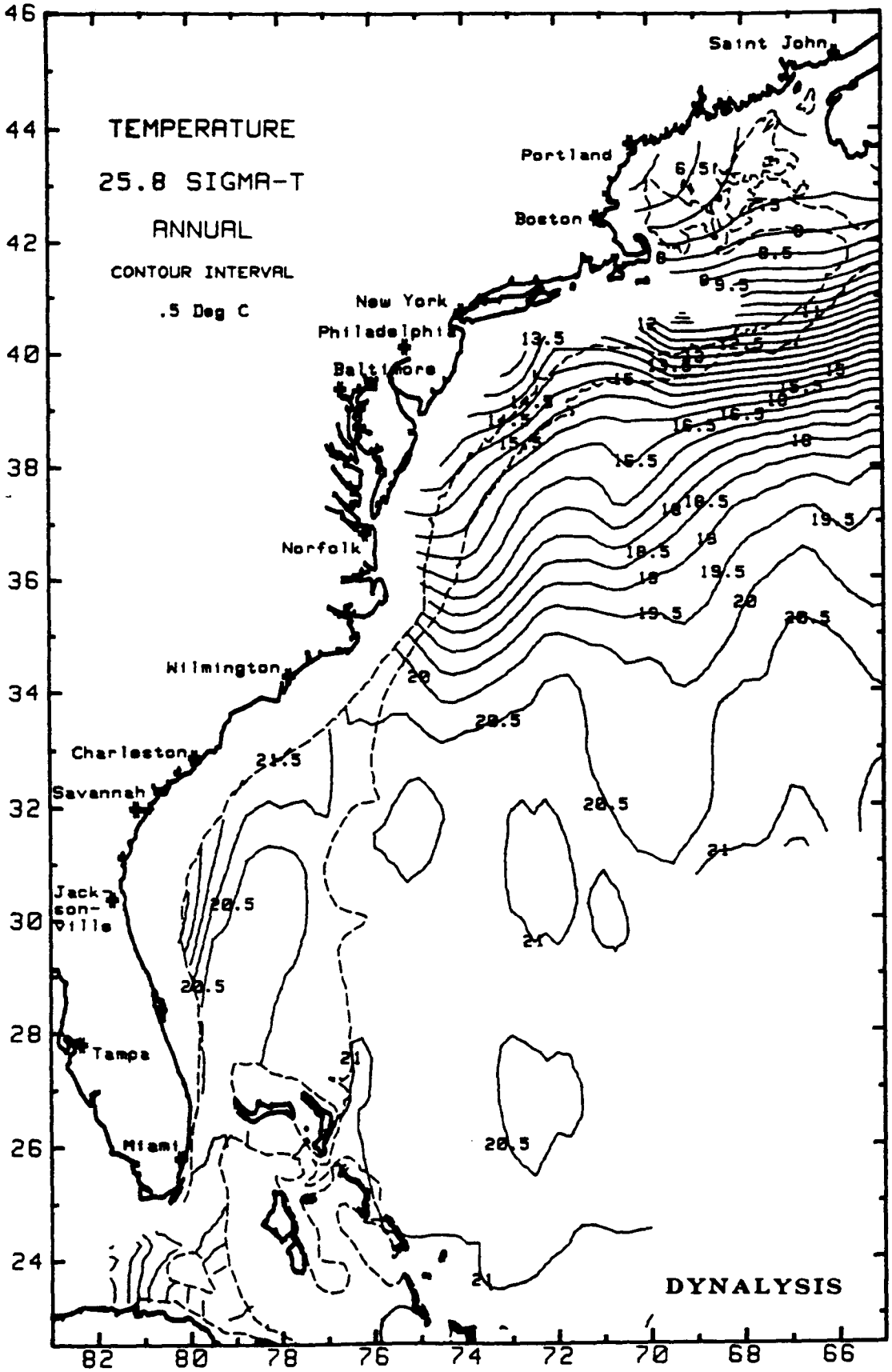

Figure 2.2.18 Temperature distribution on 25.8 σ_t surface for the annual case.

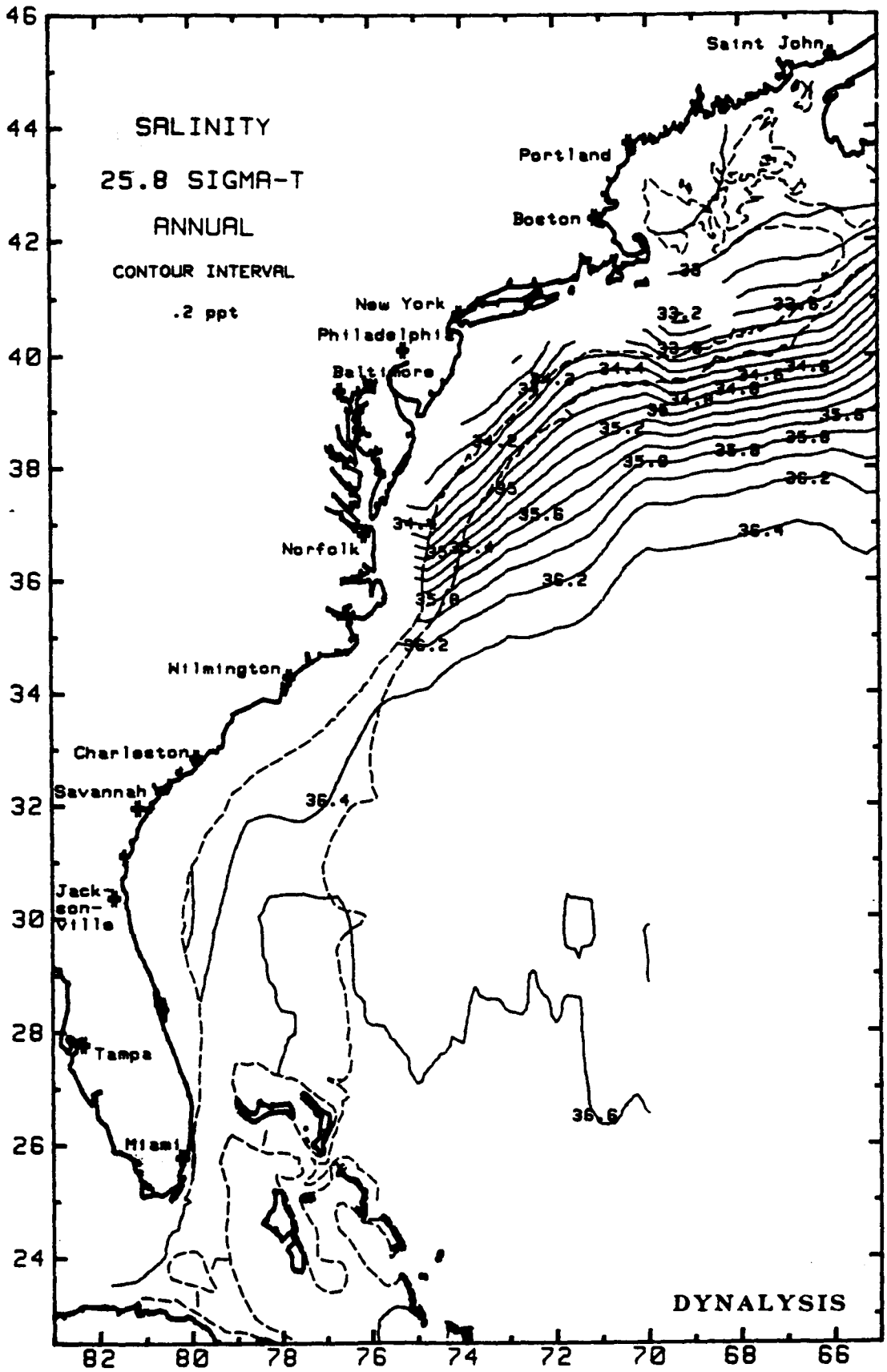

Figure 2.2.19 Salinity distribution on 25.8 σ_t surface for the annual case.

the temperature and salinity distributions on σ_t = 25.8 surface. A strong northward negative gradient is evident in both properties in the Georges Bank - Gulf of Maine region.

2.3 Characteristic Tracing Model

This Section describes the extension of a diagnostic technique (CTM 81) developed during Phase II of the South Atlantic Bight Modelling effort [Kantha, Mellor and Blumberg, 1981a and 1982], to include the effect of the bottom stresses in the planetary potential vorticity balance. The method depends on integration of the equation for the planetary potential vorticity (f/H)[1] (see Gill [1982]) along the f/H characteristics of the region to determine the transports (volume flow rate per unit width in the entire water column). Henceforth references to vorticity balance or vorticity imply the planetary potential vorticity. The extension involves inclusion of the bottom-stress forcing in the governing vorticity equation to provide a better estimate of the currents on the shelf. A second-moment turbulence closure model, employed in a one-dimensional vertical mixing routine incorporated into the Characteristic Tracing Model, properly distributes the wind-induced momentum in the upper layers and takes into account the effect of bottom stresses on the currents in the water column. The reader is referred to the above-cited papers for a detailed discussion of the technique and the governing equations, which are nothing but geostrophic equations with Ekman terms included.

The extended Characteristic Tracing Model (CTM 83) has been applied to the East Coast of the United States to provide a better depiction and

---

1 The relative vorticity, essentially the cross-stream gradient of the alongstream vertically averaged velocity, is considered negligible, even though it might be significant at the Gulf Stream Front. The model could be extended to include it, but an iterative solution technique is needed to trace along total vorticity contours.

understanding of the circulation in the South Atlantic Bight (SAB) using the climatological hydrographic fields determined from data archived at the National Oceanographic Data Center (NODC), Fleet Numerical Oceanography Center (FNOC) and other sources, and wind stress fields determined from data archived at the National Climatic Data Center (NCC). The result is the climatological distribution of transports and currents in the region both on a seasonal and annual basis. In addition, geostrophic background currents are also deduced for direct use in the MMS oil spill risk assessment model.

For a comprehensive description of the model, and the basic physics it is based upon, the reader is referred to Kantha et al. [1981 and 1982]. A brief description is included below for completeness and to point out the improvements upon the earlier version, CTM 81.

2.3.1 Model Description

The vast expanse of the oceans makes current meter measurements with extensive coverage in space and time costly and impractical. The best one can hope for, even under the most favorable circumstances, is a limited number of current meter measurements, most of them in shallow coastal shelf waters. Hydrographic measurements, on the other hand, have a relatively larger extent of coverage both in space and time. It is therefore desirable to be able to deduce, at least approximately, the prevailing currents in a region from hydrographic measurements.

The basic starting point of such diagnostic calculations is the full or the geostrophic approximation to the governing equations with or without the shear stress terms. Basically, these models are just another means of obtaining the sea surface elevation gradients, examples being Stommel Beta-spiral method [Schott and Stommel, 1978] and the conventional geostrophic calculations with the assumption of a level of no motion at some depth. Once the barotropic component of current is thus known,

knowledge of the density gradients provides the baroclinic component and hence the total currents at all levels in the vertical. These currents can be either pure geostrophic background currents in the water column (if the shear stress terms are not included in the momentum balance) or geostrophic-Ekman currents. The derivation of the latter calls for a suitable closure scheme for Reynolds stresses whose variation in the vertical is needed for distributing the wind-induced momentum in the upper layers of the water column.

Characteristic tracing is just another means of deducing the sea surface elevation. It is a diagnostic method for deducing the current and transport distributions over the domain from simple geostrophic/geostrophic-Ekman dynamics utilizing observed wind stress and hydrographic data. The technique does not require any assumption as to the level of no motion. Instead, the total transport is determined by integrating the geostrophic equation for total transport along contours of constant planetary potential vorticity which in this case are the mathematical characteristics of the problem.

It is necessary to specify only the total transport at only one point on each f/H contour or equivalently, on any one transect crossing all contours in the domain. This information is readily obtained if the velocity normal to the transect is known at any one point in the water column all along the transect. For example, if the bottom currents are known, from hydrography along the transect it is possible to obtain the transport stream function along the transect. Data on currents, especially in the deep ocean are the sparsest and most often nonexistent. In such a case, a suitable assumption is necessary; for example one could assume bottom currents to be negligible, or postulate a plausible distribution based on other indirect data. In any case, although the total transport in the water column is sensitive to inaccuracies in the prescription of

the bottom currents, the near-surface currents, especially beyond the shelf break, are not overly sensitive and if it is these that one is primarily interested in, the technique is useful.

The results of an application of such a model (CTM 81) to the South Atlantic Bight have been described by Kantha et al. [1981 and 1982]. Calculations describing the seasonal variations as well as sensitivity to the prescription of boundary conditions in a transect through the Straits of Florida have been presented in these works. CTM 81 incorporated a one-dimensional turbulence closure to account for the effect of wind and bottom stresses on the currents in the water column. It, however, ignored the bottom stress terms in the planetary potential vorticity balance. The presence of bottom stress terms (Equations (21) and (22) of Kantha et. al., 1981) effectively raises the order of the equation and changes the mathematical nature of the problem. More importantly, howsoever these terms are parameterized they depend on the bottom velocities which are not known a priori. The equations, therefore, become implicit in form, with dependent variables in the driving terms and hence not amenable to solution by characteristic tracing. The only alternative is an iterative solution technique in which the bottom stress is put to zero in the first iteration and the resulting solution used to compute a first approximation to bottom stresses, which is then plugged back into the driving terms and the next approximation to the true solution sought. However, as in all iterative procedures, convergence is not guaranteed a priori and a criterion for convergence if any, in a problem as complex as the present is hard to deduce.

It has been found that assuming linearized bottom stresses (i.e., bottom stress proportional to the bottom velocity) and using for the next iteration, the arithmetic mean of the old assumed value and the new calculated value as the guess bottom stress field assures convergence. The

rate of convergence depends on the magnitudes of the stresses and the smoothness of the bottom stress field. Nevertheless, convergence is readily achieved.

The numerical solution strategy employed is as follows. Characteristic tracing is used to derive the transport field by first ignoring the bottom stresses in the planetary potential vorticity balance. Knowledge of these and the baroclinicity prevalent in the water column provides the barotropic component of the transport in the water column or equivalently the bottom velocity. The bottom stresses are calculated from these velocities with a proportionality constant of 0.004 m s^{-1}, (equivalent to a bottom velocity of about 15 cm s^{-1} in the quadratic drag law) and the arithmetic mean of the calculated stress field and assumed field (zero in the first iteration) is used in characteristic tracing to obtain new values for the bottom velocities and hence bottom stresses. The iterative procedure is continued (about 15 iterations are needed) until bottom stress field converges. The sea surface elevation gradients that result at the end of the iterative solution are used as input to the one dimensional vertical mixing submodel (as described by Kantha et. al., 1981) to deduce the currents everywhere in the water column.

It should be noted that the magnitude of the coefficient used in the drag law for the bottom stresses is appropriate for the climatological bottom currents prevalent on the continental shelf regions, which are typically 10-20 cm s^{-1}. Also, the baroclinicity implied by climatology is weaker than synoptic values and therefore if the transports in the water column are prescribed to be the same, the barotropic component of the transport or equivalently the bottom stresses will necessarily be overestimated by the model. A lower value of the drag coefficient is therefore preferable so that the effect of the bottom stresses on the vorticity balance is not overestimated. Since the influence of the bottom

stresses is negligible if the depth of the water column is large, the results off the shelf and in the deep water (say regions with depths larger than 500m) are relatively insensitive to the magnitude of this coefficient. In fact, ignoring bottom stresses in the vorticity balance is well justified everywhere except on the shelf itself, where wind and bottom stresses constitute the main components of the balance. The value of the drag coefficient has therefore been chosen to be appropriate to the climatology of the shallow continental shelf waters.

Diagnostic techniques have a tendency to produce "noisy" results because the density field is prescribed and not allowed to evolve in conformity with the dynamic constraints. Characteristic tracing is no exception. Sharply varying bottom topography off the East Coast when averaged over ¼° grid boxes leads to rapid changes in the bottom depths across the shelf break especially near Cape Hatteras. Also, the grid points at which no solution could be found from characteristic tracing have to be filled in suitably. CTM 81 used simple Laplacian interpolation to do so. The combined effect of inadequate resolution and strong topographic changes accentuated by the lack of any horizontal diffusion in the model could then lead to 'noisy' circulation patterns. To alleviate this problem, an objective analysis scheme - specifically the Herring Poisson Solver (see Appendix A of Blumberg, Herring, Kantha and Mellor, 1983) - was used to fill in stream function values at grid points which have no solution. Actual bottom topography at ¼° resolution, derived from SYNBAPS data tape [Vanwyckhouse, 1973] containing 5' x 5' high resolution digitized topography of the worlds oceans, has been used in CTM 83 without any smoothing, unlike CTM 81, which used smoothed bottom topography. Characteristic tracing yields total transport in the water column and it is necessary to compute the baroclinic part of this from known density fields before the barotropic part (equivalently the elevation

gradients) can be deduced and hence the current distribution in the vertical. Numerical problems associated with the calculation of the baroclinic component from the density gradient near a steep break can lead to spurious currents in the nearshore band and unrealistically large cross-shore elevation gradients on the shelf. This problem is avoided by converting the integrals of density gradients to gradients of density integrals in the momentum equations as described in Kantha, Mellor and Blumberg, [1982]. The vertical integrals of the density are well defined and their horizontal gradients produce meaningful current fields.

Refinements to characteristic tracing technique in CTM 83 prevents grid points with near-zero gradients of f/H from making large spurious contributions to the stream function for a characteristic passing through them that could give rise to spurious eddy patterns. If the characteristic originating from a grid point passes through such a region, characteristic tracing for that point is terminated and the point is assumed to have no solution. Stream function values for such points along with those for which the characteristics do not trace to the southern transect are later filled in, using objective analysis techniques.

The refinements discussed above, in combination with much smoother climatological properties obtained from the hydrographic data analysis procedures described in Section 2.2 lead to much smoother circulation and current distributions from CTM 83, when compared with that of CTM 81. Also, the inclusion of bottom stresses leads to more realistic currents on the shelf itself. These results are described in the next Section.

2.3.2 Diagnostic Circulation

CTM 83 described in Section 2.3.1 has been applied to the ECS to deduce the circulation in these waters both on a seasonal and annual basis. Only the annual results are presented in this section. The seasonal circulations deduced can be found in Appendix B.3. In addition to the cli-

matological temperature and salinity fields in the water column and the wind stress at the surface, the model needs information on a transect crossing f/H contours.

As described in the beginning of Section 2, the climatological data reduction and analysis, as well as CTM 83 calculations for the ECS domain were accomplished in two stages, in the first for the domain north of 26.5°N and in the second for the domain south of 26.5°N and extending southward to 22.75°N. The transect for the northern domain has been chosen at 26.75°N latitude to pass through the Straits of Florida , where excellent transport measurements are available, adequate enough to deduce even the seasonal variation (see Brooks, 1979; Brooks and Niiler, 1977; Knauss, 1969; Lee, Brooks and Duing, 1977; Mooers and Brooks, 1977; Niiler and Richardson, 1973; Richardson, Schmitz and Niiler, 1969; Schmitz and Richardson, 1968; and Anderson and Corry, 1983). These measurements indicate that the transport through the Straits of Florida is roughly 24.5, 26.5, 33.0 and 32.0 Sv during winter, spring, summer and fall respectively, with an annual average of about 29.0 Sv. For the southern domain, the same values were prescribed but at 80.5°W longitude, spanning the Straits from the Florida keys to the Cuban coast. Because of the rough topography in this domain and existence of many closed f/H contours, a large number of grid points in the domain failed to yield solutions and Laplacian filling had to be employed to obtain continuous fields. This problem is almost nonexistent in the northern domain, where by far principally the grid points in the center of the Gulf of Maine region had to be filled in because of a vorticity island in the region.

The distribution across the Straits is difficult to ascertain, but the observations of Brooks [1979] are consistent with a roughly parabolic distribution used in the model. Beyond the Little Bahama Bank, there are no observations available on either transports or velocities in the water

column so that an assumption was definitely needed. Assuming bottom velocities to be negligible and then using the baroclinicity to derive the transports in the water column has been shown to be a justifiable procedure [Kantha et al., 1981; Blumberg et al., 1983] and this is the procedure used in this study. Since most of the f/H contours in the entire domain in regions on and near the shelf pass through the Straits of Florida, this procedure should not affect the results in these regions. The deeper water especially on the Hatteras Abyssal Plain do have f/H contours intersecting the southern transect beyond the Little Bahama Bank. For this reason and because the sampling in deep waters of the Plain is sparse, the results there are to that extent less reliable.

Figures 2.3.1 and 2.3.2 show the total transport in the water column and the stream function. As expected, the Gulf Stream dominates the transport in both the SAB and MAB. The deflection of the Gulf Stream at and beyond the Charleston Bump should be noticed. The Bump is a topographic feature located off Savannah, Georgia. It is clearly manifest in 500m bottom depth contour and appears to exert an important effect on the Gulf Stream. Principally, it often appears to force the Gulf Stream to deflect offshore, which might cause amplification of its instabilities. The narrow signature of the Stream even on an annual climatological basis is noteworthy. The increase in its transport as it passes through the ECS is significant and consistent with the observations of Knauss [1969]. The southward transport all along the shelf break in the MAB is presumably due to the cold waters coming in from the Labrador region. The cyclonic circulation and the meandering of the Gulf Stream in the MAB are evident in the results. The union of the northward flowing Gulf Stream and the southward flow from the MAB near Cape Hatteras to form a more voluminous and energetic Gulf Stream that departs from the coast should be noted.

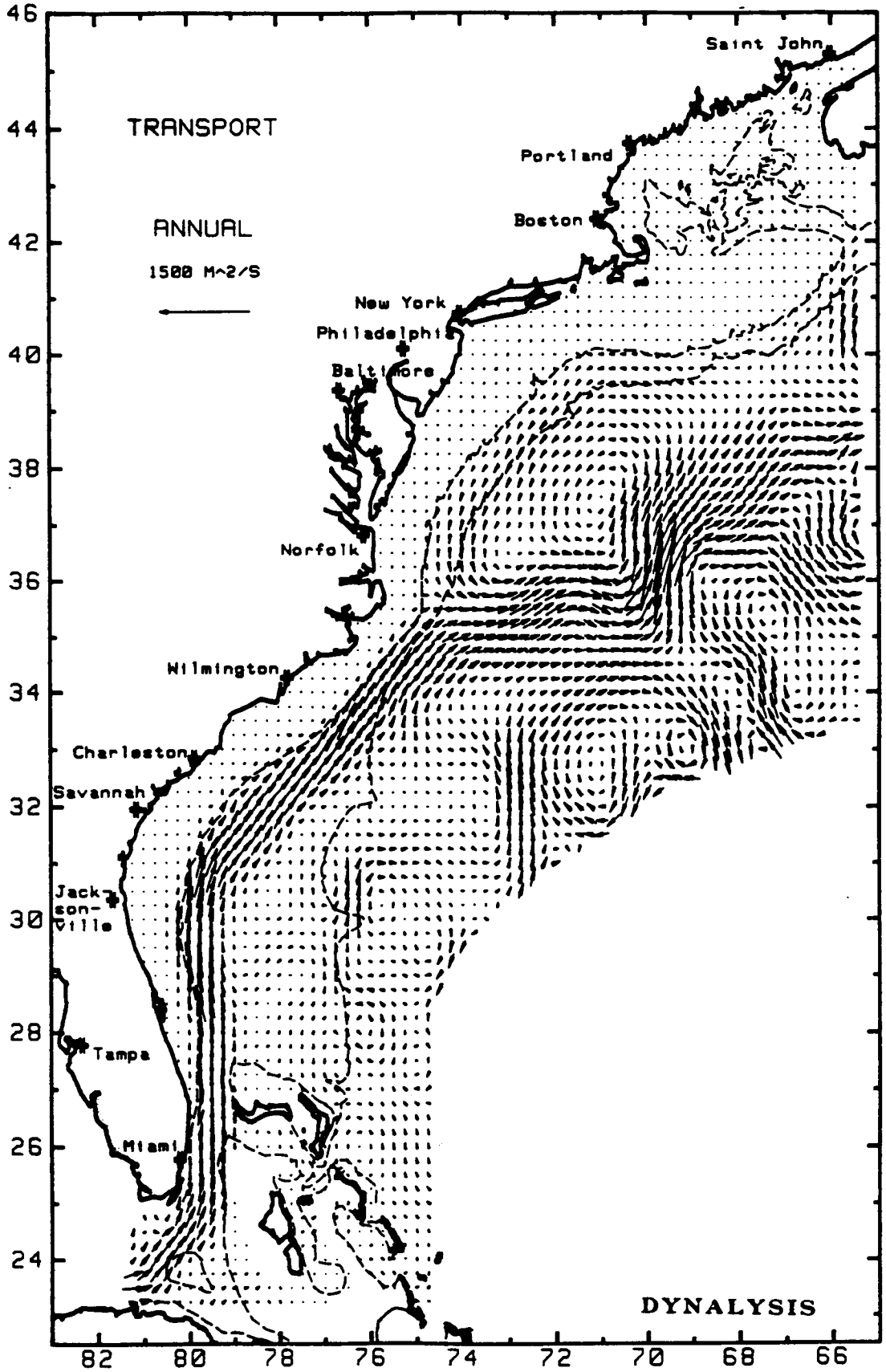

Figure 2.3.1 Total transport in the water column for the annual case.

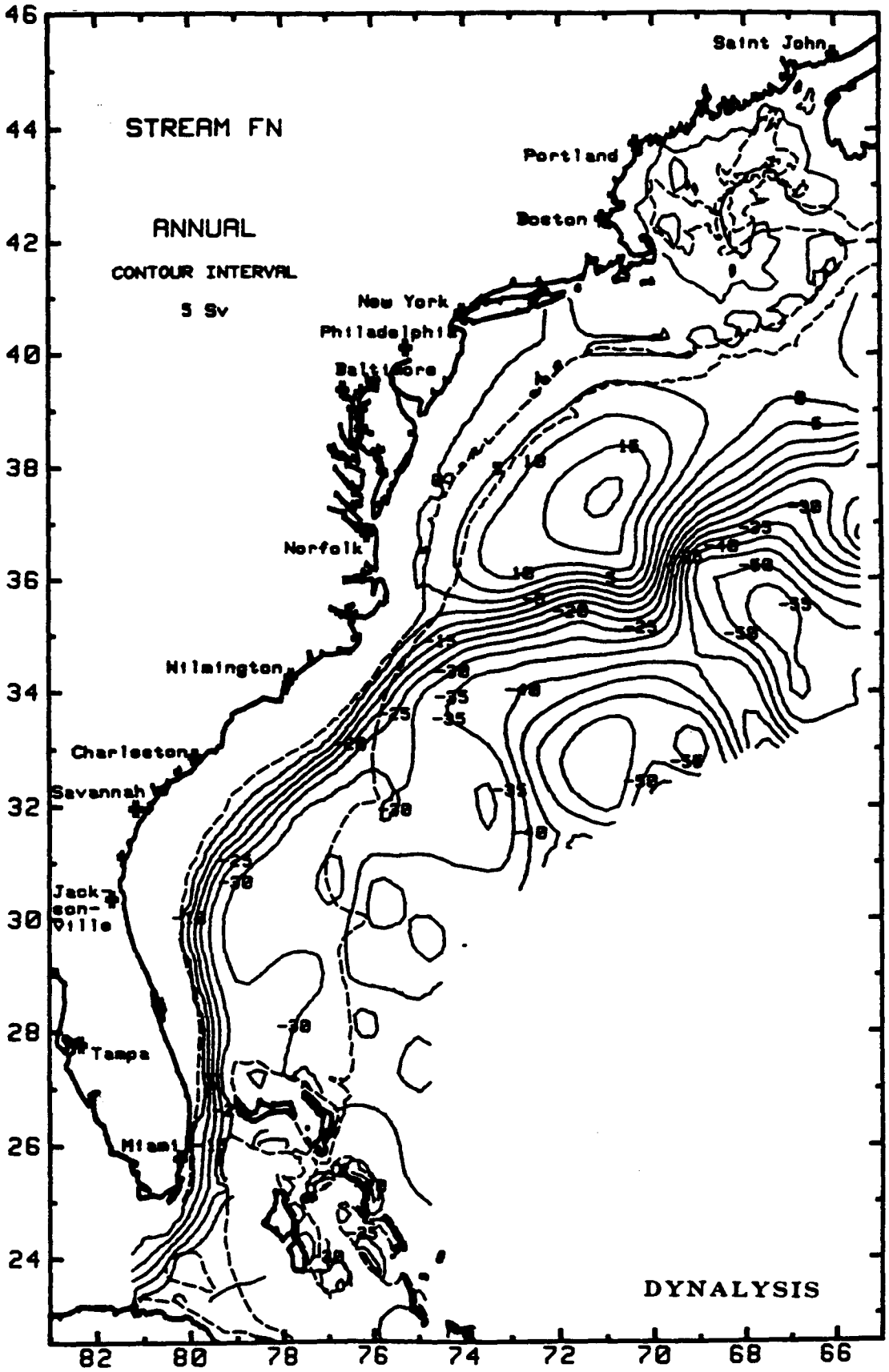

Figure 2.3.2 Distribution of stream function for the annual case.

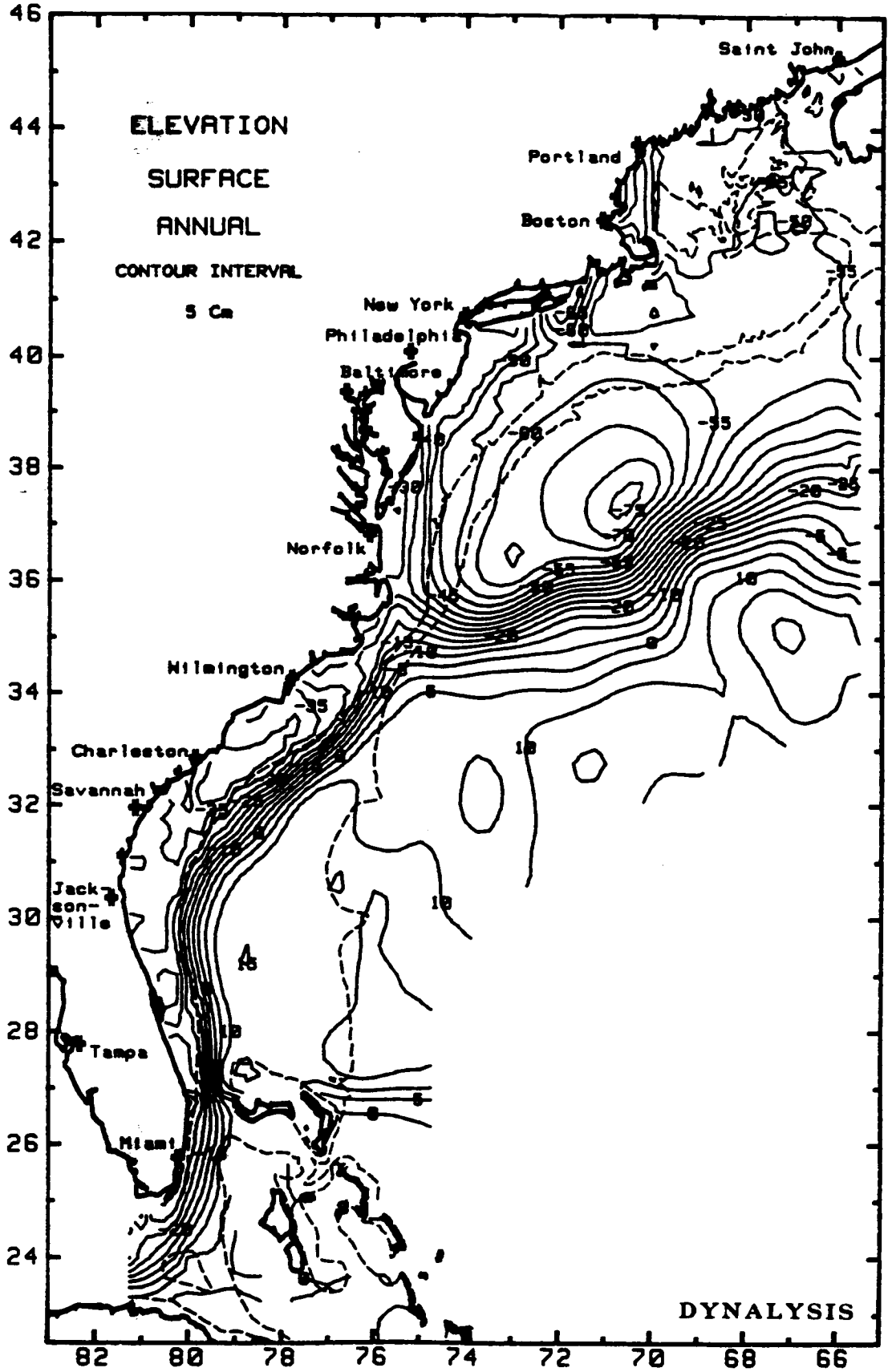

Figure 2.3.3 Distribution of sea surface elevation for the annual case.

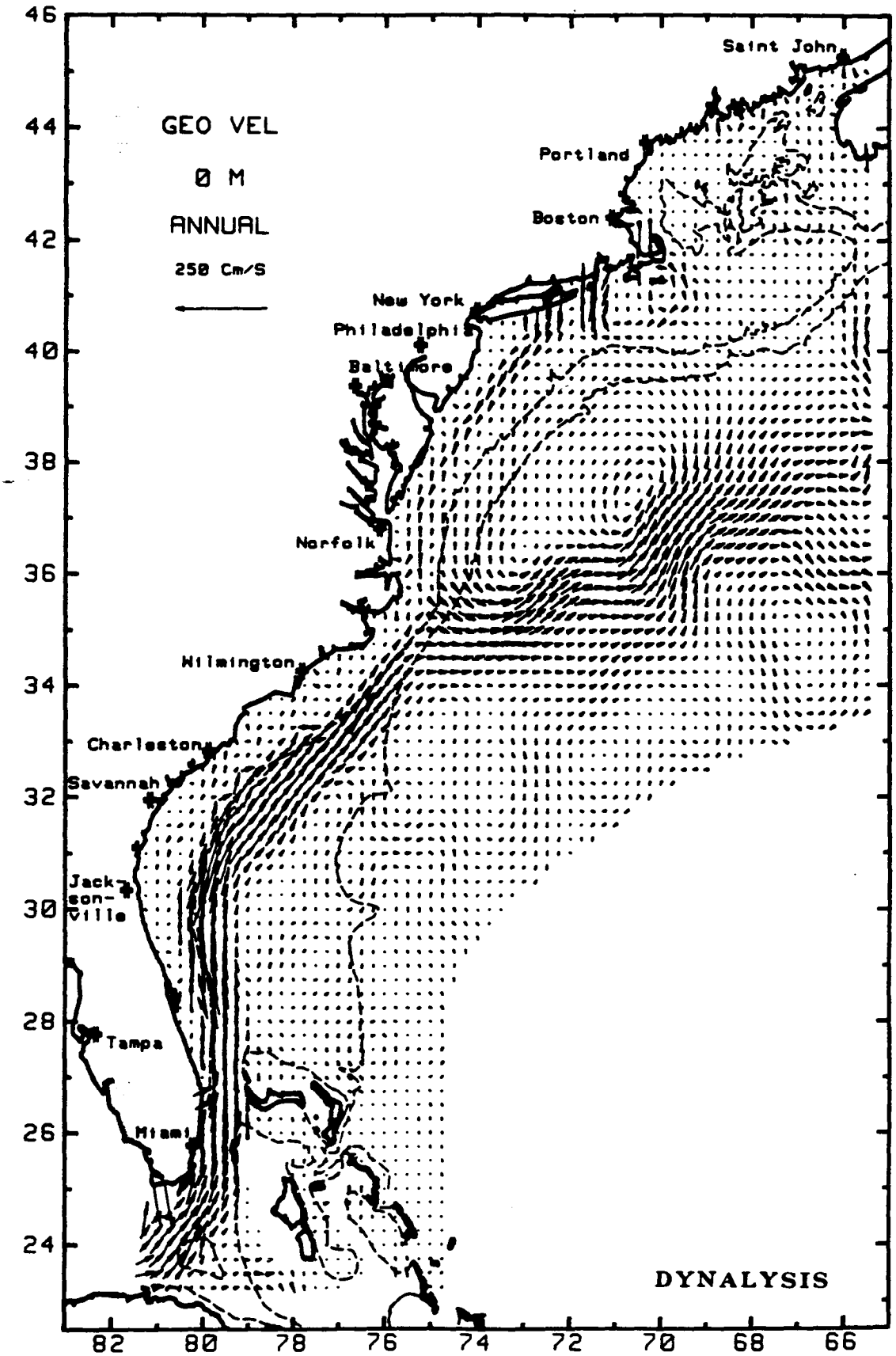

Figure 2.3.4 Distribution of geostrophic velocity at the surface for the annual case.

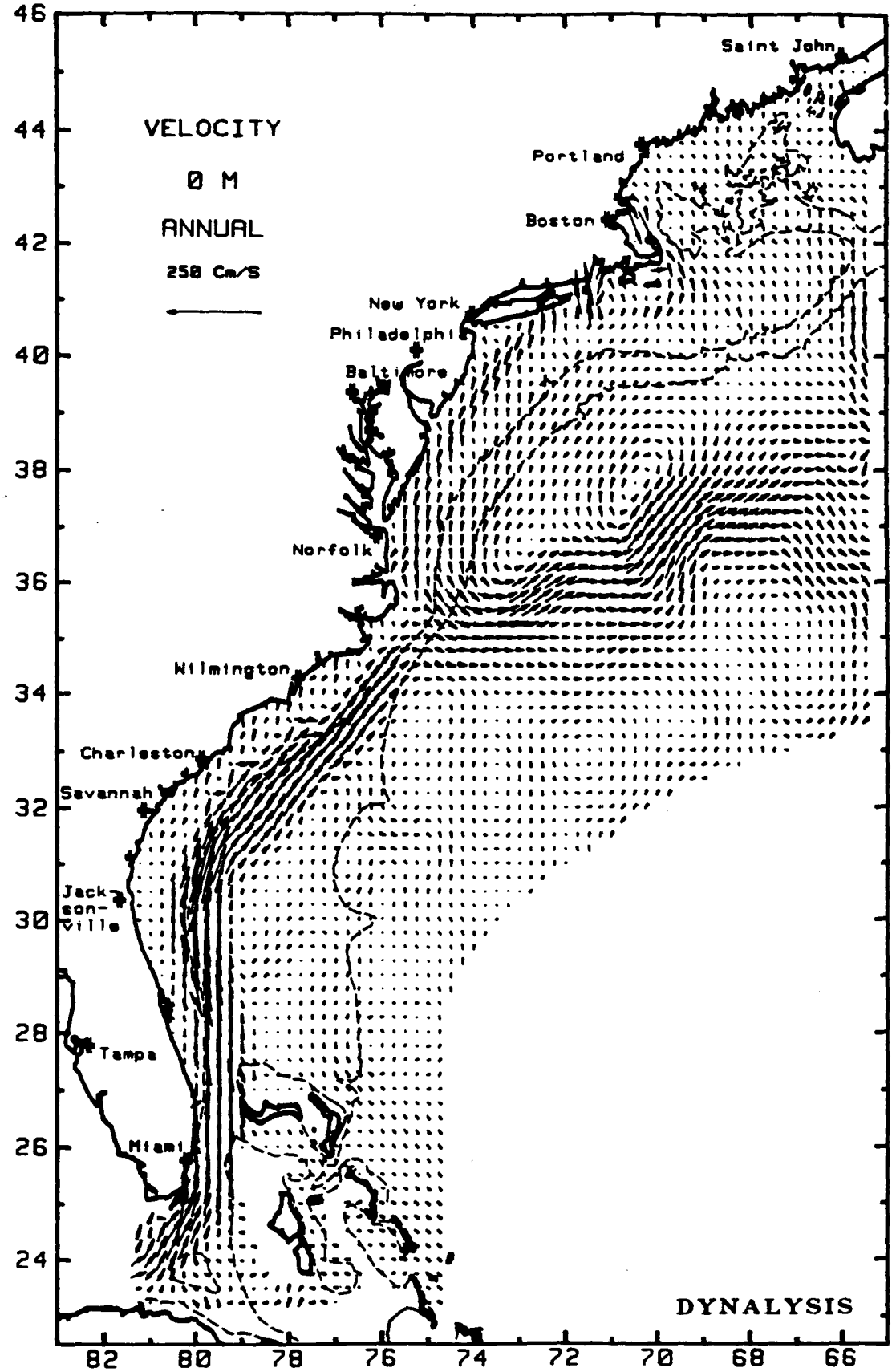

Figure 2.3.5 Total velocity at the surface for the annual case.

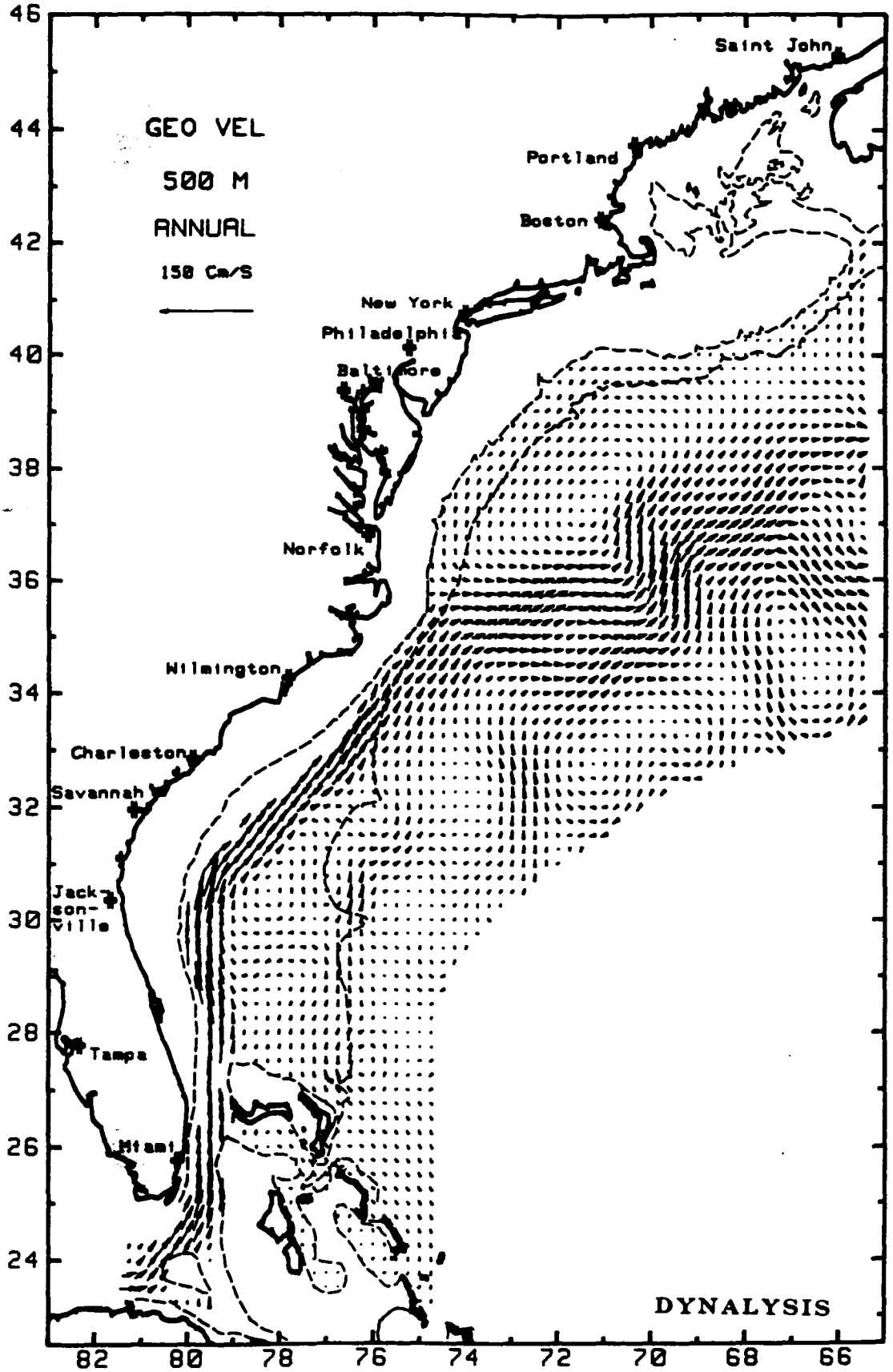

Figure 2.3.6 Geostrophic velocity at 500 m depth for the annual case.

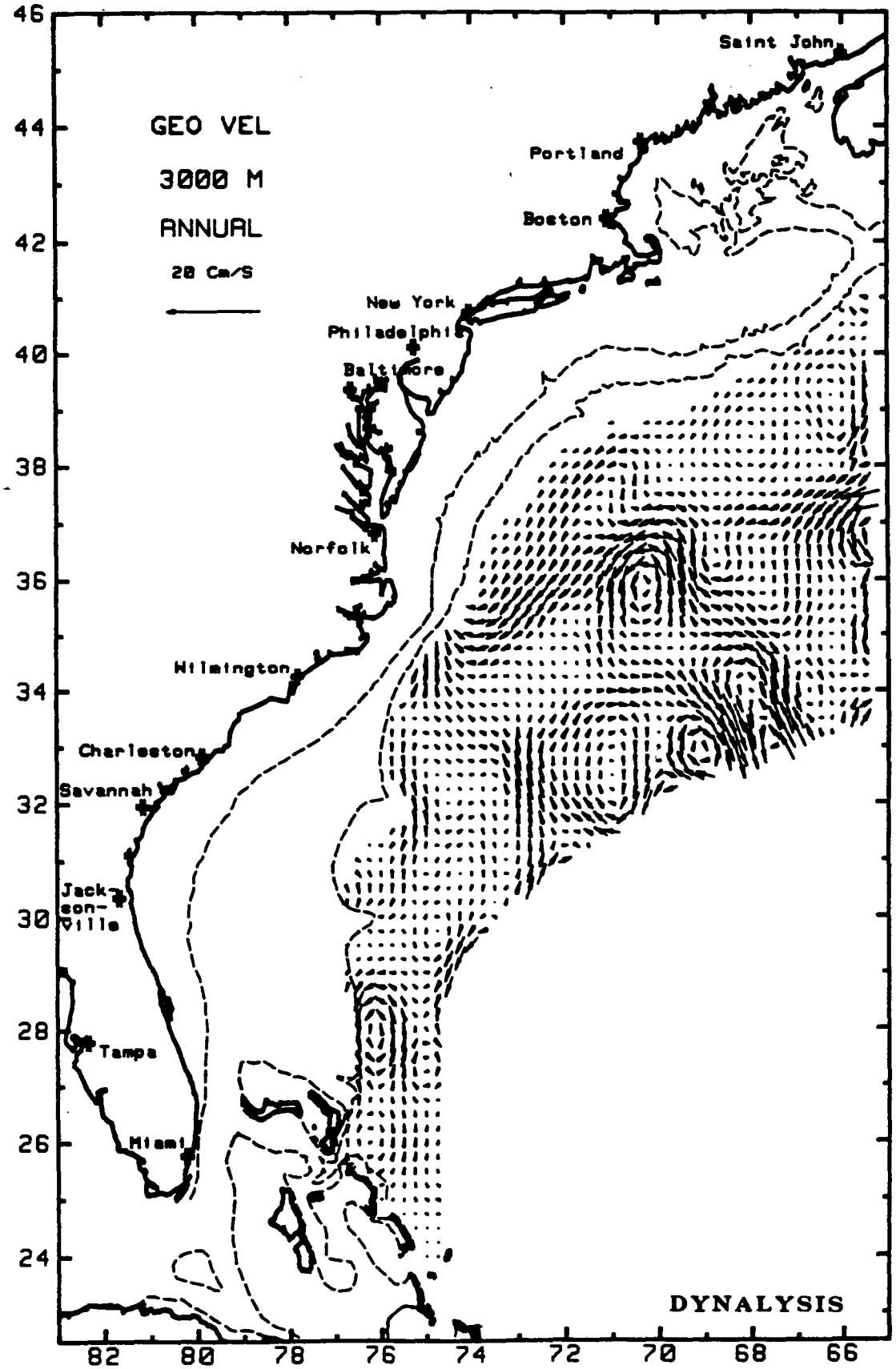

Figure 2.3.7 Geostrophic velocity at 3000 m depth for the annual case.

Figure 2.3.3 shows the elevation distribution and Figure 2.3.4 the surface geostrophic velocities. The cyclonic eddy in the MAB is clearly evident in the elevation distribution. The alongshore pressure gradient thought to be responsible for the southwestward flow on the MAB shelf [Csanady, 1978] and the flow on the Georgia Bight shelf [Atkinson et al., 1983] are readily evident in the elevation distributions. The surface geostrophic velocities essentially reflect the sea surface elevation gradients and clearly depict the southwestward flows on the MAB shelf.

Figures 2.3.5 through 2.3.7 show the distributions of total velocity at the surface, and of geostrophic velocities at 500m and 3000m depths. The Gulf Stream can be clearly seen at all but 3000m depths. The penetration of the flow from MAB southward of Cape Hatteras is noteworthy as well as the strong flow southward of this flow all along the shelf break in the MAB. The deflection of the Gulf Stream at the Charleston Bump can be clearly seen at 500m depth, as well as the swing inshoreward of the Gulf Stream near Jacksonville. The noisy distributions at 3000m are undoubtedly due to sampling biases. Nevertheless, the flow toward the equator by the undercurrent below the Gulf Stream is apparent in the distribution at 3000m. The surface velocity distributions exhibit many well-known circulation features in the ECS as described below.

The principal difficulty in comparing the model results to observations is the lack of <u>long term</u> current meter data that can be considered to be representative of the climatological values desired. It is hard to find records more than a few months or a year long in most regions of the ocean. The coastal shelves on the east coast are no exception. Despite the "large" amount of data available on this coast, which is certainly extraordinary, it is difficult to derive climatological averages that are sufficiently representative. Therefore most of the comparison attempted is rather "anecdotal" in nature.

It is convenient to divide the ECS into three regions, the South Atlantic Bight (SAB) south of 36°N latitude, Middle Atlantic Bight (MAB) between 36°N and 42°N, and the Gulf of Maine (GOM) and Georges Bank regions in the north. We will discuss the model results for these three regions and compare the salient features with the available observations.

A comprehensive and the most recent discussion of the circulation in the Gulf of Maine and Georges Bank at the northern end of the ECS can be found in Butman et. al. [1982]. They have summarized the existing knowledge of the currents in these waters based on the earlier investigation of Bigelow [1927], drifter-bottle studies of Bumpus [1973 and 1976] and Bumpus and Lauzier [1965] and their own extensive observational program. Modelling of the Gulf of Maine and a brief description of the salient features of the circulation in the Gulf of Maine and Georges Bank can be found in Greenberg [1983]. From these investigations, it appears that the salient features of the circulation in the northern ECS are the anticyclonic circulation around Georges Bank of 5-10 cm s^{-1}, which is a large cyclonic gyre (the Maine eddy) in the Gulf of Maine with flow into the Gulf and the Bay of Fundy around Nova Scotia. Anticyclonic circulations are frequently present around Nantucket Shoals [Bigelow, 1927; Bumpus, 1973; Butman et al., 1982] and Browns Bank [Smith, 1983]. There have been suggestions [Csanady, 1974] that the circulation features in the Gulf and on the Georges Bank are driven by the wind. Wind stress data presented in Section 2.1 should help clarify the driving mechanism. The flow to the west of Nantucket Shoals is consistently west-southwestward at 5-10 cm s^{-1} and continues along the Middle Atlantic Bight shelf southwestward with similar intensities, leading Butman et al. [1982] to suggest the source of much of the MAB waters to be the Georges Bank region. Flow around Georges Bank is clockwise at all depths according to Butman et al. [1982] although it gets weaker with depth.

Seasonal variations in the circulation patterns are not as clearly defined. Bumpus and Lauzier [1965] found no gyre on the Georges Bank in fall and winter and no definite pattern in the Gulf of Maine in winter. These circulation patterns are apparently strongest in spring [Butman et al., 1982]. However a clear delineation of seasonal variations is yet to be made.

There are many similarities between the above depiction of currents and the present results. Since seasonal variations are not well known, only annual results will be used for comparison. Clockwise flow around Nantucket Shoals is clearly seen. The flow into the Bay of Fundy around Nova Scotia is present as well as flow along the Maine coast and out of the Gulf near Cape Cod. West-northwestward flow of the right magnitude can also be discerned around the Nantucket Shoals and along the MAB shelf and offshore waters. Strong flow below 1000 m along the isobaths from way up north all along the entire northern portion of the ECS is noteworthy as well as its union with Gulf Stream waters near Cape Hatteras. Some of this flow appears to continue southward into the SAB as an undercurrent below the Gulf Stream. The reason for the strong, most probably spurious, coastward flows near New York Bight and Long Island Sound is not clear. It might be that the model basin is too shallow in this region compared to reality and strong winds or baroclinic effects then tend to produce unrealistically large currents.

Circulation in the Middle Atlantic Bight has been summarized most recently by Beardsley and Boicourt [1981]. From their work and the earlier studies of Beardsley, Boicourt and Hansen [1976], Beardsley and Flagg [1976], Beardlsey and Winant [1979] and Hansen [1977] as well as the drifter-bottle studies of Bumpus [1973], it is apparent that the characteristic feature of the circulation in the MAB is the southwestward mean flow at all depths along the shelf of roughly 2-10 cm s^{-1}. This is

presumably driven by an alongshore sea level slope of about 2×10^{-7} at the shelf break due to the large scale circulation offshore. The average currents generally increase in magnitude offshore and decrease with depth. Superimposed on these are fluctuations due to the wind stresses. Flow off the shelf break exhibits large variability associated with the meanders and eddies of the Gulf Stream. Such variability is clearly evident in satellite IR imagery of the region.

The model results are consistent with the knowledge gleaned from the above studies. The longshore pressure gradient is well reproduced in the model results. Both in the annual and seasonal calculations, the mean southwestward flow along the shelf is clear. The source of nearshore waters in the MAB is the flow around Nantucket Shoals.

The dominant feature of the circulation in the SAB is the Gulf Stream flowing northward off the shelf break. The currents in the Gulf Stream are generally of the order of 1.5 m s^{-1}. The Gulf Stream hugs the shelf break rather tightly as far as Cape Hatteras where it suddenly veers off the coast into the Atlantic Ocean. Near the Charleston Bump, the Gulf Stream undergoes a small deflection in the crossshore direction and this is clearly evident both in annual and seasonal circulations. The flow on the shelf itself appears to be generally in the southerly direction nearshore and northward near the shelf break. The magnitudes are typically less than 10 cm s^{-1}. Unlike the MAB and the GOM, there is no recent comprehensive review of the mean circulation in the SAB, although there does exist a recent compendium on oceanography of the region [Lee, 1983], in which Atkinson et al. [1983] discuss the measurements in the Georgia Bight which confirm the presence of northward flows on the shelf near the shelf break. They also infer an alongshore pressure gradient

similar to that found in MAB to be responsible for the northward mean flow at midshelf. This gradient is equivalent to a sea level slope of roughly 10^{-7} and the model results are consistent with this.

The results of this study are also in agreement with those of the CTM 81 undertaken during Phase II except that a better depiction of the currents of the shelf has now been possible because of the inclusion of the bottom stresses in the vorticity balance. The currents on the shelf, though dynamically more complete, are not much different from those deduced from CTM 81 [Kantha et al., 1981]. It should however be pointed out that while CTM 81 used smoothed topography, CTM 83 does not and in view of this, the circulation deduced is remarkably smooth and certainly less "noisy" than that of CTM 81.

3. GULF STREAM FRONTAL VARIABILITY

Circulation on the South Atlantic Bight shelf and slope is strongly influenced by the mesoscale variability of the western front of the Gulf Stream. The Gulf Stream, once it enters the South Atlantic Bight through the Straits of Florida, flows along the shelf break all the way to Cape Hatteras before veering off the coast into the North Atlantic. The presence, therefore, of the Gulf Stream just off the shelf break profoundly influences the water masses and circulation on the shelves of Florida, Georgia and the Carolinas, especially the outer shelves beyond the 50 m isobath. It is known that the Gulf Stream frontal disturbances such as wave-like meanders and cold core frontal eddies govern the low frequency variability of the flow and water masses on the South Atlantic Bight shelf on time scales of the order of 2 to 14 days [Lee and Atkinson, 1983; see also Allen et al, 1983]. Gulf Stream frontal eddies propagating northward are a primary mechanism for exchange of water, momentum and nutrients between the shelf and the deep ocean. Strong upwelling in the cold core, cyclonic eddies provides a major source of nutrients to the outer shelf [Lee and Atkinson, 1983]. These frontal disturbances propagate northward at typical speeds of 50 to 70 cm s^{-1} (40 to 60 km d^{-1}) and apparently play an important role in transfer of energy between the mean flow and the eddies also.

3.1 Known Characteristics

Gulf Stream frontal eddies occur all along the western edge of the Gulf Stream in the SAB, but appear especially prominent downstream of the Charleston Bump located off Savannah, Georgia. The Bump appears to force the Gulf Stream to deflect offshore [Brooks and Bane, 1981; 1983; and

Bane, Brooks & Lorenson, 1981]. Downstream of the Bump, large wave-like meanders, apparently kinematically akin to the frontal meanders off the Georgia shelf [Lee and Atkinson, 1983], are strikingly evident in satellite thermal imagery of the Gulf Stream (see Figures 18 and 19 of Lee and Atkinson, 1983 for example). Clearly, at least in the vicinity of the Charleston Bump, the lateral excursions of the Gulf Stream appear to trigger frontal disturbances and give rise to wave-like meanders and frontal eddies. Since the axis of the Gulf Stream (or the Florida Current) has been observed to shift laterally even in the region of the Straits of Florida, it is possible that the frequent lateral excursions (natural or forced) of the Gulf Stream might be the primary triggering mechanism for the frontal variability observed all along the SAB shelf.

The morphology of the cyclonic, cold core frontal eddies is such that there is invariably a warm filament to the shoreward side of the eddy [Chew, 1981; Lee, Atkinson and Legeckis, 1981; Pietrafesa, 1983; and Lee and Atkinson, 1983]. Thus the cold cyclonic feature is sandwiched between warm water masses. These features have also been termed shingles and spin-off eddies. The warm filament is narrow and long, typically 10 to 20 km wide and less than 100 km long and appears to be a shallow feature, typically a few tens of meters deep. The warm filament is clearly visible in a cross-shore temperature section and so is the cold dome (see Figure 2 of Chew, 1981 or Figure 7 of Brooks and Bane, 1983).

The wave-like meanders (and frontal eddies), the primary form of mesoscale variability from the Florida Keys to Cape Hatteras, have a life span of up to 3 weeks, wavelengths from 90 to 260 km and move northward at speeds of 20 to 60 km d^{-1} [Chew, Bane and Brooks, 1985]. The residence time of the cold water forming the cold dome appears to be of the order of a week [Chew et al, 1985]. The predominant period of the meanders

downstream of the Charleston Bump appears to be 7-8 days from the current meter records [Bane et al, 1981; see also Brooks and Bane, 1981] and the wavelength 230 km and phase speed 32-35 km d^{-1}. Bane et al [1981] mapped the temperature structure of two meanders using AXBTs and found that these features were very much similar to those observed by Lee, Atkinson and Legeckis [1981] off the Georgia shelf. The meanders involved a cold dome sandwiched between a warm filament and the main body of the Gulf Stream.

Pietrafesa [1983] describes a Gulf Stream frontal event on the Florida/Georgia shelf observed during 1980 using current meters and satellite imagery. The event consisted of a warm tongue inshore of a cold dome with upwelling found both in the cold dome region and below the warm tongue, and anticyclonic rotation in the warm filament. Li et al [1985] studied the low frequency current fluctuations on the Georgia shelf using inverted echo sounders and current meter moorings and found a strong coherence between low frequency fluctuations on the outer shelf and lateral displacements of the Gulf Stream. Lee et al [1981] and Lee and Atkinson [1983] provide a detailed description of the structure of meanders, filaments and frontal eddies off Georgia, and Brooks and Bane [1983] and Bane [1983] describe these features off the coast of North Carolina, using current meter records, hydrography and satellite imagery. The reader is especially referred to Lee and Atkinson's [1983] Figures 20 and 21 for an illuminating display of surface features of a propagating filament structure and the associated cold dome in April of 1980.

3.2 Previous Studies

There have been very few attempts at modelling the Gulf Stream frontal variability or the underlying instabilities of a baroclinic jet. Orlanski [1969] investigated the influence of bottom topography on the stability of a baroclinic jet in a two-layer fluid using an analytical

model. He found that a large amplitude bottom topography can be destabilizing and that the most unstable disturbances differ in characteristics upstream and downstream of Cape Hatteras. Orlanski and Cox [1973] used a three-dimensional numerical model to study unstable waves on an idealized western boundary current, which is in geostrophic equilibrium with a temperature field prescribed by the analytical expression

$$T(x,z) = T_o - \Delta T \left[3 - 2(\delta x + 1)e^{-\delta x}\right]\left[\varepsilon z - 1 \quad e\right]^{2\varepsilon z}, \qquad (3.1)$$

where x is the horizontal, and z the vertical coordinate and the values for T_o, ΔT, δ and ε are 4°C, 7°C, 1.25×10^{-5} m^{-1} and 0.65×10^{-3} m^{-1} respectively. Prescribed bottom topography corresponded to a typical cross-shore variation of bottom depth, except that the shelf was very narrow and therefore the coast was more akin to a vertical wall. The value of horizontal viscosity was typically 100 m^2 s^{-1}, and the cross-shore and alongshore resolutions typically 7.5 km and 20 km respectively. The response of the system to a small random perturbation from equilibrium state was through the development of large meanders of the jet in about 7 to 8 days, with a typical wavelength of about 110 km. There appeared to be a transfer of kinetic energy from eddies to the mean flow consistent with the observations of Gulf Stream frontal eddies (the source of eddy kinetic energy is the mean potential energy). The wave-like meander of the jet did not however have a cold-dome feature associated with it, contrary to the common observations of such features in Gulf Stream frontal meanders. The absence of a wide shelf and the use of unrealistic horizontal shear and transport [Luther and Bane, 1985] might be responsible to some extent for the unrealistic aspects of the meanders.

Luther and Bane [1985] conducted a numerical model study of unstable normal modes of an idealized western boundary current that approximates

the Gulf Stream south of Cape Hatteras using a linear model. The current is in geostrophic equilibrium with a temperature field similar in form to that used by Orlanski and Cox [1983], except that $\hat{c} = 3 \times 10^{-5}\ m^{-1}$ and $\varepsilon = 1.3 \times 10^{-3}\ m^{-1}$, more realistic values according to the authors. Another notable difference is that there exists a broad shelf in the prescribed topography, with a temperature field with no horizontal gradient:

$$T(x,z) = T_o - \Delta T(\varepsilon z - 1)e^{2\varepsilon z} \tag{3.2}$$

and zero velocity. Thus there exists a sharp thermal front with a strong barotropic shear across it. Naturally, both barotropic and baroclinic instabilities can occur in such a system and indeed one unstable normal mode corresponding to a 8-day wave has 80% of the perturbation energy derived from mean potential energy, and the instability is clearly mixed barotropic-baroclinic. The wave motion corresponds to a lateral meander of the current core and has associated warm filaments and cold dome consisting of upwelled water. The phase speed appears to be 40 km d^{-1}, close to the observed values. However the meandering flow was not skewed. Chew, Bane and Brooks [1985] consider skewness of the wave motion (intense offshore current alternating with broad onshore flow) and cold dome to be essential features of Gulf Stream frontal meanders. Moreover, the model does not shed any light on triggering mechanisms of such waves.

Stern [1985] studied the temporal evolution of large amplitude disturbances in a flow with piecewise uniform potential vorticity. He showed that for sufficiently large amplitude disturbances on a front such as the western edge of the Gulf Stream, the waves break laterally; the low vorticity fluid is engulfed into the higher vorticity fluid and is slowly

stretched by the shear flow over long periods of time. Remarkable resemblance of the stretched feature to the observed warm filament feature is noteworthy. Thus it appears that sufficiently large amplitude meanders of the Gulf Stream front might lead to "shingle" formation. Stern [1985] did not address the question of how such a disturbance might be initiated but did not entirely rule out a local barotropic-baroclinic instability as a triggering mechanism.

Chew, Bane and Brooks [1985] conducted a diagnostic study of a cold dome meander and stress the importance of vertical motion in such features. They showed that vertical motion and translation of the meander are closely related and both play a part in the skewness of the meandering flow.

It is clear, from this brief review, that although observationally much is known about the Gulf Stream frontal meanders in the SAB, and their importance to the shelf dynamics is well acknowledged, theoretical studies to understand the initiation and evolution of these features are rather sparse. All that can be said from the studies so far is that barotropic-baroclinic instability might be the underlying cause and a lateral deflection of the Gulf Stream due either to natural shifts in its axis or due to a topographic feature such as the Charleston Bump might be the trigger. No known efforts have been made to simulate their evolution in a realistic context. It is the object of the following Section to describe a series of numerical experiments to study the initiation and evolution of Gulf Stream cold dome meanders using a three-dimensional numerical model.

3.3 General Circulation Model

The model, as described in Oey, Mellor and Hires,[1985], is a full three-dimensional time dependent model which includes the solutions of 8

simultaneous differential equations. Vertical mixing is determined with the use of a two variable second order turbulence closure model.

This model is a subset of the more complete orthogonal curvilinear coordinate system model presented in Blumberg, Kantha, Herring and Mellor, [1984]. In the latter model the curvilinear coordinate system may be shaped to conform to coastal features and variable grid spacing used to place high resolution in regions of interest. These capabilities increase efficiency by eliminating wasted grid points which would be required to obtain equivalent resolution in a more conventional rectangular grid. The vertical grid is also a variable, topographically conformal grid. Therefore, the profile in shallow regions is resolved with the same number of grid points as that in the deep.

The ultimate objective is, of course, to predict actual Gulf Stream variability for comparison with observational data. However, the more limited purpose of the present study is to ascertain possible causes of this variability and demonstrate the capability of the model to reproduce these characteristic features. For these purposes, the rectangular but non-uniform grid is the optimum choice.

The focal point of the study is the western boundary of the Gulf Stream in the region southeast of the coast of North and South Carolina. The path of the Gulf Stream here is relatively straight and therefore may be well represented on a rectilinear coordinate system. A possible coordinate system is illustrated schematically in Figure 3.3.1. This grid has a high resolution band which approximately coincides with the mean western boundary of the Gulf Stream. The lateral high resolution portion is 5 km increasing to 45 km out to sea. The longitudinal spacing is 10 km throughout.

For simplicity of interpretation and comparison with other research studies a further simplification has been made. Although there is some

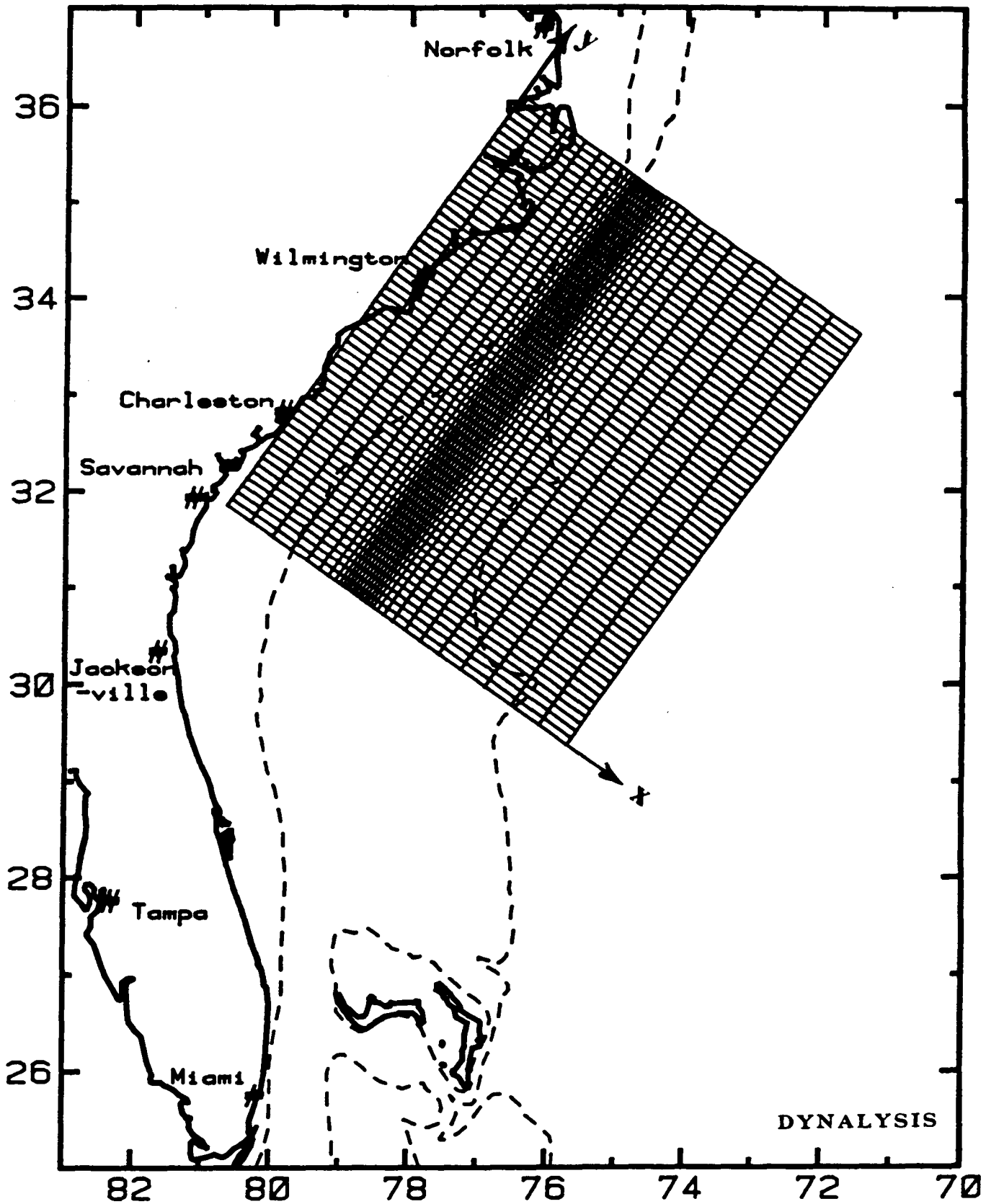

Figure 3.3.1 The computational grid shown schematically off the coast of the Carolinas.

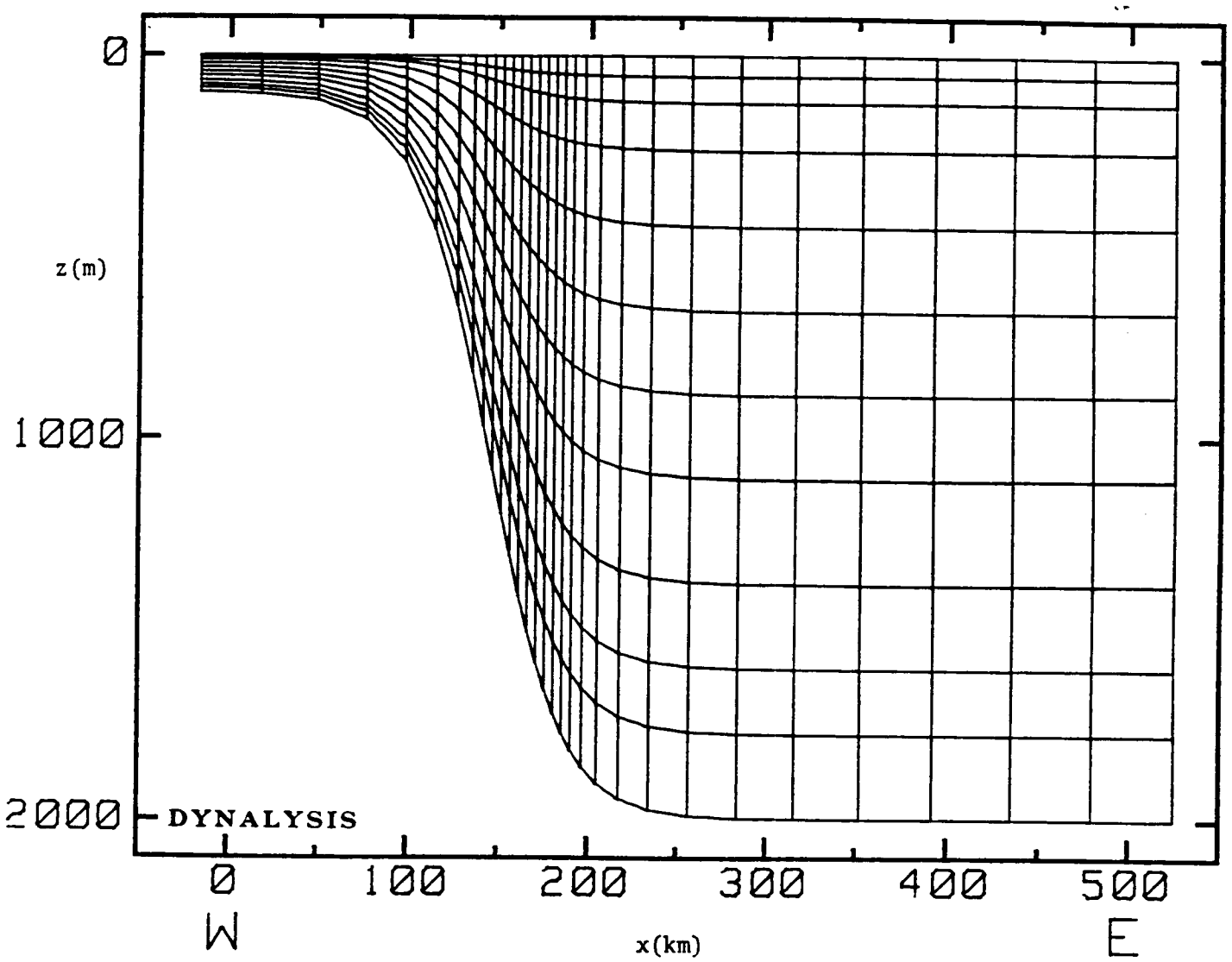

Figure 3.3.2 Vertical cross-section of the computational grid shown in Figure 3.3.1.

topographic variation in the region shown in Figure 3.3.1, the generally monotonic characteristics and relative uniformity of the bottom may be approximated by topography uniform along the y coordinate. The topography is set according to the relation

$$D = 100 + 950 \left[1 + \mathrm{Tanh} \left(\frac{x - 145}{40} \right) \right] , \tag{3.3}$$

in accordance with Luther and Bane [1985]. The topography and grid spacing are shown in Figure 3.3.2 and specified in Table 1.

For all cases the initial temperature distribution is prescribed as

$$T(x,z) = T_o - \Delta T \left[3 - 2(\delta x_b + 1)e^{-\delta x_b} \right] (\varepsilon z - 1)e^{2\varepsilon z}, \tag{3.4}$$

following the Luther and Bane version of Equation (3.1) where $x_b = x - x_f$ and δ, ε and x_f are 3.0×10^{-5} m^{-1}, 1.3×10^{-3} m^{-1} and 100 km respectively. Similarly the surface velocity distribution is

$$v(x,o) = 3ga\Delta T(2f\varepsilon)^{-1} \delta^2 x_b e^{-\delta x_b} , \tag{3.5}$$

where $a = 1.15 \times 10^{-4}$ $°C^{-1}$ and g and f are the acceleration due to gravity and the Coriolis parameter respectively. The subsurface velocity field was prescribed to be in geostrophic equilibrium with the temperature field.

The boundary conditions, with some important variations, as described below, were prescribed consistent with Equations (3.4) and (3.5) throughout the calculation. On the upper, outflow boundary the temperature was upwind differenced so that it was fully advected out of the domain.

Table 1. COMPUTATIONAL GRID DEFINITION

Horizontal East-West Grid

I	x(km)	Δx(km)	D(m)	$A_M(m^2/s)$
1	0.0	34.0	1.00	767
2	34.0	30.0	107.36	767
3	64.0	25.0	131.90	663
4	88.0	19.0	204.39	555
5	108.0	14.0	352.63	452
6	122.0	10.0	555.20	364
7	132.0	7.0	751.68	302
8	139.0	5.0	906.24	269
9	144.0	5.0	1031.00	258
10	149.0	5.0	1144.68	256
11	154.0	5.0	1257.95	256
12	159.0	5.0	1363.22	256
13	164.0	5.0	1462.44	256
14	168.0	5.0	1549.98	256
15	173.0	5.0	1628.65	256
16	178.0	5.0	1695.17	256
17	183.0	5.0	1752.79	256
18	188.0	5.0	1799.99	258
19	193.0	7.0	1842.69	270
20	200.0	10.0	1886.37	303
21	210.0	15.0	1929.76	365
22	225.0	19.0	1965.32	453
23	244.0	25.0	1986.70	558
24	269.0	30.0	1996.13	669
25	299.0	34.0	1999.13	773
26	333.0	38.0	1999.84	868
27	372.0	42.0	1999.98	947
28	413.0	44.0	2000.00	1011
29	457.0	45.0	2000.00	1051
30	502.0	45.0	2000.00	1051

Vertical Grid

K	$\sigma = z/D$	$\Delta\sigma$
1	0.000	0.02800
2	-0.028	0.02800
3	-0.056	0.05500
4	-0.111	0.11100
5	-0.222	0.11100
6	-0.333	0.11100
7	-0.444	0.11100
8	-0.555	0.11200
9	-0.667	0.11100
10	-0.778	0.11100
11	-0.889	0.11100
12	-1.000	

On the lower and upper boundaries, the external mode (barotropic) velocities were determined from the vertical integral of the geostrophic velocity obtained from Equations (3.4) and (3.5). On the right and left hand boundaries the velocities were set equal to zero.

The internal mode (baroclinic) velocities normal to the inlet and outlet boundaries were determined by the Sommerfeld radiation condition. The tangential velocities were null on the inflow boundary and freely advected outward on the outflow boundary.

The north-south grid increment was 10 km whereas the east-west increment varied according to Table 1 where we also tabulate the depth, H, and the horizontal eddy viscosity. The latter is by and large derived from experience as that which reduces numerical grid noise to an acceptable level. The thermal diffusivity, A_H, was, in the main, set equal to A_M. For the calculations described in Section 3.4.3, calculations were also performed where A_M was doubled whereas A_H was halved; only a very small change in the results was obtained.

3.4 Results from Numerical Experiments

A null case was run to serve as a benchmark and also to explore the possibility of triggering a frontal instability without the aid of any external forcing. The null case simulation consisted of a 20-day prognostic run in which the temperature and velocity fields were initialized to near equilibrium conditions (geostrophy, which of course ignores nonlinearity and horizontal diffusion). These fields were then allowed to evolve with steady temperature and velocity prescriptions on the southern boundary. Despite the high resolution (5 km) in the vicinity of the front, no instabilities developed. Instead the Gulf Stream diffused slightly as it traversed the domain from south to north, but by and large,

the fields remained the same. It is likely that the alongstream extent of the domain has to be several times the one used (400 km), or periodic boundary conditions as described by Orlanski and Cox [1973] are needed for the instability to manifest itself. Perhaps horizontal viscosity (minimum 256 $m^2\ s^{-1}$) also needs to be decreased. Clearly some kind of external perturbation is needed to coax the Stream to manifest frontal activity of the kind observed in satellite imagery.

A survey of the previous studies concerning Gulf Stream frontal variability suggests three primary modes of external forcing for exciting such frontal activity:

1. Surface forcing by a propagating wind stress curl,
2. Modulation of the Gulf Stream intensity, and
3. Modulation of the lateral position of the Gulf Stream.

Accordingly three sets of numerical experiments were conducted to ascertain whether cold dome meanders of the Gulf Stream front could be triggered. The following sections describe the results of these three cases.

3.4.1. Propagating Wind Stress

In this numerical experiment, the lateral temperature boundary conditions were fixed. The system was forced by wind stress implied by the calculations of Luther and Bane [1985] whereby

$$(\tau_{ox}, \tau_{oy}) = \left(A \cos \left(2\pi \left(\frac{t}{t_p} - \frac{y}{\lambda} \right) \right), 0 \right) \tag{3.6}$$

and where t_p = 8 days and λ = 30 km and A = 5 dynes/cm^2. The wind stress value is rather large and corresponds to a weak propagating storm. Note that the wind stress curl is nonzero and therefore the case is equivalent to the propagating wind stress curl forcing of Luther and Bane [1985].

Note also that the wave length is unrealistically short but we are able here to generate the evolved disturbance and phase for the normal velocity at y = 200 km.

Figures 3.4.1 to 3.4.10 display the near-surface temperature and velocity fields, temperature at 100 m depth and the temperature section on a cross-shore transect at y = 200 km (center of the domain) at intervals of a day from day 11 to day 20 of the simulation. A propagating meander of small amplitude is clearly visible in the horizontal distributions. The propagation speed is about 30 km d^{-1}. It is noteworthy that the surface forcing does not appear to excite any strong frontal activity at the western edge of the Gulf Stream but instead large perturbations do appear on the eastern edge of the Stream. These are clearly evident in the temperature fields, and the sea surface temperature features produced bear a remarkable resemblance to the features observed at the eastern edge of the Gulf Stream in satellite IR imagery (see Figure 19 of Lee and Atkinson, [1983], for example). The implications of this resemblance is not clear but does encourage speculation that the streamer-like features observed on the seaward side of the Gulf Stream might be at least partly wind-related! More experiments with more realistic distribution of wind stress are needed to shed more light on this phenomenon and also to rule out production of cold dome meanders by surface forcing.

3.4.2 Modulation of Gulf Stream Intensity

In this numerical experiment, the system was forced at the southern boundary by a temperature perturbation given by

$$T'(x,z) = A_T \frac{(x - x_c)}{\sigma_x} \exp\left[- \left(\frac{(x - x_c)}{\sigma_x} \right)^2 + \frac{z}{\sigma_z} \right] \cos\left(2\pi \frac{t}{t_v}\right) \qquad (3.7)$$

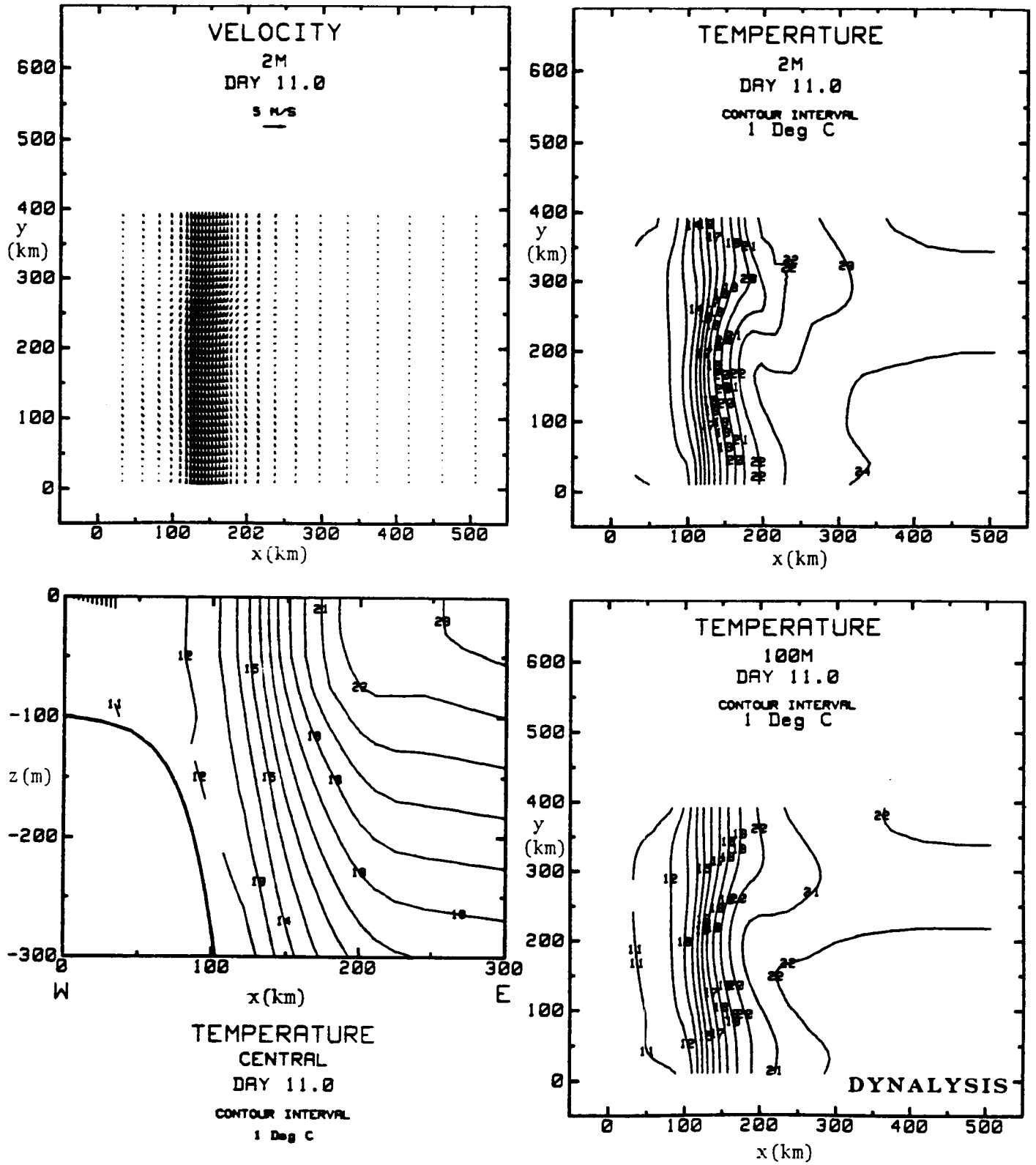

Figure 3.4.1 Calculated fields on day 11 for propagating wind stress experiment.

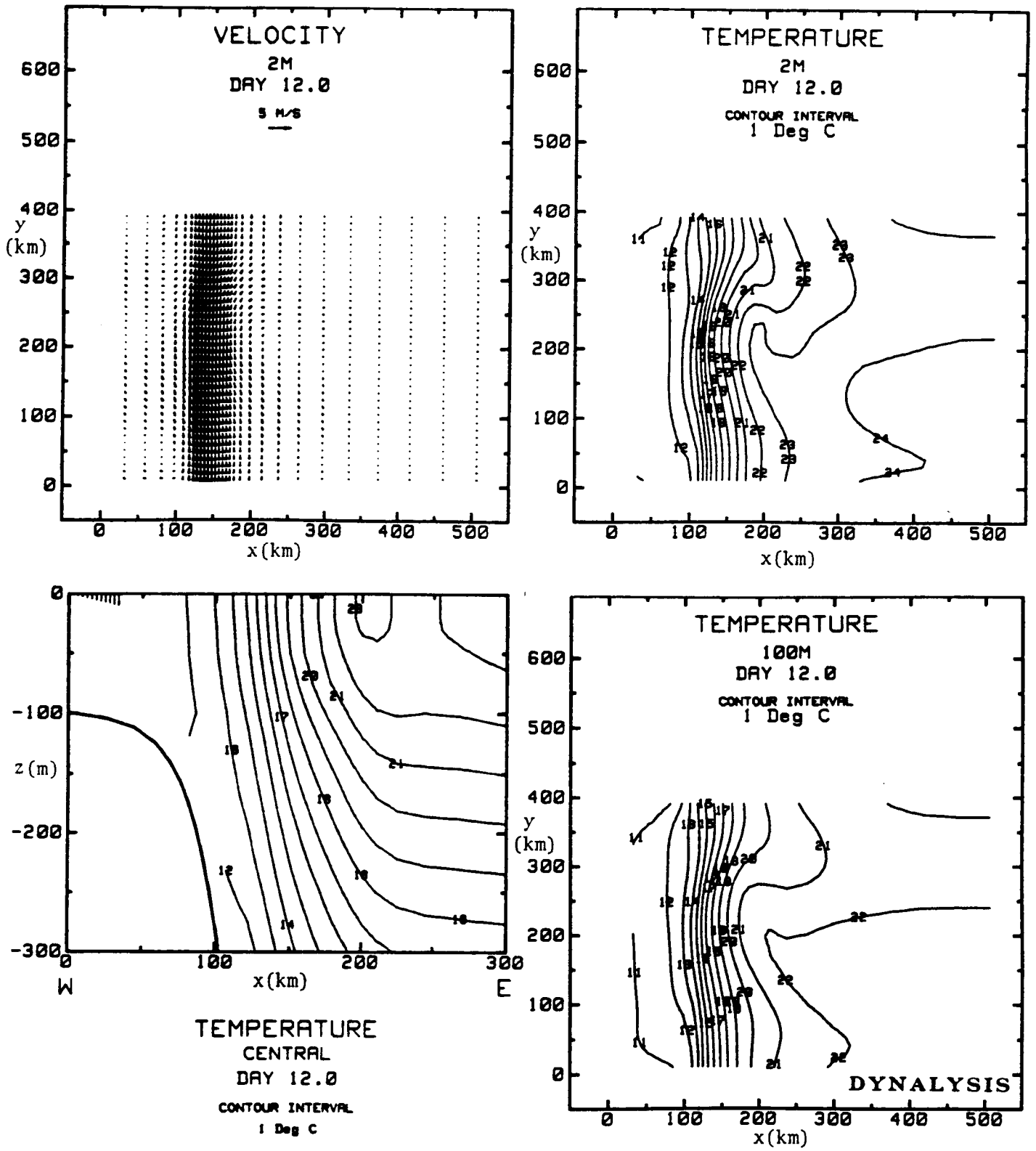

Figure 3.4.2 Calculated fields on day 12 for propagating wind stress experiment.

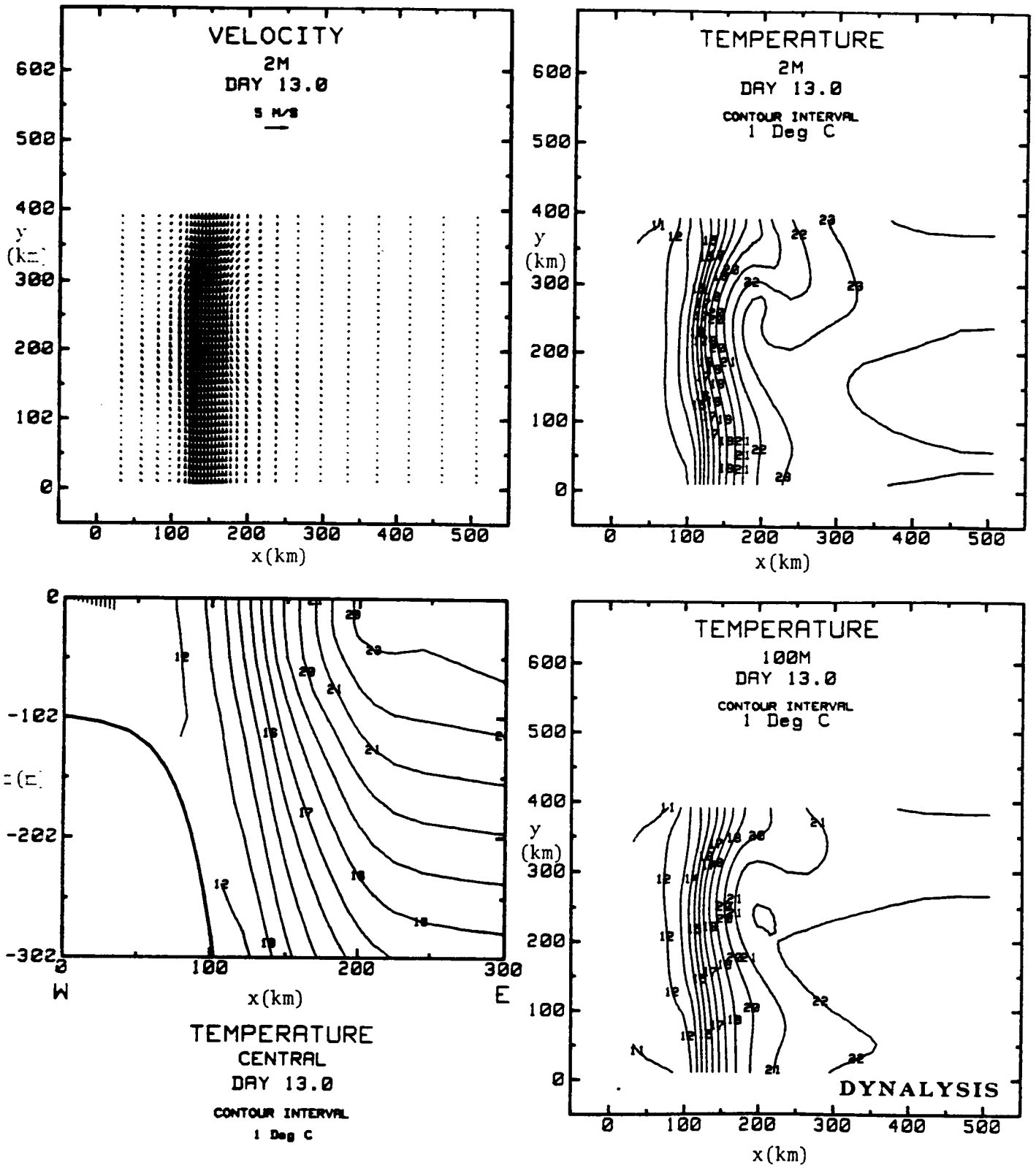

Figure 3.4.3 Calculated fields on day 13 for propagating wind stress experiment.

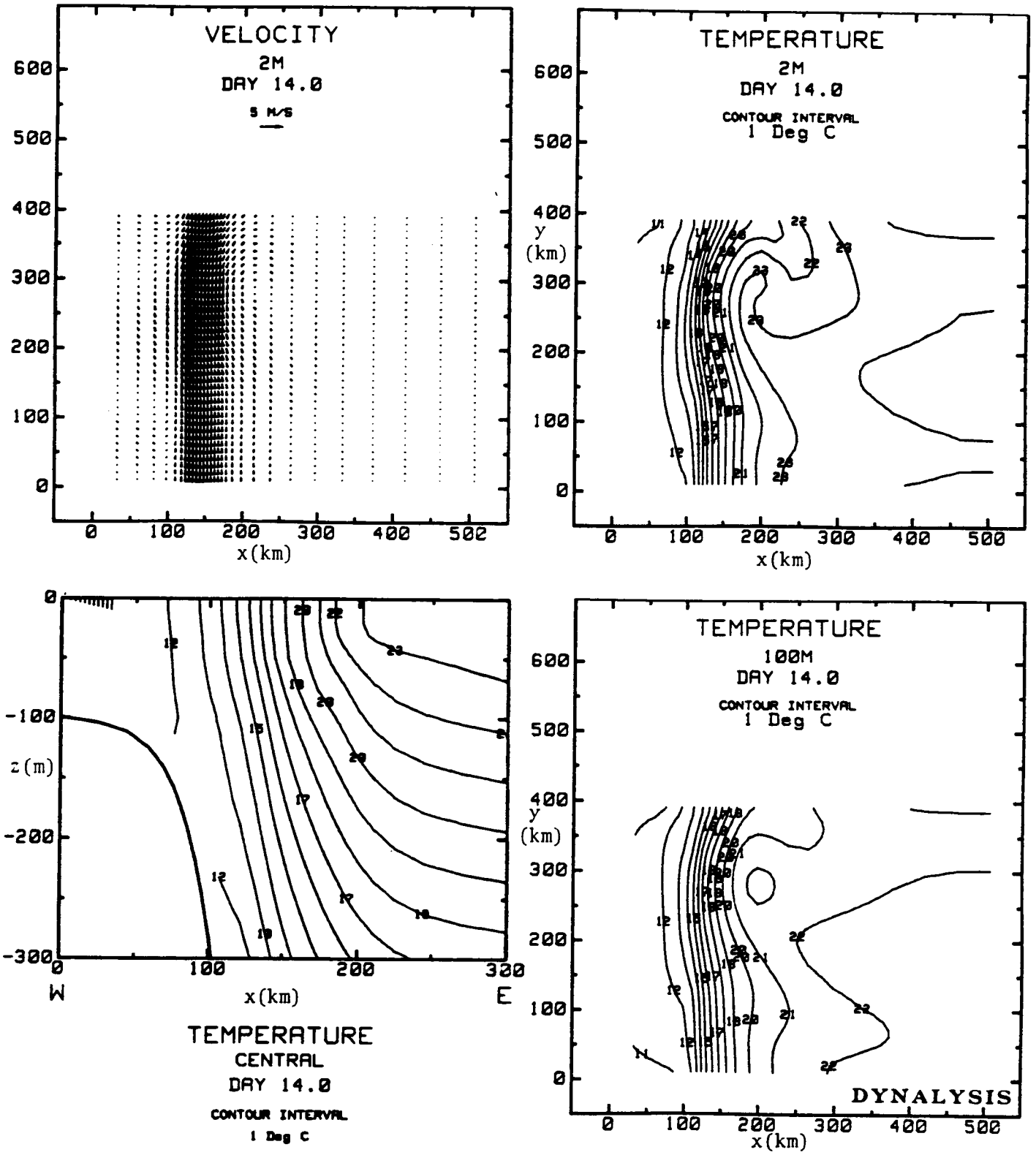

Figure 3.4.4 Calculated fields on day 14 for propagating wind stress experiment.

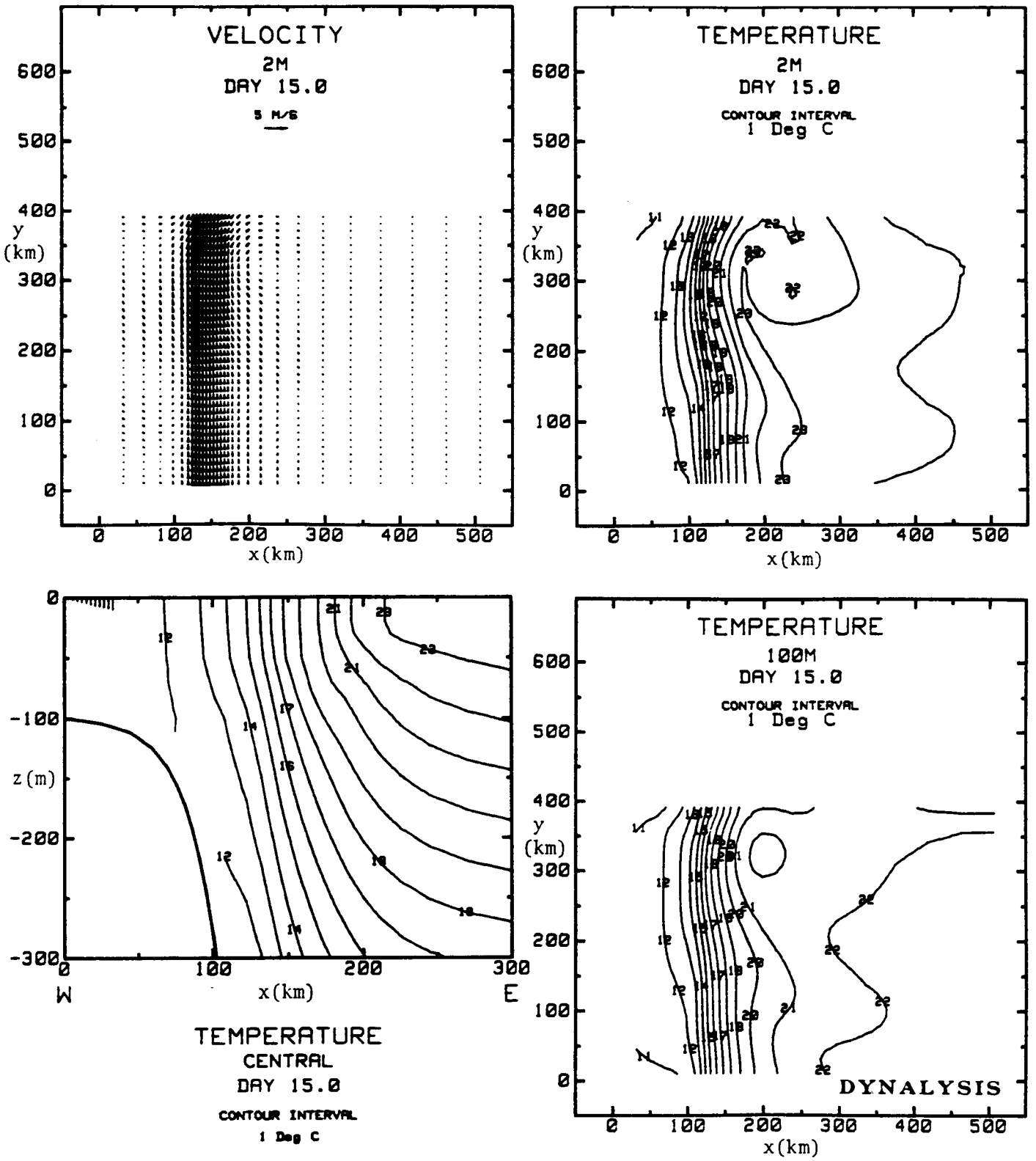

Figure 3.4.5 Calculated fields on day 15 for propagating wind stress experiment.

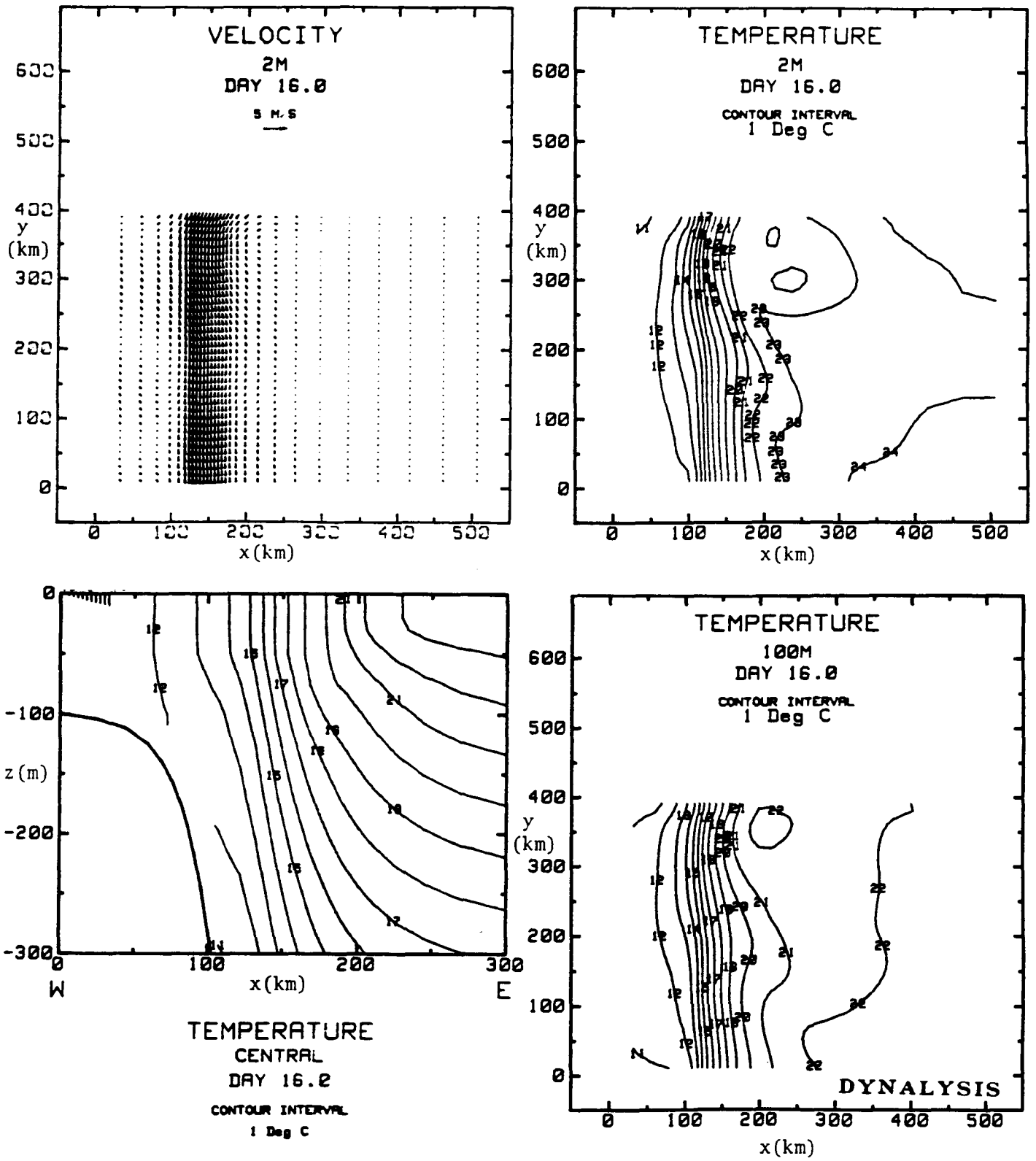

Figure 3.4.6 Calculated fields on day 16 for propagating wind stress experiment.

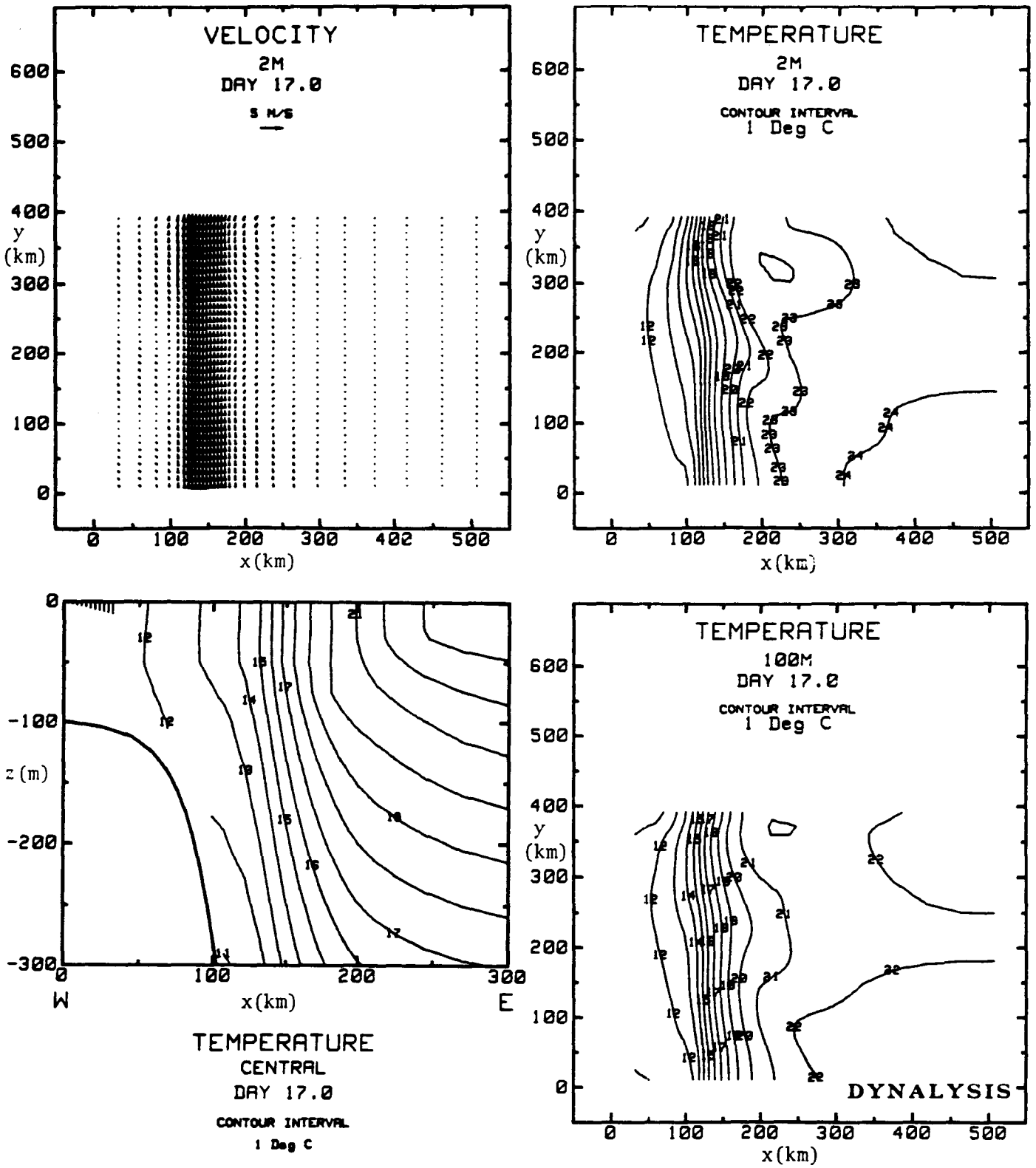

Figure 3.4.7 Calculated fields on day 17 for propagating wind stress experiment.

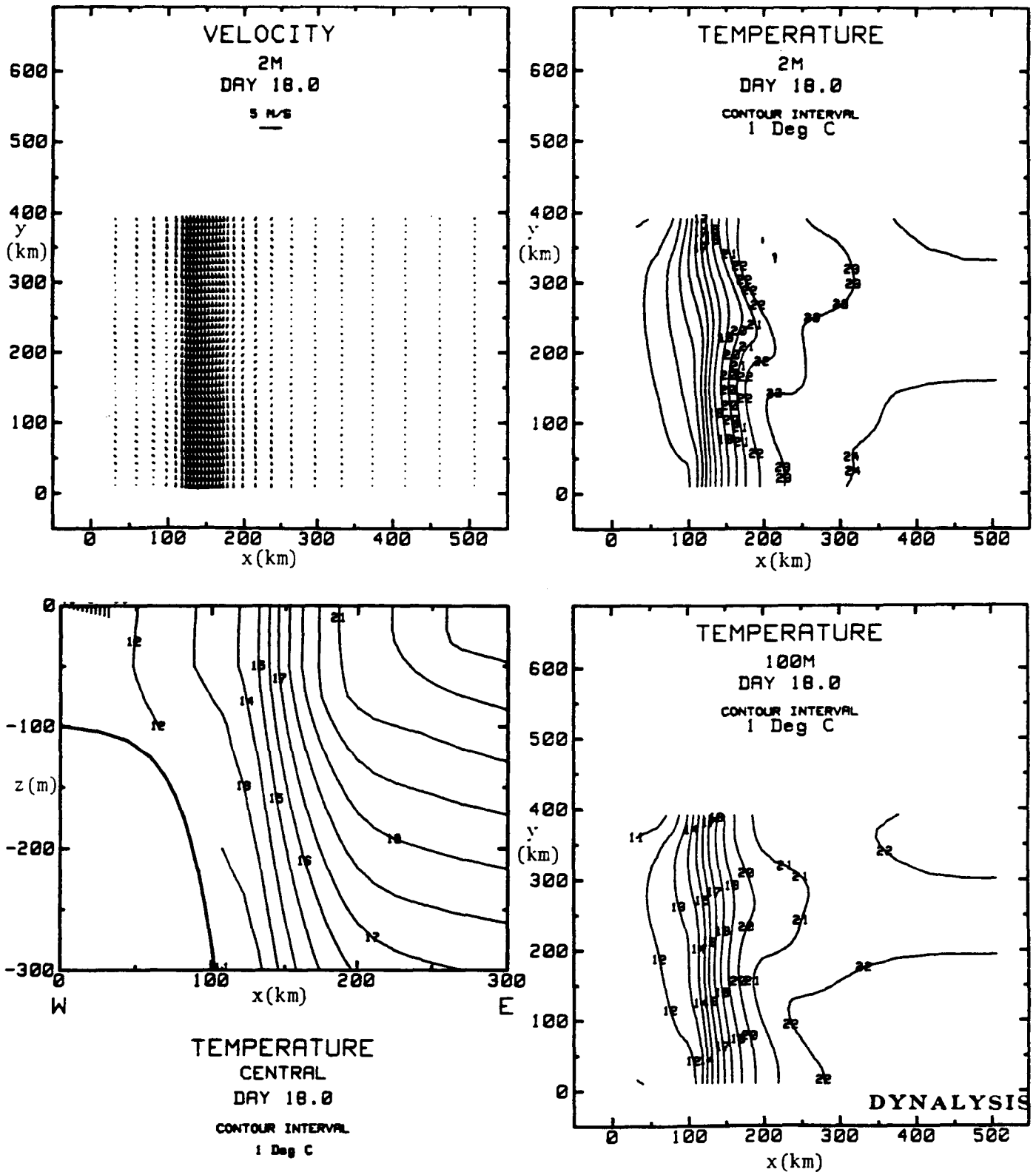

Figure 3.4.8 Calculated fields on day 18 for propagating wind stress experiment.

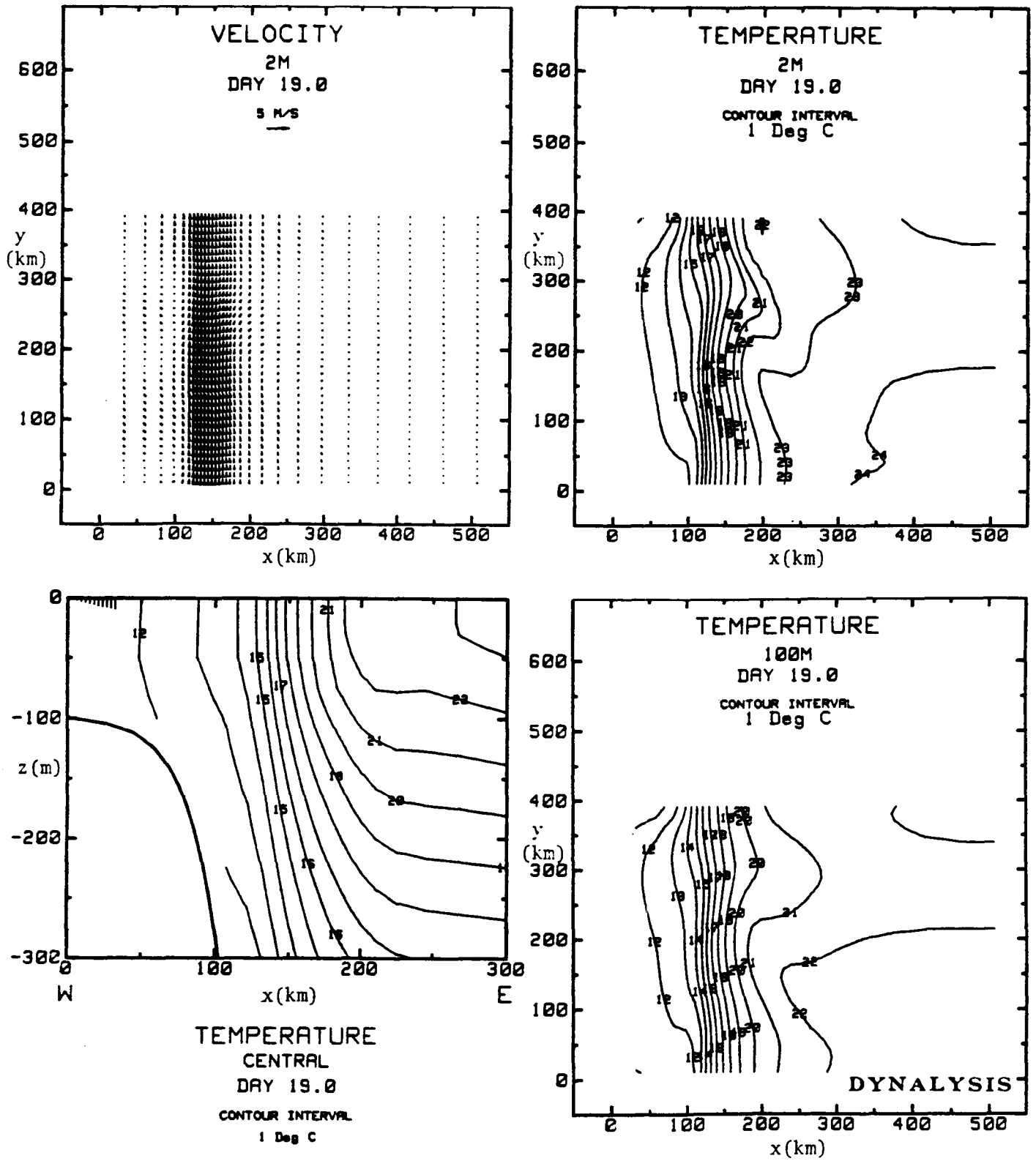

Figure 3.4.9 Calculated fields on day 19 for propagating wind stress experiment.

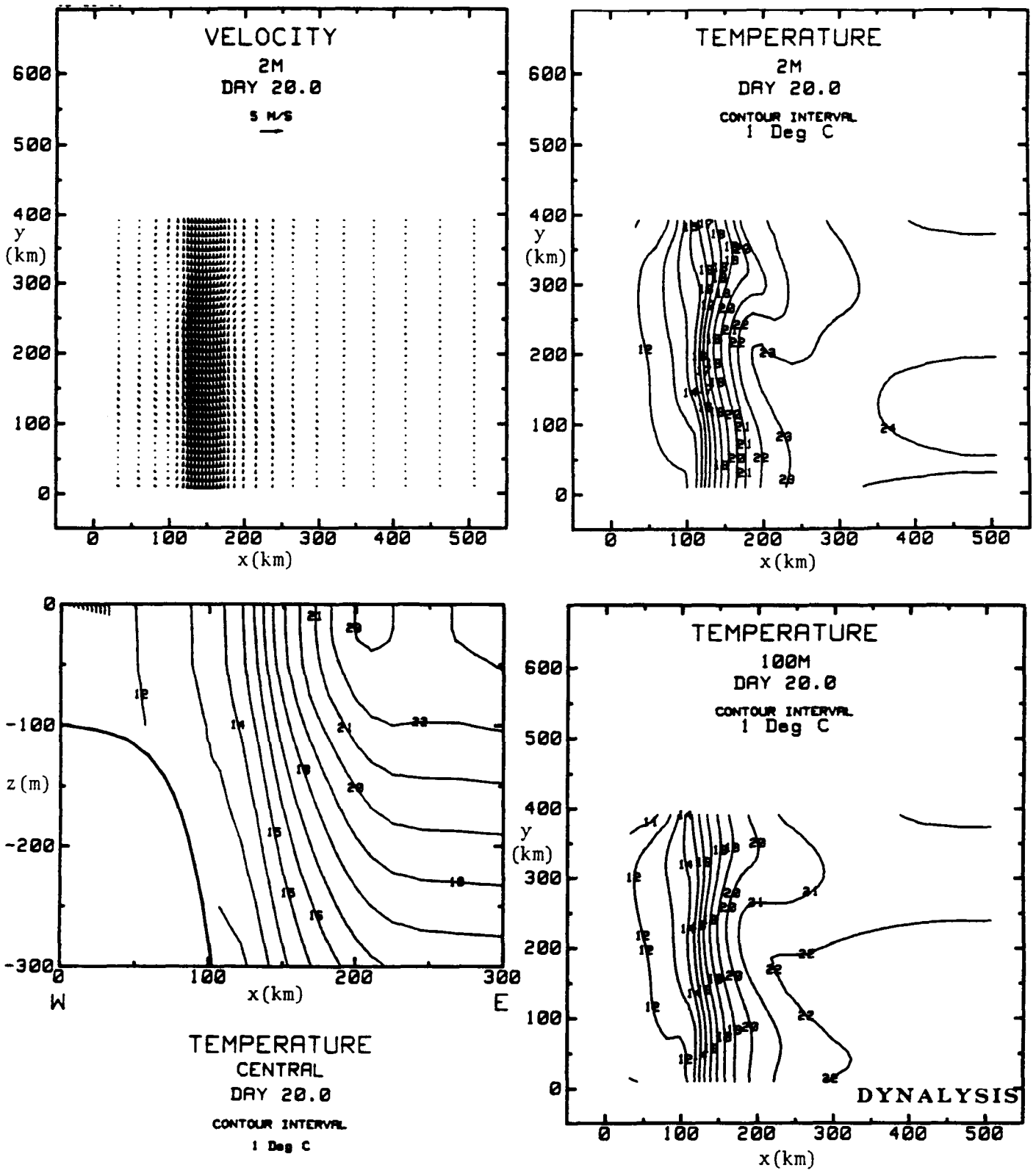

Figure 3.4.10 Calculated fields on day 20 for propagating wind stress experiment.

where A_T = 10°C (note however, that the largest temperature variation is about 4°C), x_c = 135 km, σ_x = 35 km, σ_z = 200 m and t_v = 8 days. This form of perturbation is suggested by the 8-day unstable second mode of Luther and Bane [1985].

Figures 3.4.11 to 3.4.20 show the near surface temperature and velocity fields, the temperature field at 100 m and the temperature section on a cross-shore transect at y = 200 km (center of the domain) at intervals of a day from day 11 to day 20 of the simulation. Again a propagating meander of about 300 km wavelength propagating northward at about 30 km d^{-1} is evident in the surface fields. Once again, apart from the tendency of the Gulf Stream front to sharpen up, no dramatic frontal activity is apparent. Instead the eastern side of the Gulf Stream does tend to have significant perturbations (see the near surface temperature fields) but not as dramatic as the case of the propagating wind stress. No cold dome or warm filament structures are evident in the temperature sections.

It is quite possible that a larger perturbation of the southern boundary temperature is needed to produce cold dome meanders. The wavelength of the meander produced is not believed to be conditioned by the domain size. Once again, a calculation with a larger alongshore extent is needed to establish this.

3.4.3 Modulation of the Lateral Position of the Gulf Stream

This is by far the most elegant way of perturbing the Gulf Stream at the southern boundary in an effort to produce cold dome meanders. Examination of the behavior of the Gulf Stream downstream of the Charleston Bump is strongly suggestive of the fact that an offshore shift in the axis of the Gulf Stream could produce cold dome meanders. Therefore in this experiment southern temperature disturbance was simply

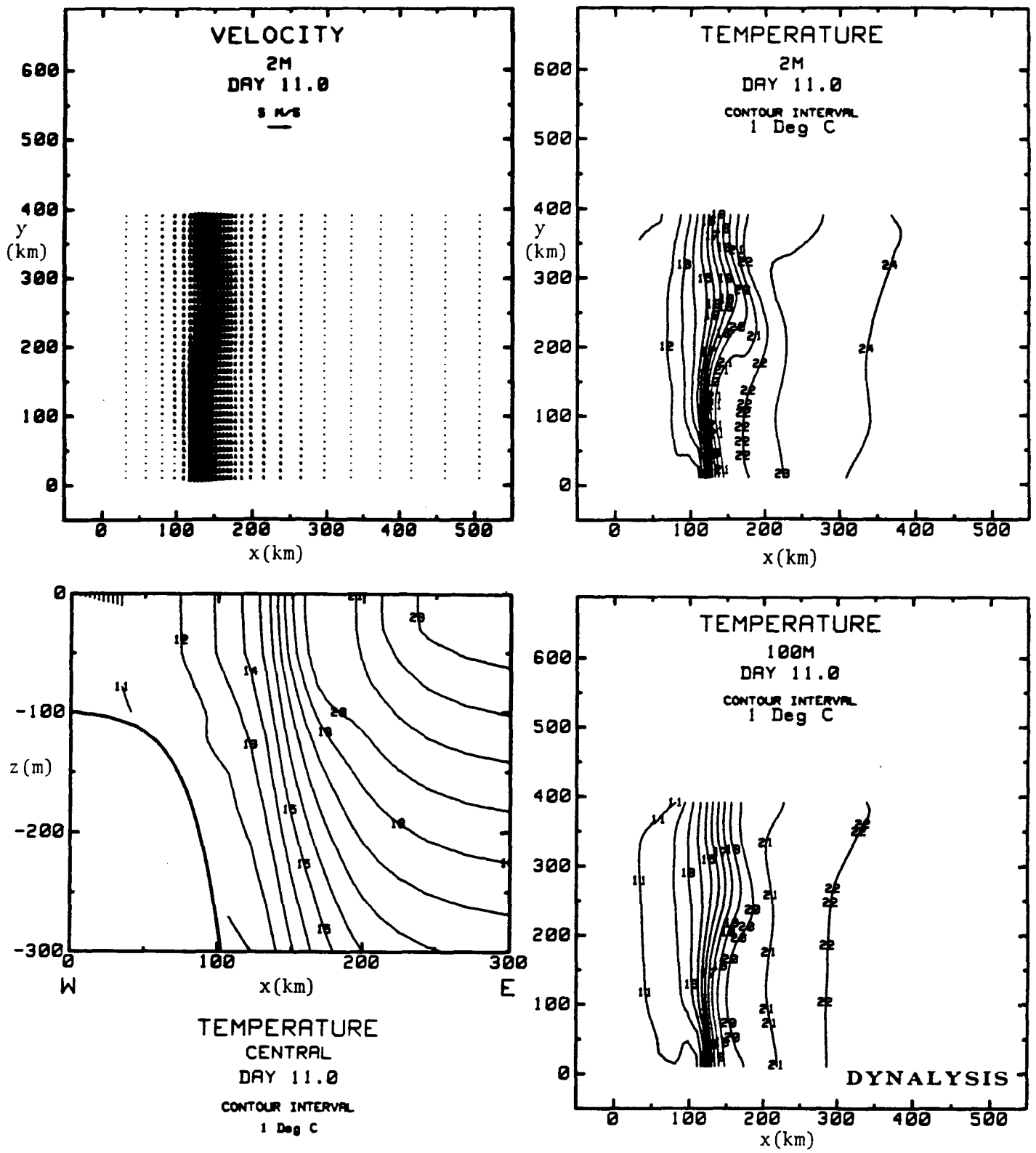

Figure 3.4.11 Calculated fields on day 11 for Gulf Stream intensity modulation experiment.

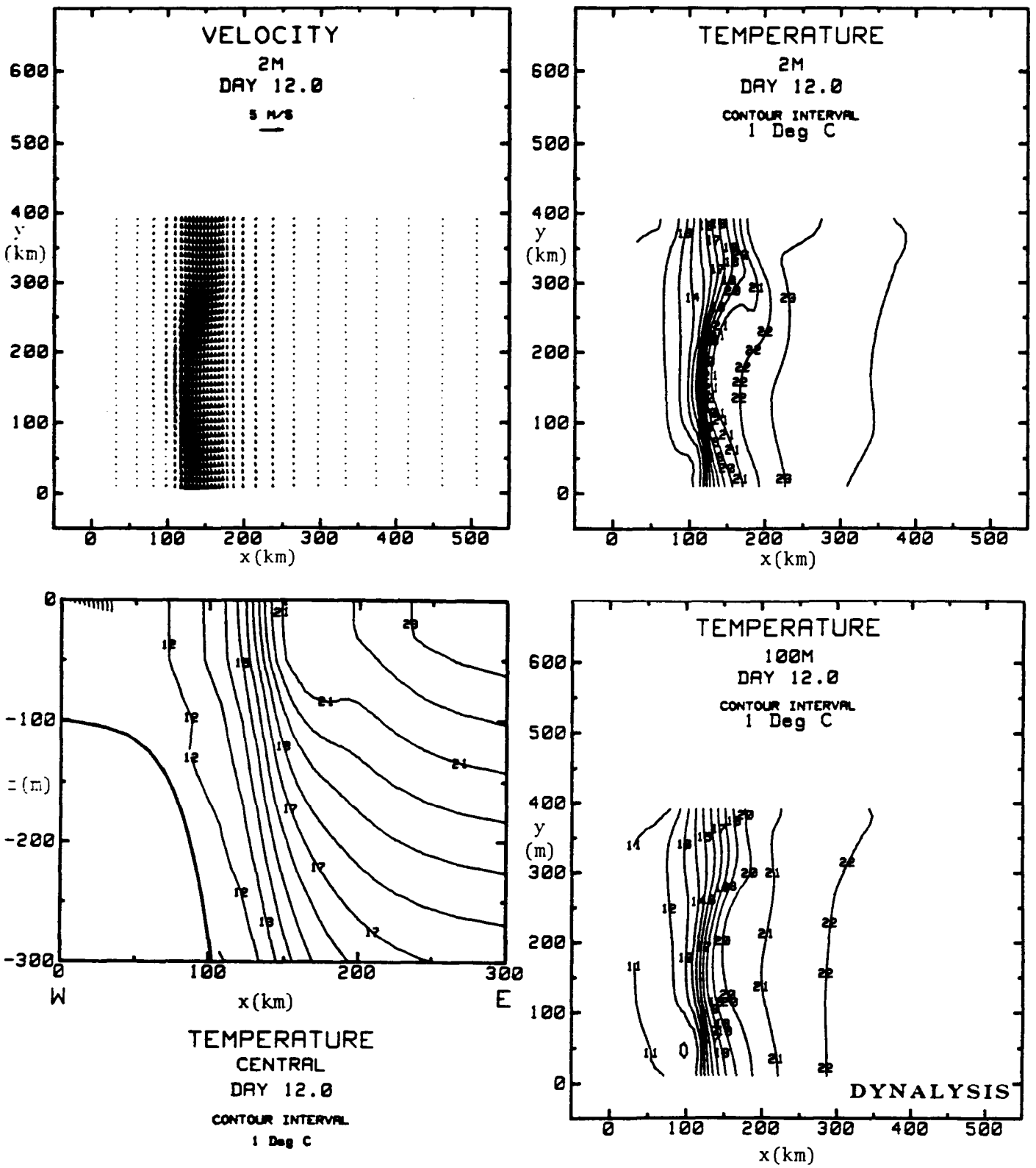

Figure 3.4.12 Calculated fields on day 12 for Gulf Stream intensity modulation experiment.

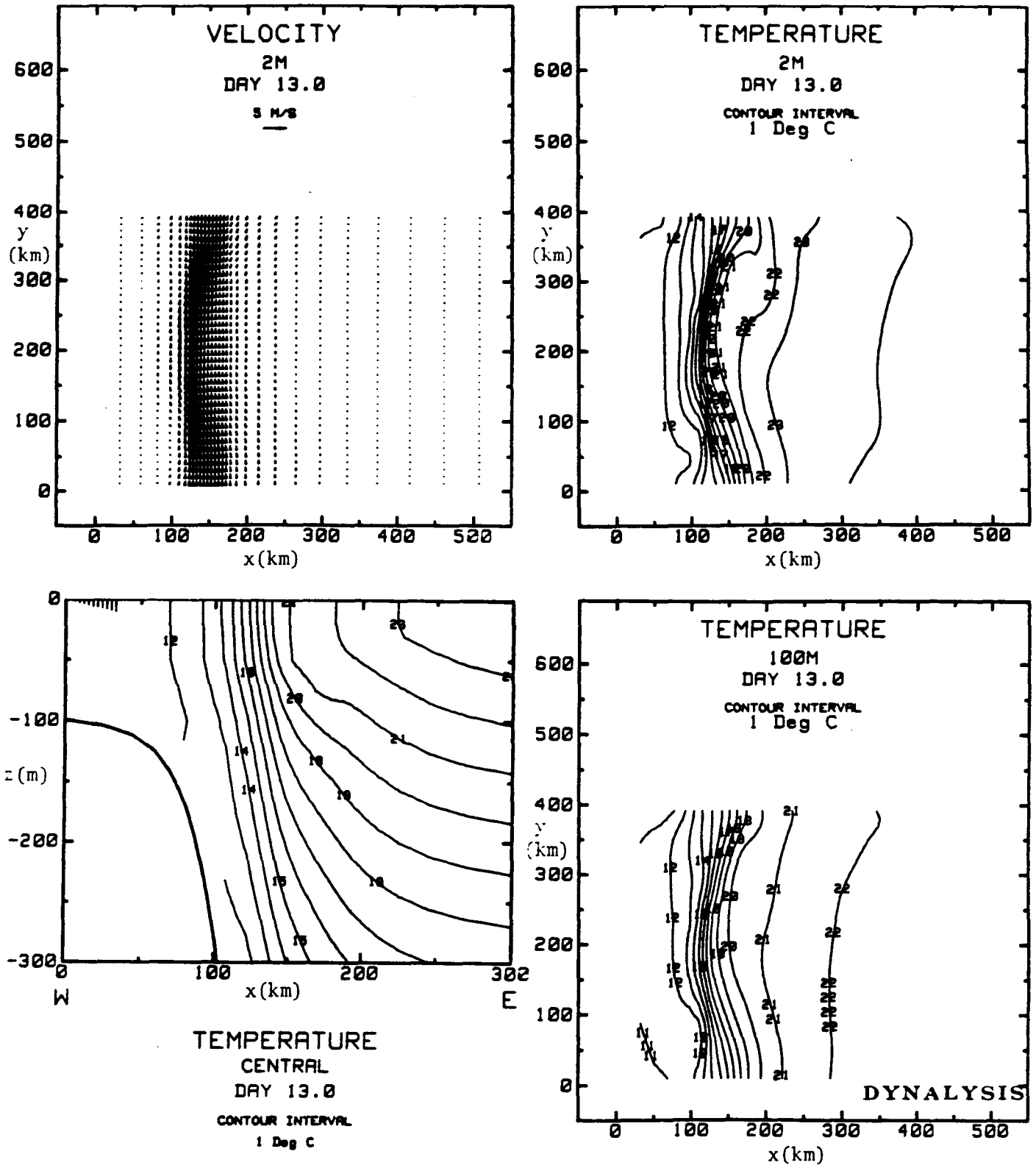

Figure 3.4.13 Calculated fields on day 13 for Gulf Stream intensity modulation experiment.

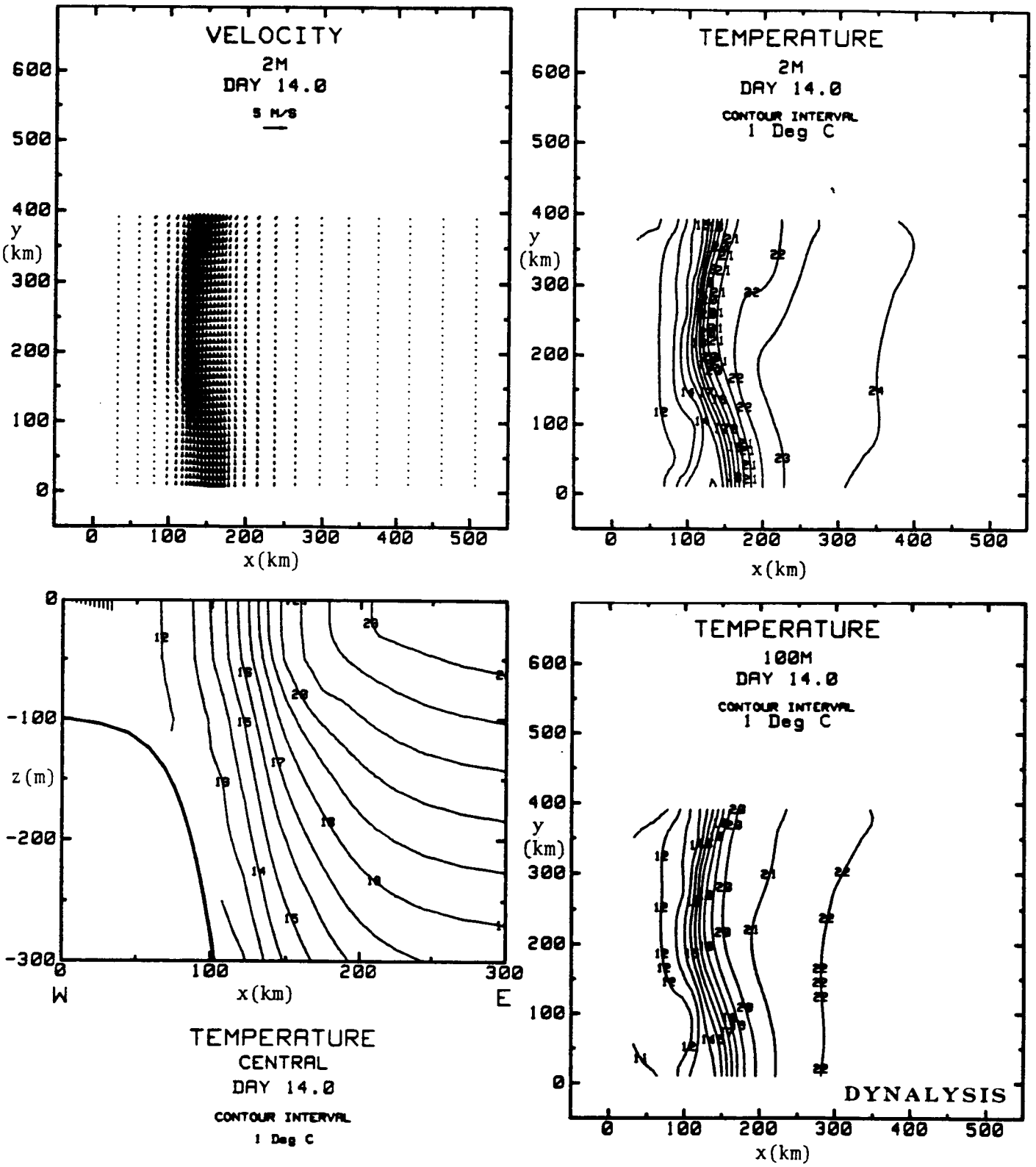

Figure 3.4.14 Calculated fields on day 14 for Gulf Stream intensity modulation experiment.

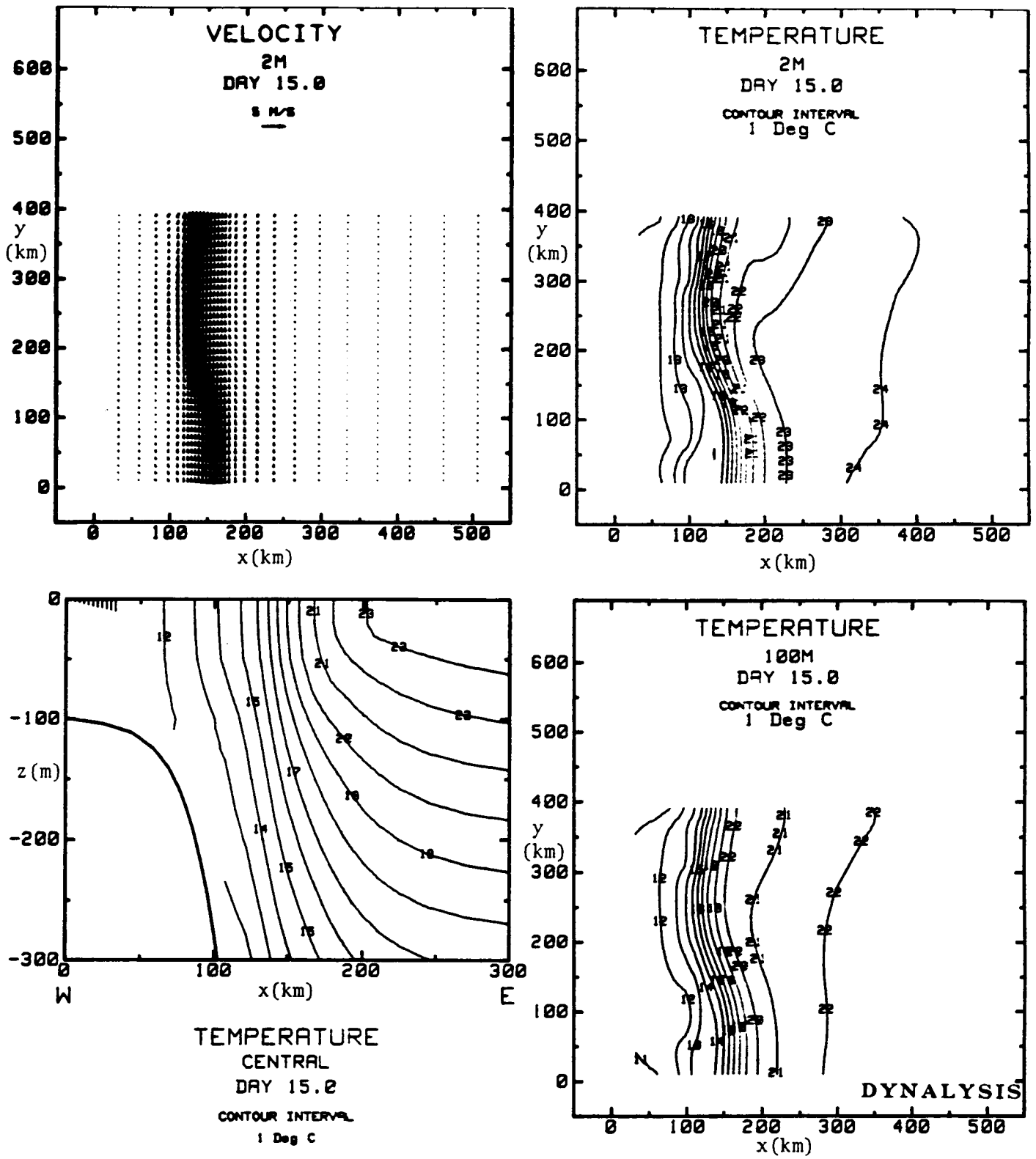

Figure 3.4.15 Calculated fields on day 15 for Gulf Stream intensity modulation experiment.

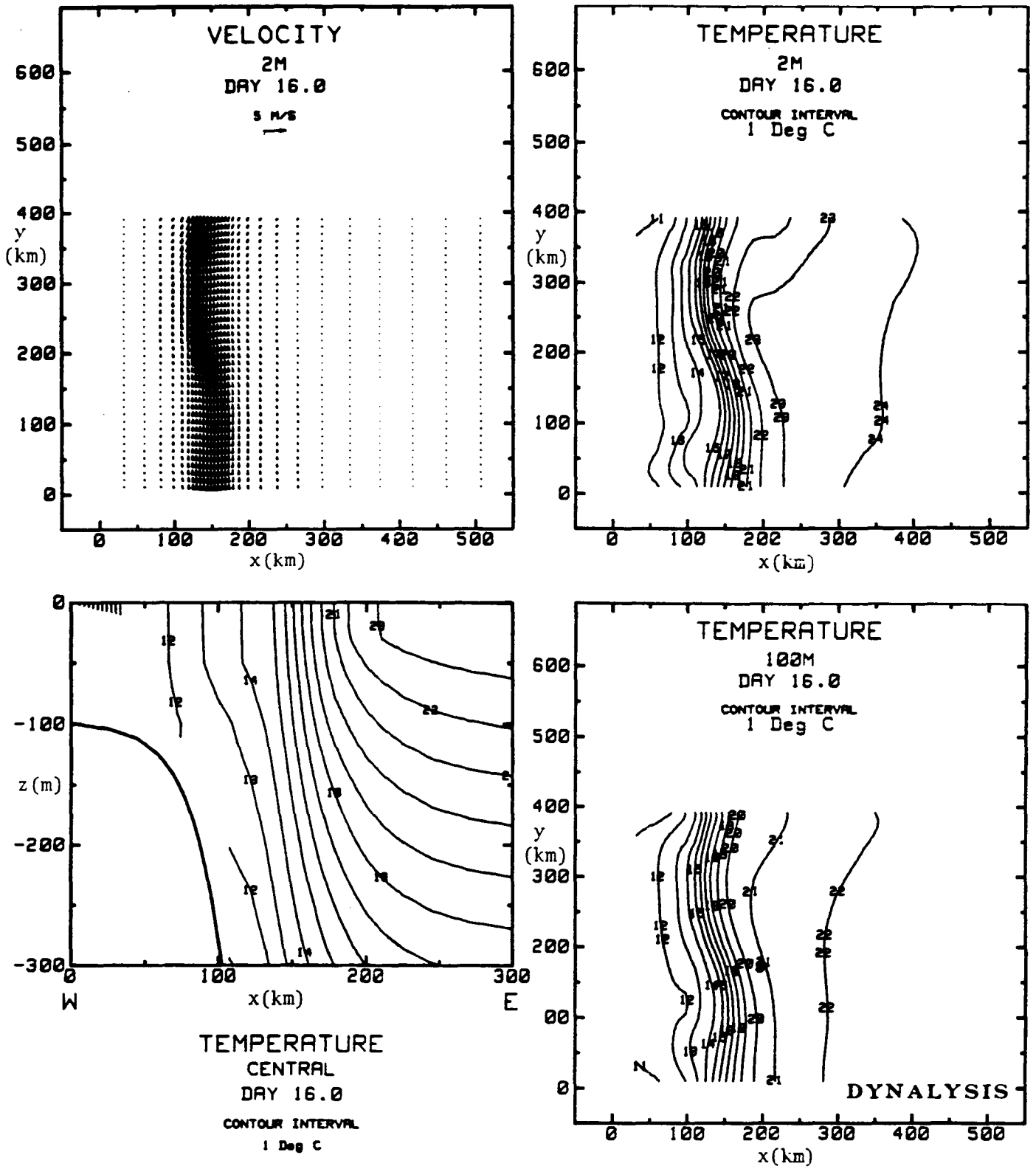

Figure 3.4.16 Calculated fields on day 16 for Gulf Stream intensity modulation experiment.

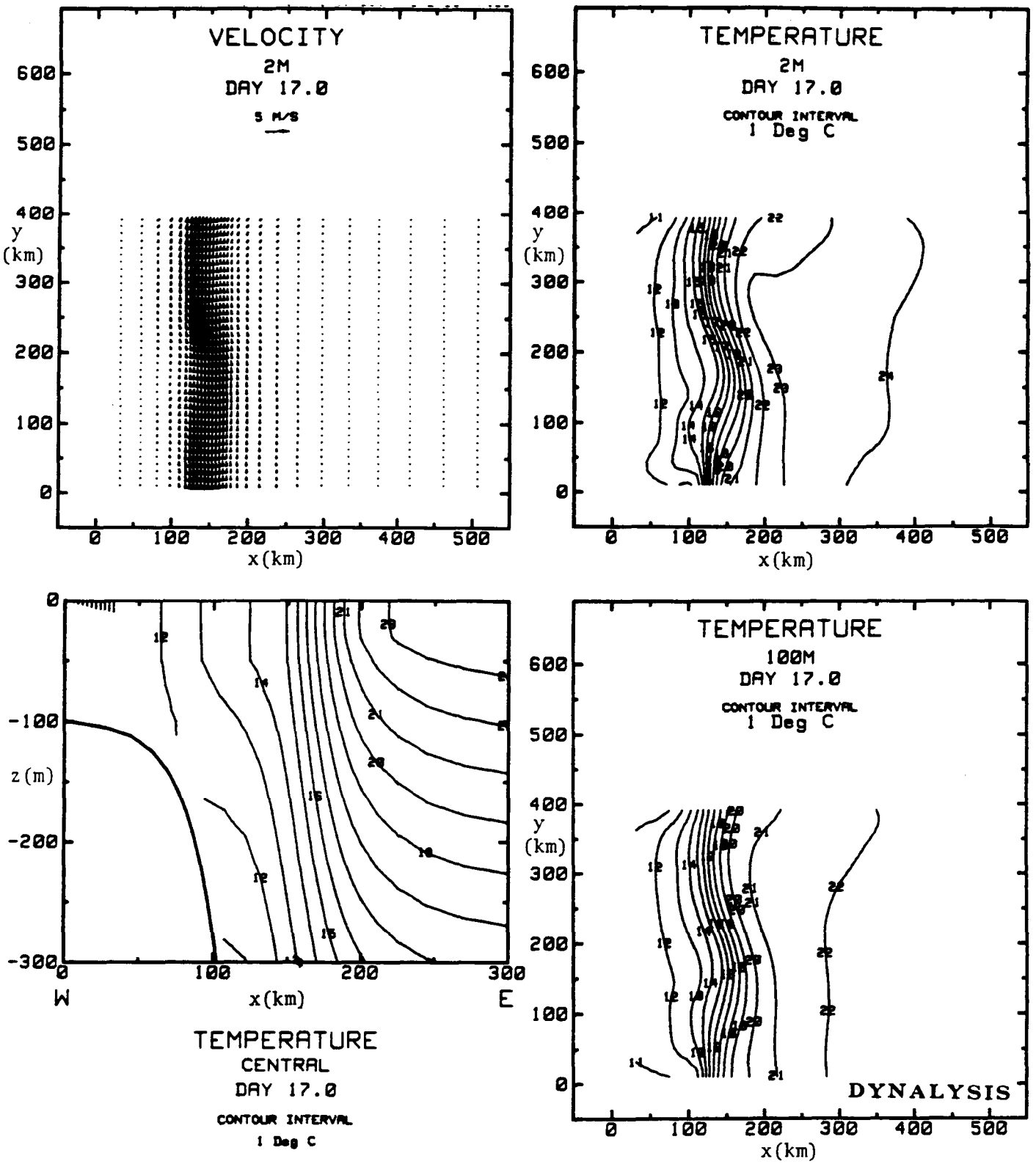

Figure 3.4.17 Calculated fields on day 17 for Gulf Stream intensity modulation experiment.

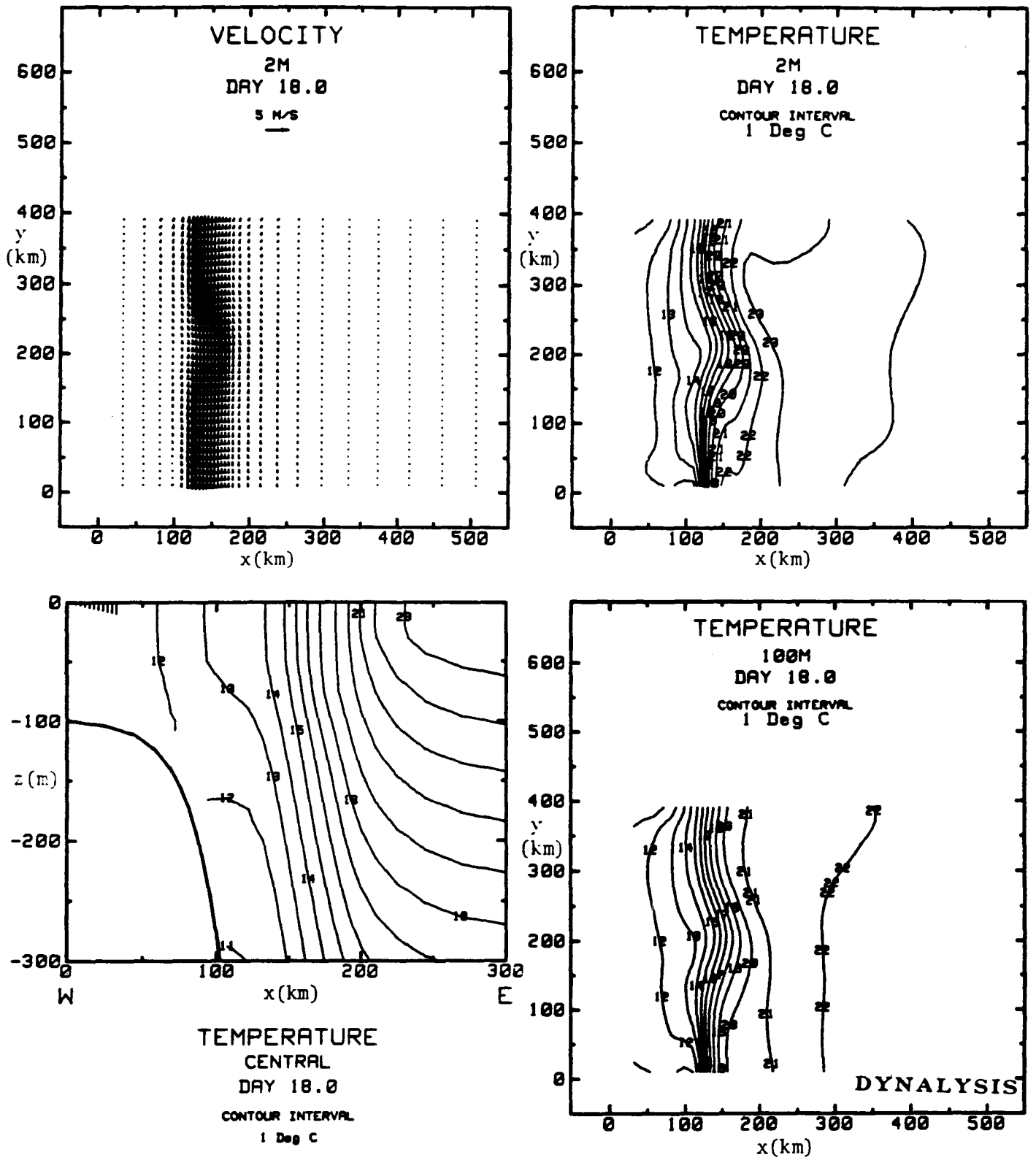

Figure 3.4.18 Calculated fields on day 18 for Gulf Stream intensity modulation experiment.

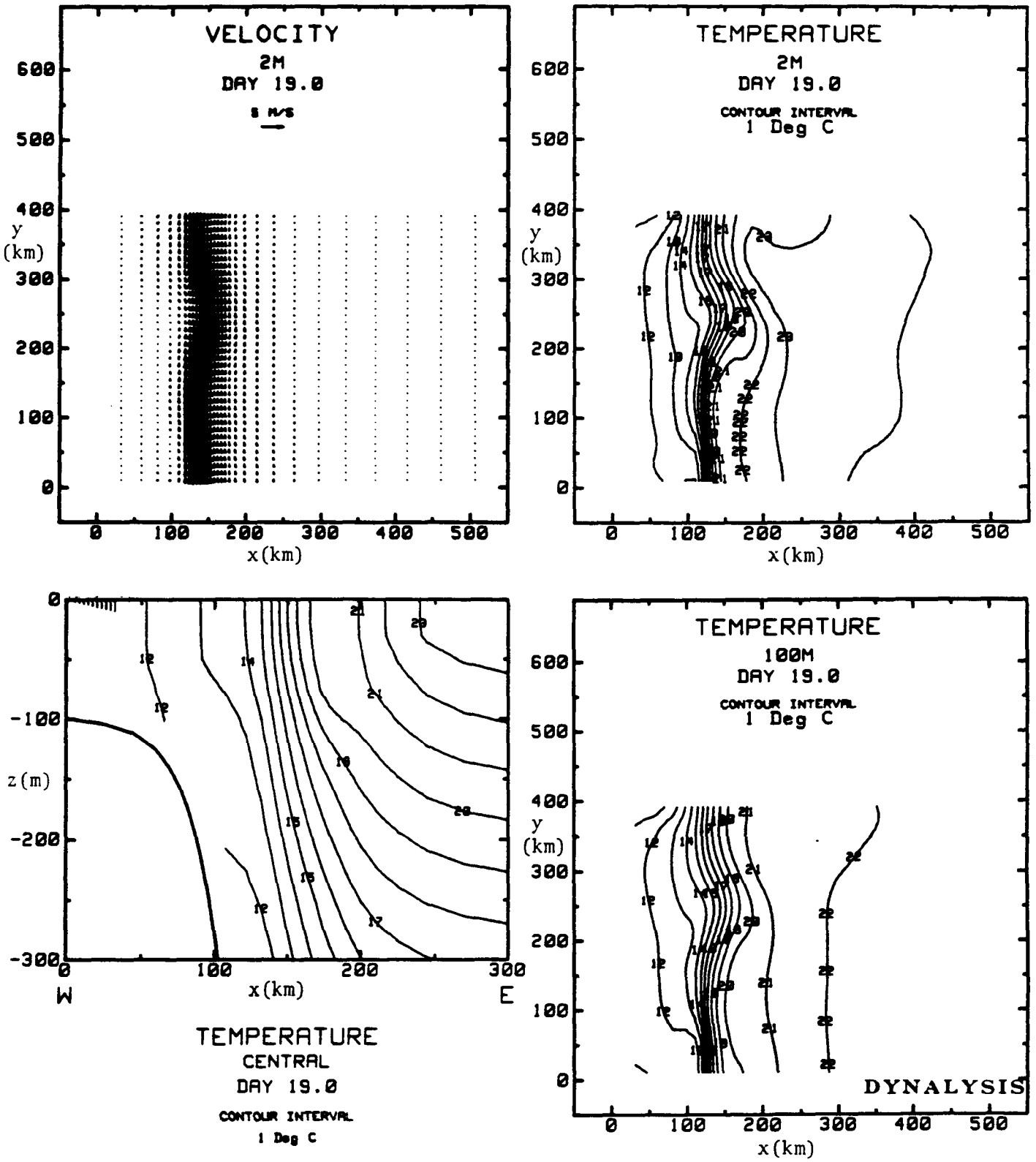

Figure 3.4.19 Calculated fields on day 19 for Gulf Stream intensity modulation experiment.

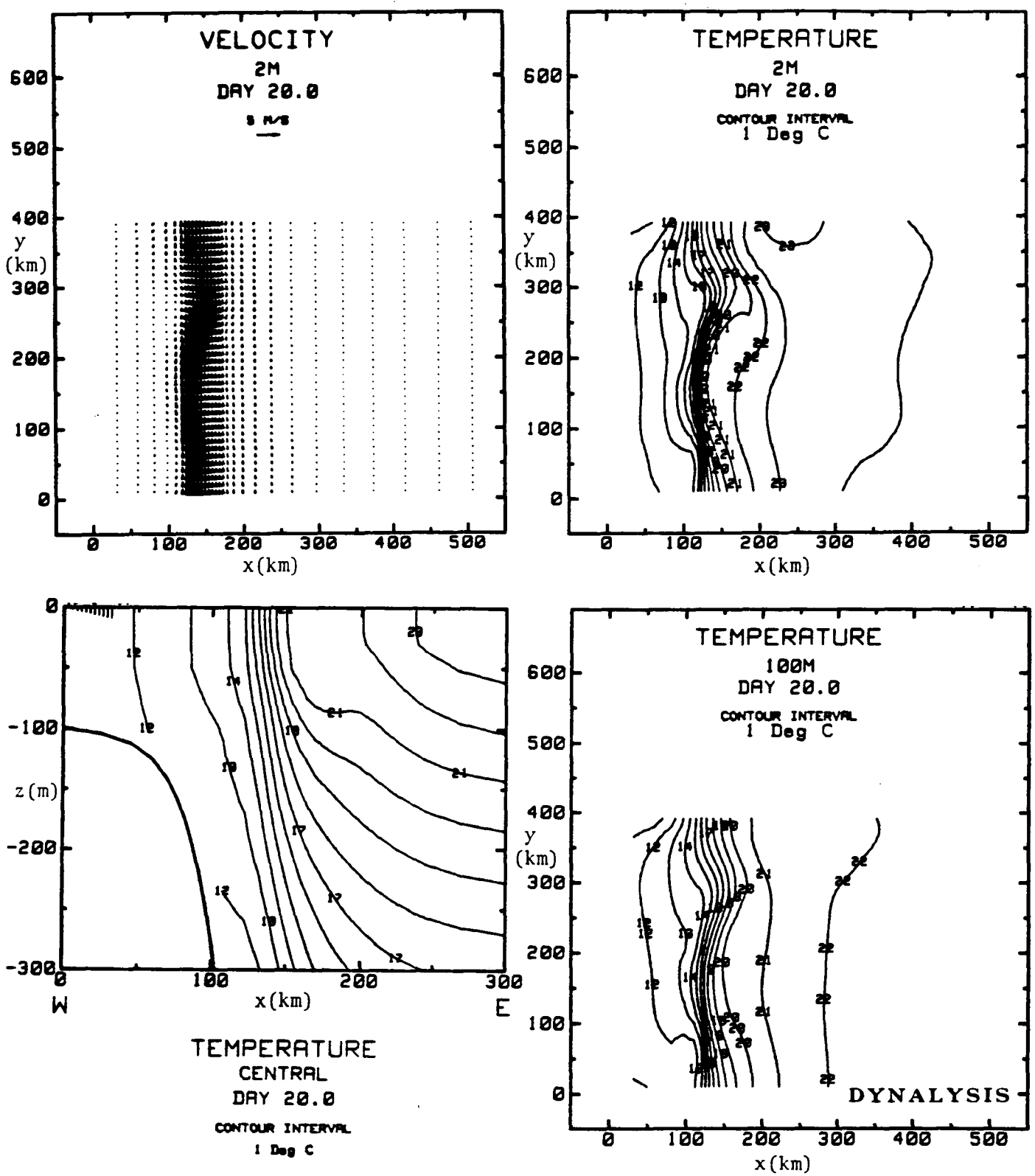

Figure 3.4.20 Calculated fields on day 20 for Gulf Stream intensity modulation experiment.

created by the difference of the result of Equation (3.4) displaced offshore by Δx and the result of Equation (3.4) displaced onshore by Δx. Again this disturbance oscillated with a frequency of 8 days to correspond to the most unstable mode of Luther and Bane [1985] and also to account for the fact that the characteristic period of significant Gulf Stream meanders is about 8 days.

Two experiments were run with Δx = 10 km and Δx = 25 km. Figures 3.4.21 and 3.4.22 display the nearsurface temperature fields for the former case at intervals of a day for days 13 to 20. A meander of about 300 km wavelength and propagating northward at a speed once again of about 30 km d^{-1} is evident in the seasurface temperature. A weak cold core eddy is also evident on day 16, but it dissipates rapidly while propagating northward.

Figures 3.4.23 to 3.4.32 display the nearsurface velocity and temperature fields, the temperature field at 100 m and the temperature section on a cross-shore transect at y = 200 km (center of the domain) at intervals of a day for days 11 to 20 for the case Δx = 25 km. The dramatic appearance of cold dome meanders is clearly evident from day 14 onwards. It is possible to follow the evolution of one cold dome from its incipience at the southern boundary around day 14 and gradual dissipation to day 20, when it is positioned just beyond the center of the domain. Once again, the propagation speed appears to be between 30 and 40 km d^{-1}, consistent with the observed propagation speeds. The spacing between two cold domes on days 14 and 15 suggest a wavelength of about 250 km, once again consistent with the observations cited in Section 3.1.

Examination of the surface temperature at the center of the cyclonic cold core that begins to evolve at the southern boundary around day 14 reveals an increase from 11°C on day 14 to about 14°C on day 20 suggesting

a gradual collapse of the doming isotherms. The residence time of the cold waters in the dome, suggested by this collapse is certainly on the order of a week to 10 days, a value not inconsistent with observational data. The spacing between two cold domes of about 250 km is larger than that observed downstream of the Charleston Bump (140 km - see Figure 19 of Lee and Atkinson, [1983]), but may be a function of the period of oscillation of the Gulf Stream axis or some other parameter, yet unknown. More experiments are needed to clarify this issue and perhaps an experiment in which a feature like the Charleston Bump is embedded in the domain of sufficient alongshore extent to display two to three cold domes is warranted. Perhaps more realistic Gulf Stream temperature and velocity fields (from actual observations rather than a contrived analytical expression) in concert with actual topography throughout the domain are well-advised. In other words, simulation of the domain around the Bump with observed topography and Gulf Stream features would be highly valuable.

Examination of the temperature section on day 19, when the cross shore transect happens to intersect the cold dome, (Figure 3.4.31) displays a remarkable resemblance to observed sections across the cold dome (see Figure 2 of Chew, [1981] or Figure 7 of Brooks and Bane, [1983]). A shallow warm filament is clearly visible on the shoreward side and so is the upward doming of the isotherms in the cold core. The signature of the warm filament is also discernible in surface temperature fields but unfortunately the characteristic elongation of the filament in the alongstream direction is somewhat weakly evident. The cause is believed to be the fact that the cross-shore resolution of the grid begins to get coarse (12 to 15 km) just at the point where the filament should manifest itself. A finer resolution (perhaps 5 km, the same as the finest

resolution in the model) would resolve the filament better and therefore produce the characteristically elongated warm filament observed in satellite imagery. Nevertheless, a shallow warm filament is clearly present in the temperature fields and the cold core is embedded between this filament and the main body of the Gulf Stream. The currents in the warm filament region, i.e., on the shoreward side of the cold core eddy appear to be about 50 cm s^{-1}, a value, once again consistent with observations.

The perturbation of the sea surface temperature on the eastern side of the Gulf Stream in the vicinity of the cold domes is also noteworthy. It is possible that if there were a wind field with an offshore component, these features would be elongated into features resembling those observed on the eastern side of the Gulf Stream (in the vicinity of the Charleston Bump) in the satellite imagery, just by Ekman drift. A parallel experiment with the additional superimposition of a realistic wind stress is needed to substantiate this speculation.

It should also be pointed out that the initiation of a cold dome at the southern boundary appears to be associated with the outward deflection of the Gulf Stream axis. This is again consistent with the fact that the Charleston Bump deflects the Gulf Stream outward away from the shore and this deflection is the apparent cause of the cold domes downstream of the Bump.

Finally a numerical experiment was run for the Δx = 25 km case, in which the horizontal viscosity was doubled but the diffusivity halved. Figures 3.4.33 and 3.4.34 show the near surface temperatures at intervals of a day for days 13 to 20 for this case. A comparison with corresponding fields for the previous case shows insignificant changes from the previous case, except perhaps a slight weakening of the intensity of the cold dome,

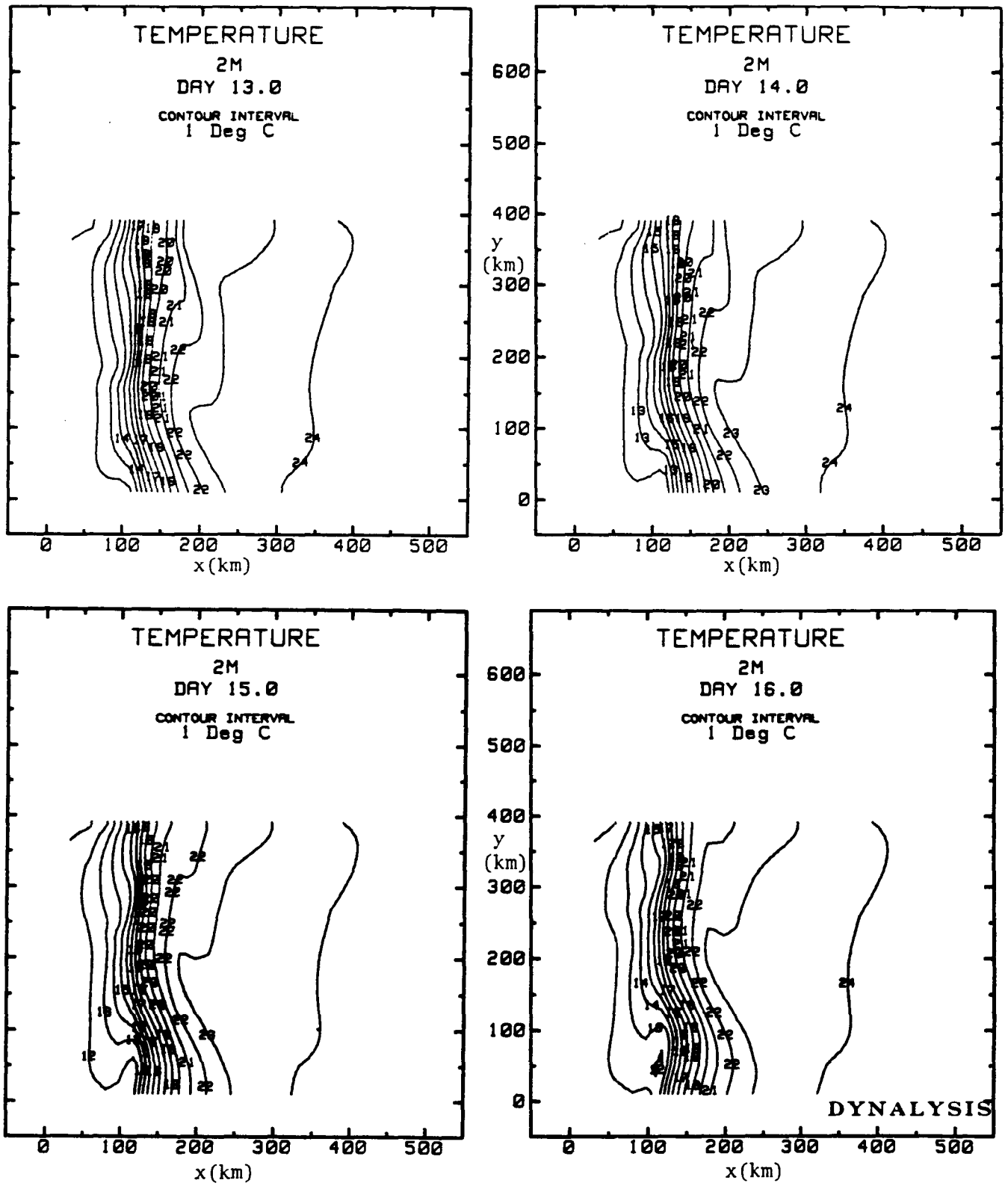

Figure 3.4.21 Calculated surface temperature fields for days 13 to 16 for Gulf Stream lateral position modulation experiment with Δx = 10 km.

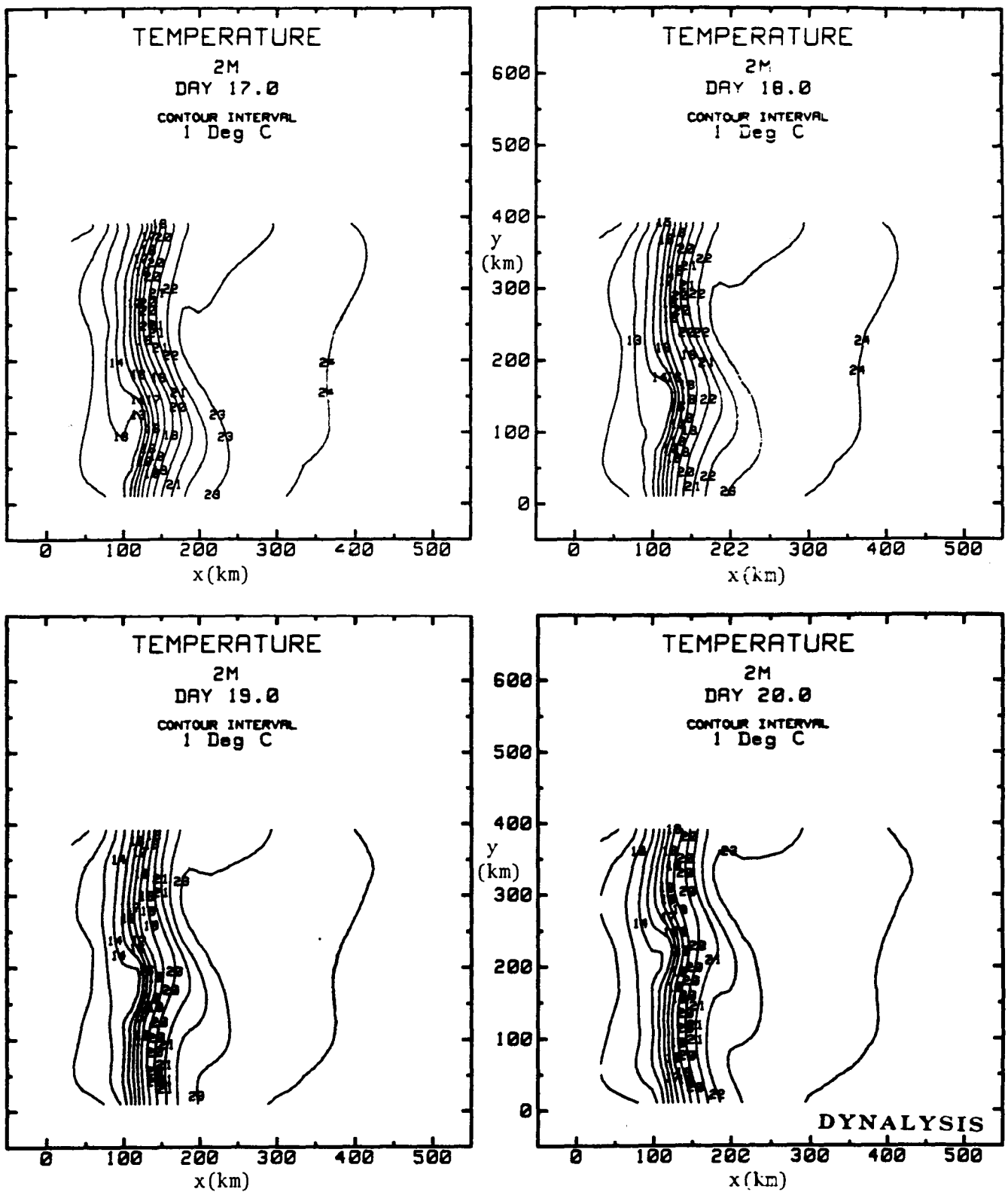

Figure 3.4.22 Calculated surface temperature fields for days 17 to 20 for Gulf Stream lateral position modulation experiment with Δx = 10 km.

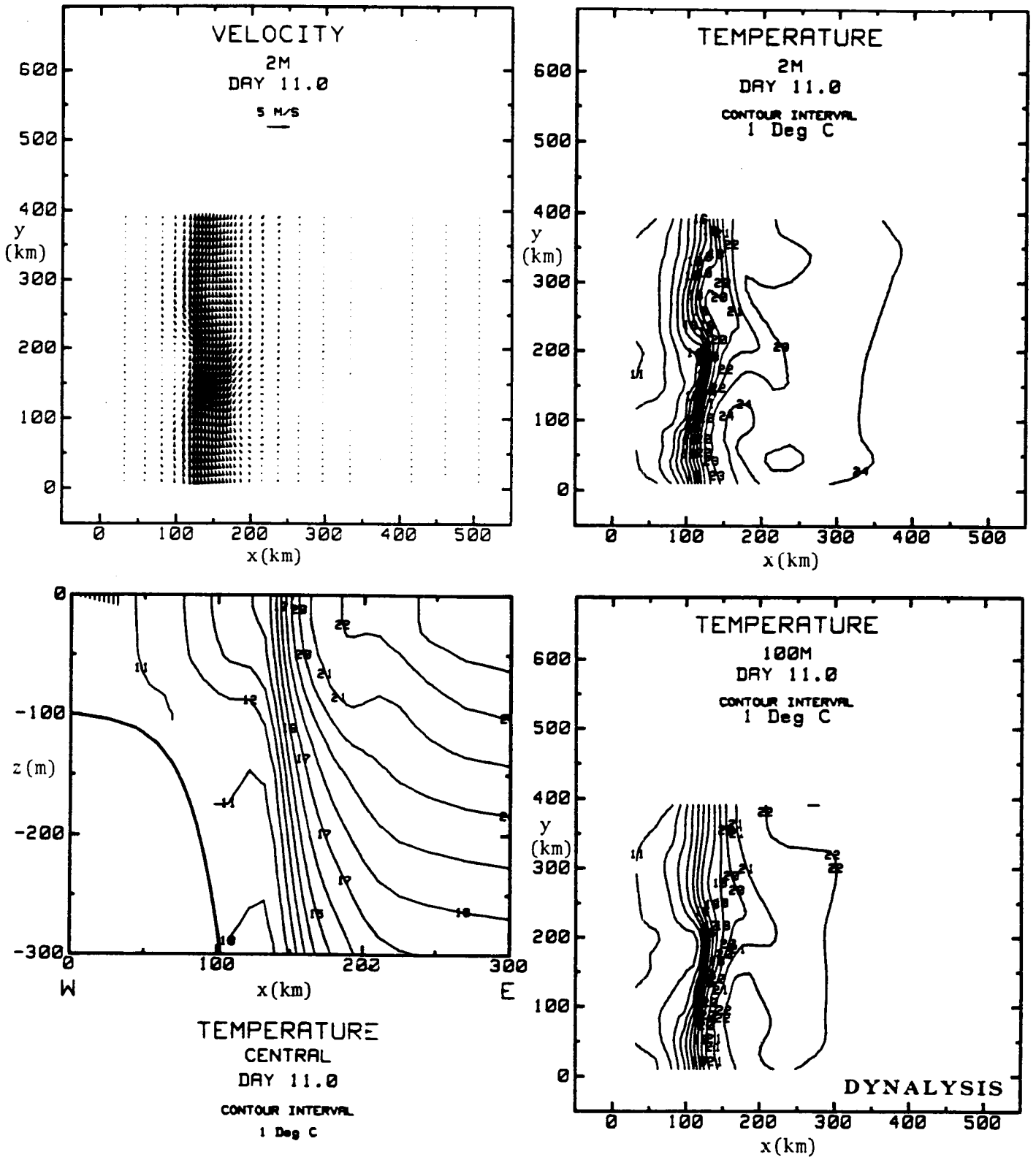

Figure 3.4.23 Calculated fields on day 11 for Gulf Stream lateral position modulation experiment with Δx = 25 km.

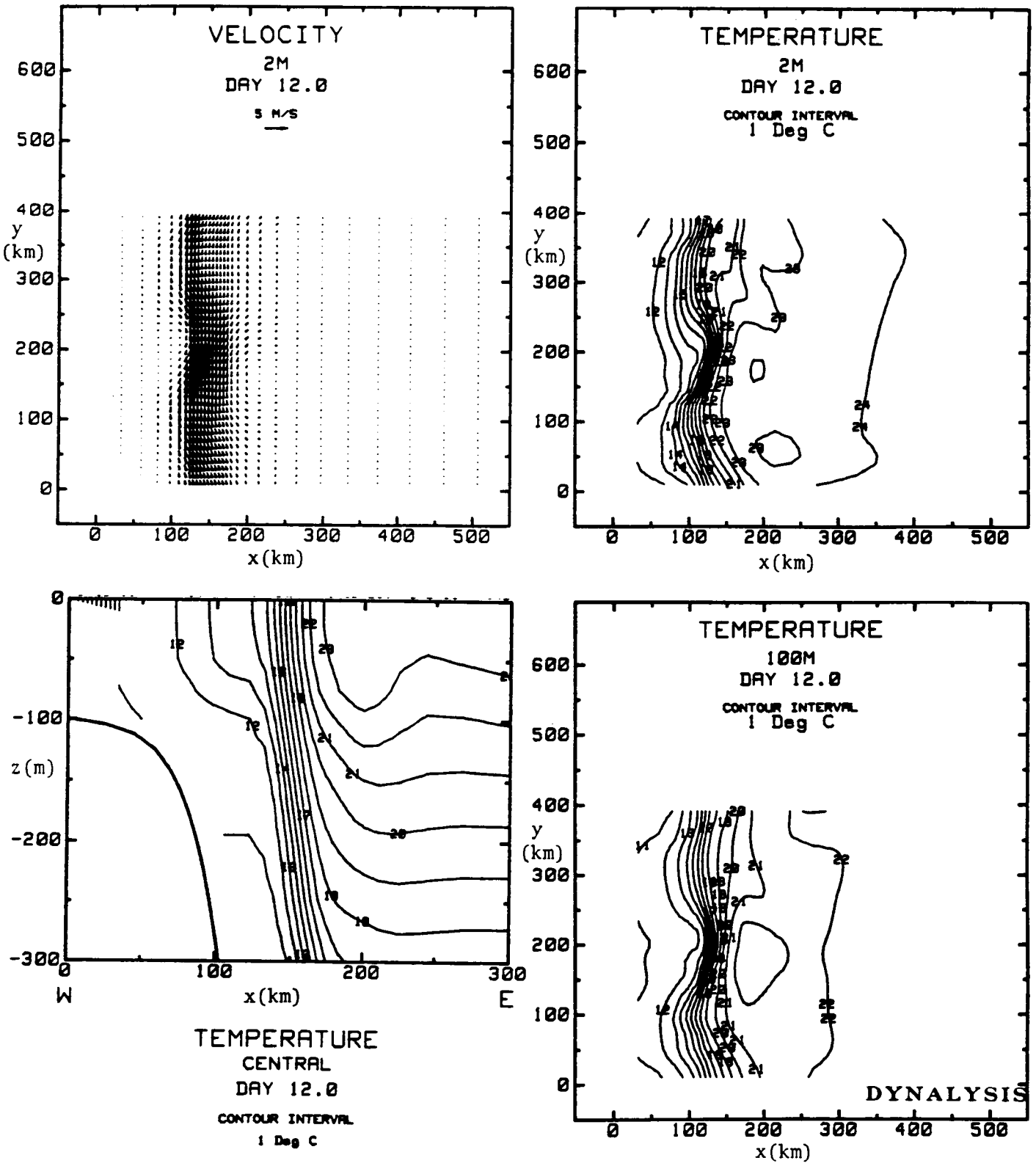

Figure 3.4.24 Calculated fields on day 12 for Gulf Stream lateral position modulation experiment with Δx = 25 km.

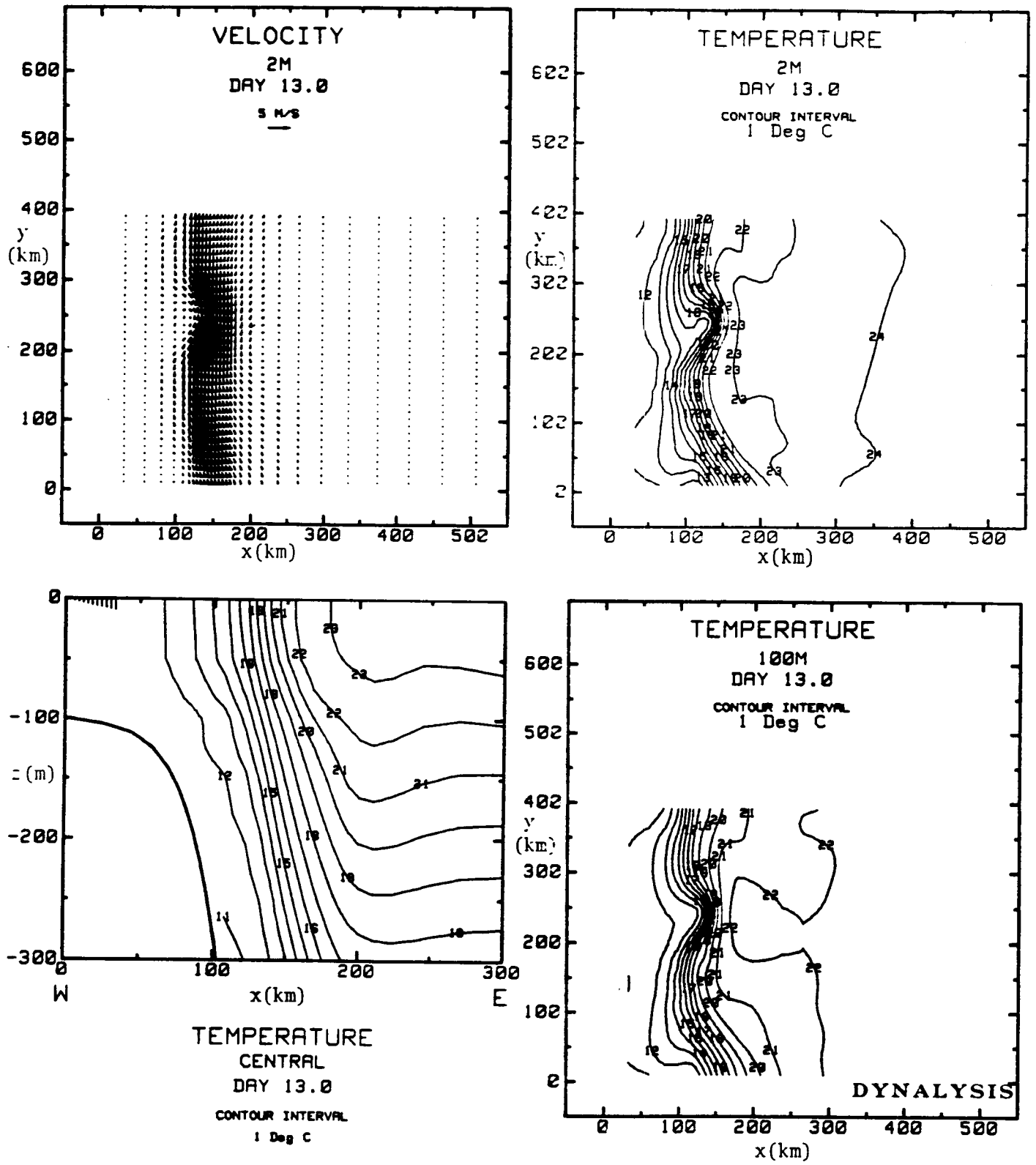

Figure 3.4.25 Calculated fields on day 13 for Gulf Stream lateral position modulation experiment with Δx = 25 km.

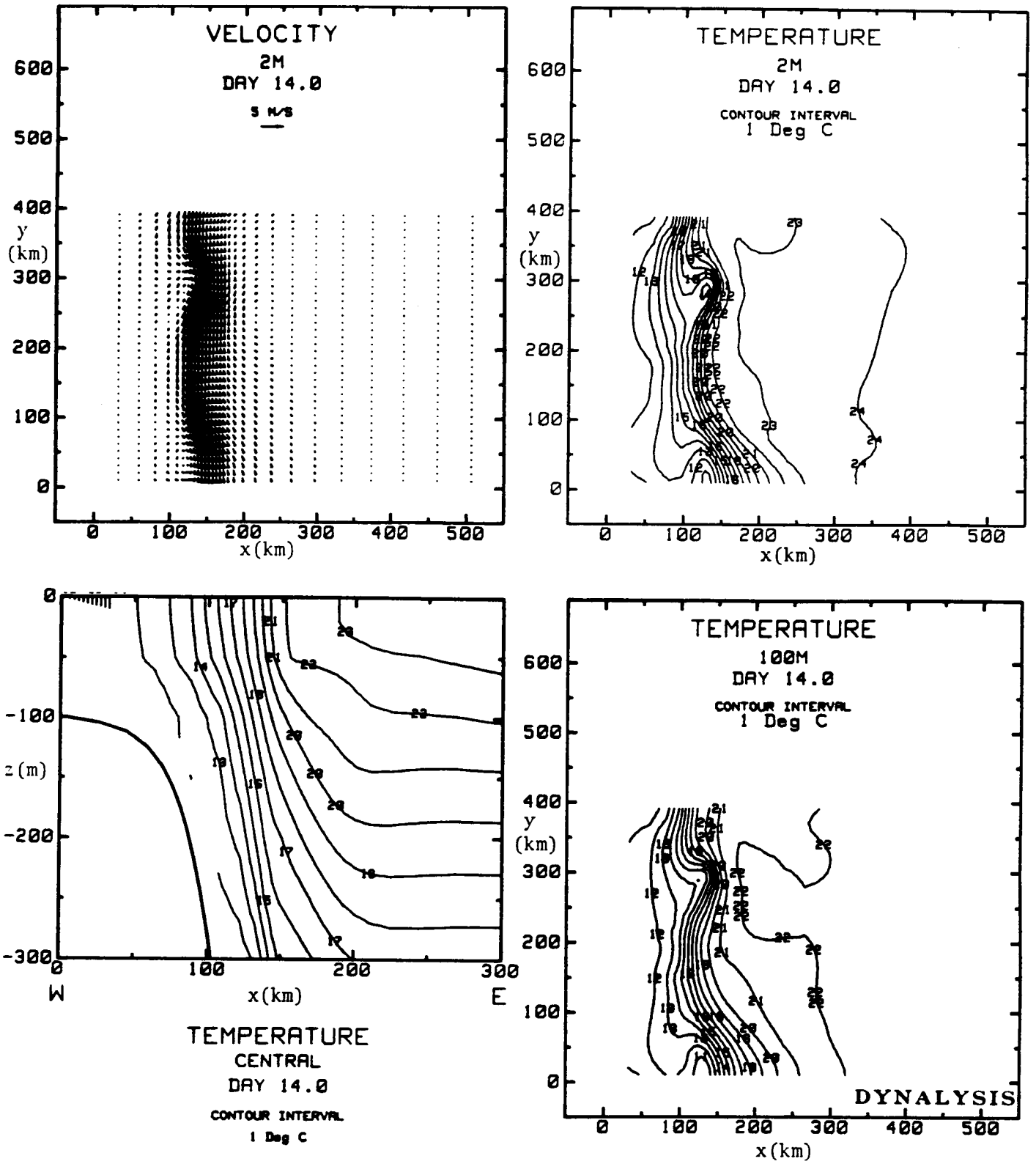

Figure 3.4.26 Calculated fields on day 14 for Gulf Stream lateral position modulation experiment with Δx = 25 km.

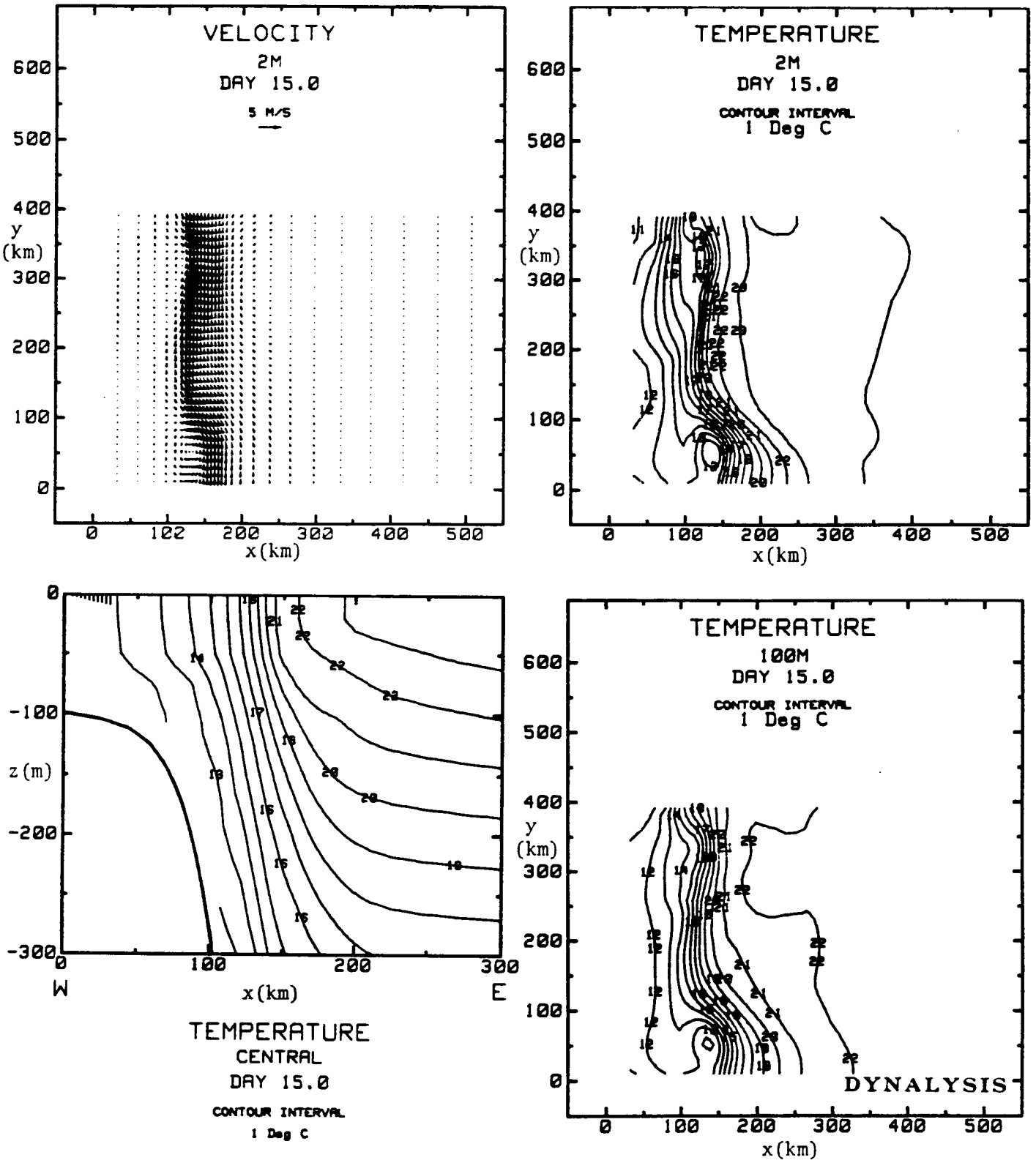

Figure 3.4.27 Calculated fields on day 15 for Gulf Stream lateral position modulation experiment with Δx = 25 km.

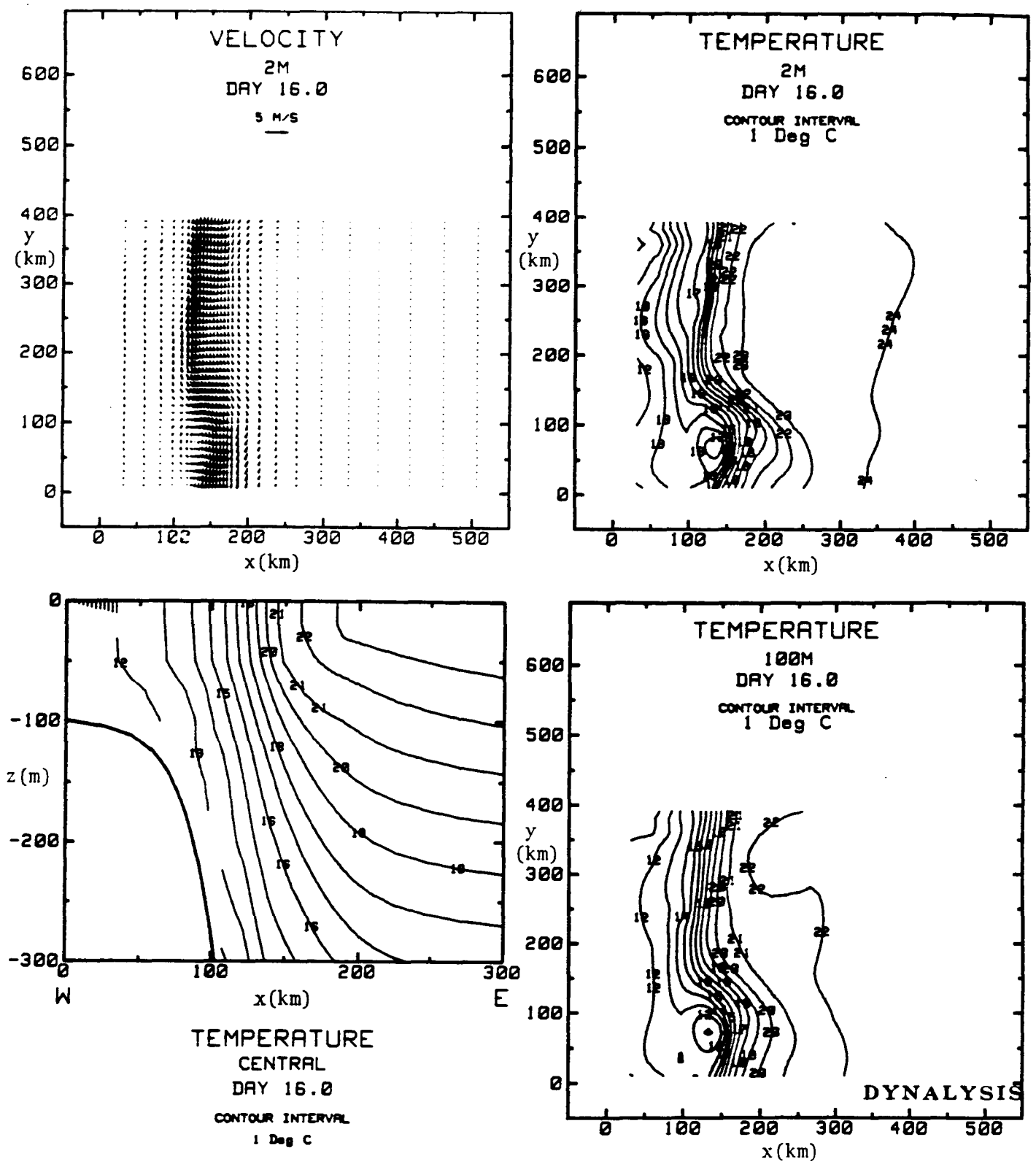

Figure 3.4.28 Calculated fields on day 16 for Gulf Stream lateral position modulation experiment with Δx = 25 km.

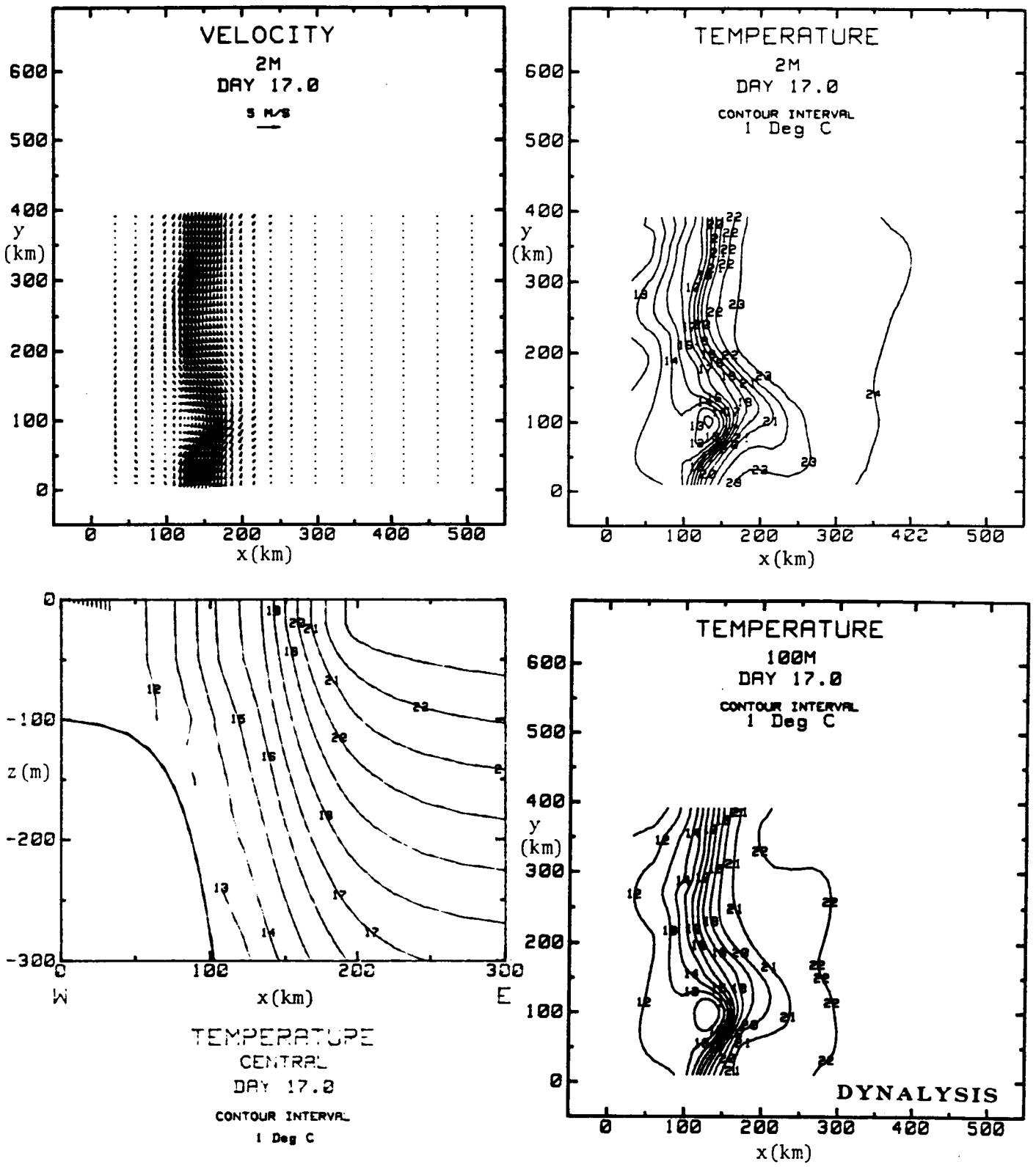

Figure 3.4.29 Calculated fields on day 17 for Gulf Stream lateral position modulation experiment with Δx = 25 km.

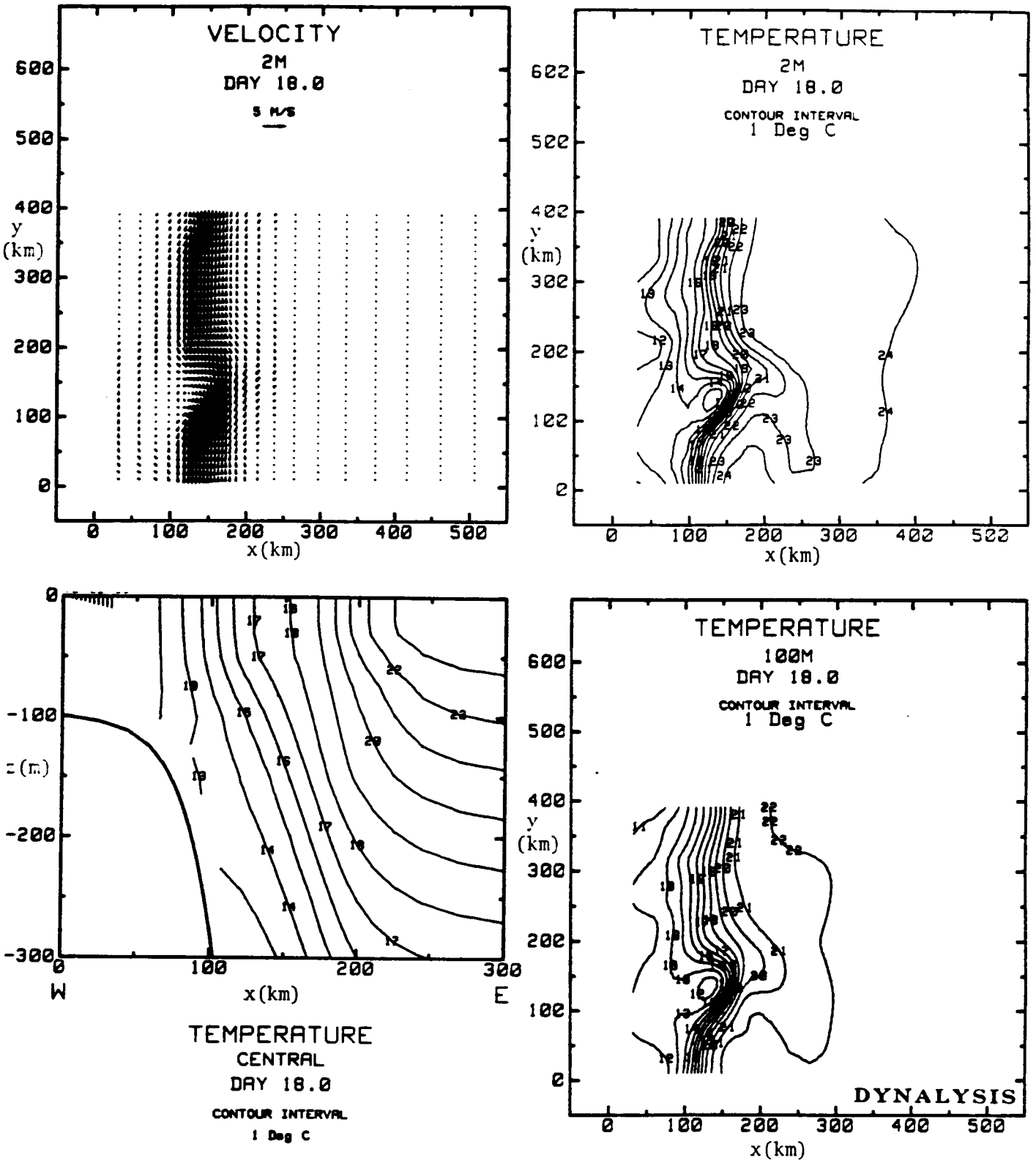

Figure 3.4.30 Calculated fields on day 18 for Gulf Stream lateral position modulation experiment with Δx = 25 km.

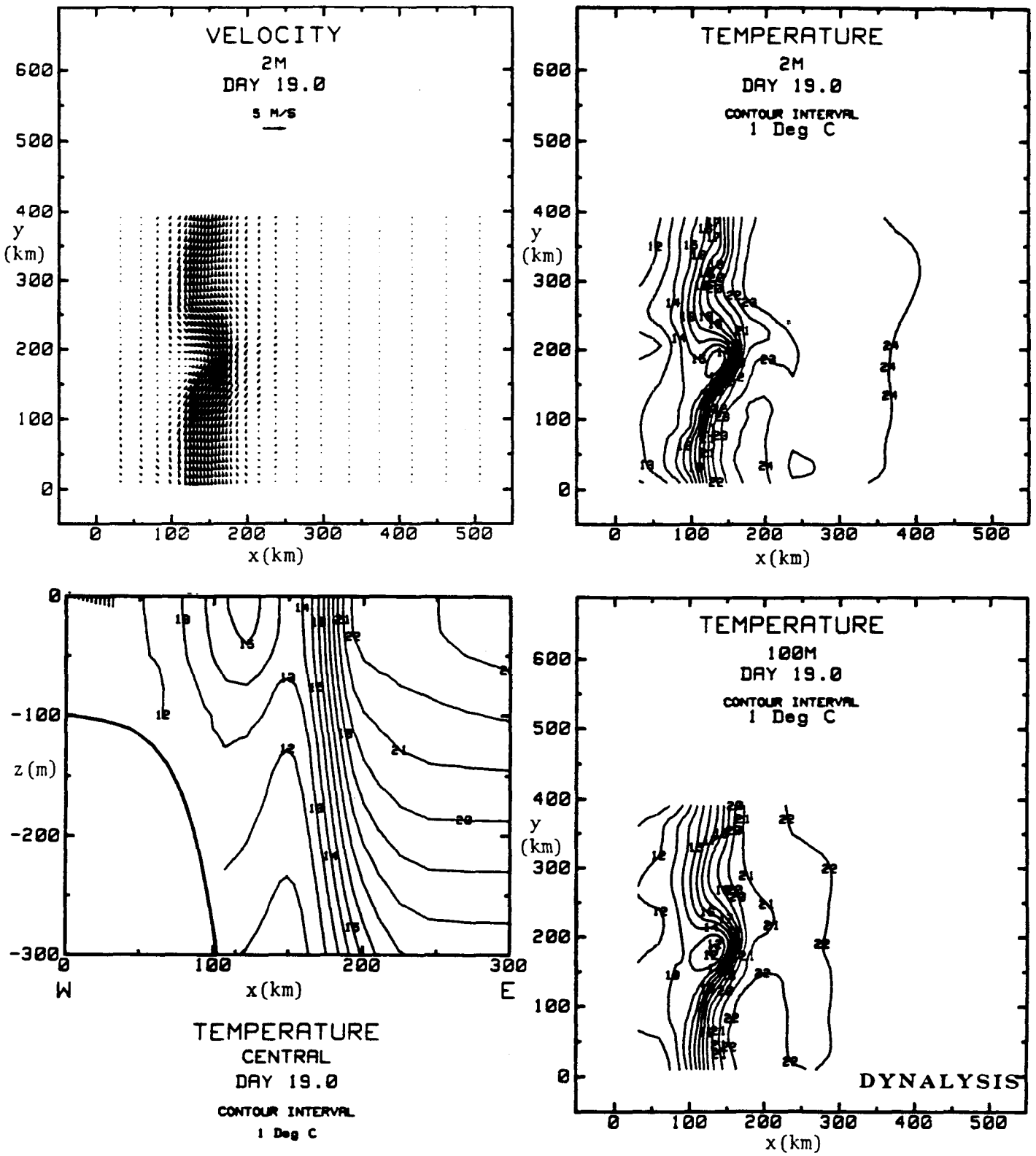

Figure 3.4.31 Calculated fields on day 19 for Gulf Stream lateral position modulation experiment with Δx = 25 km.

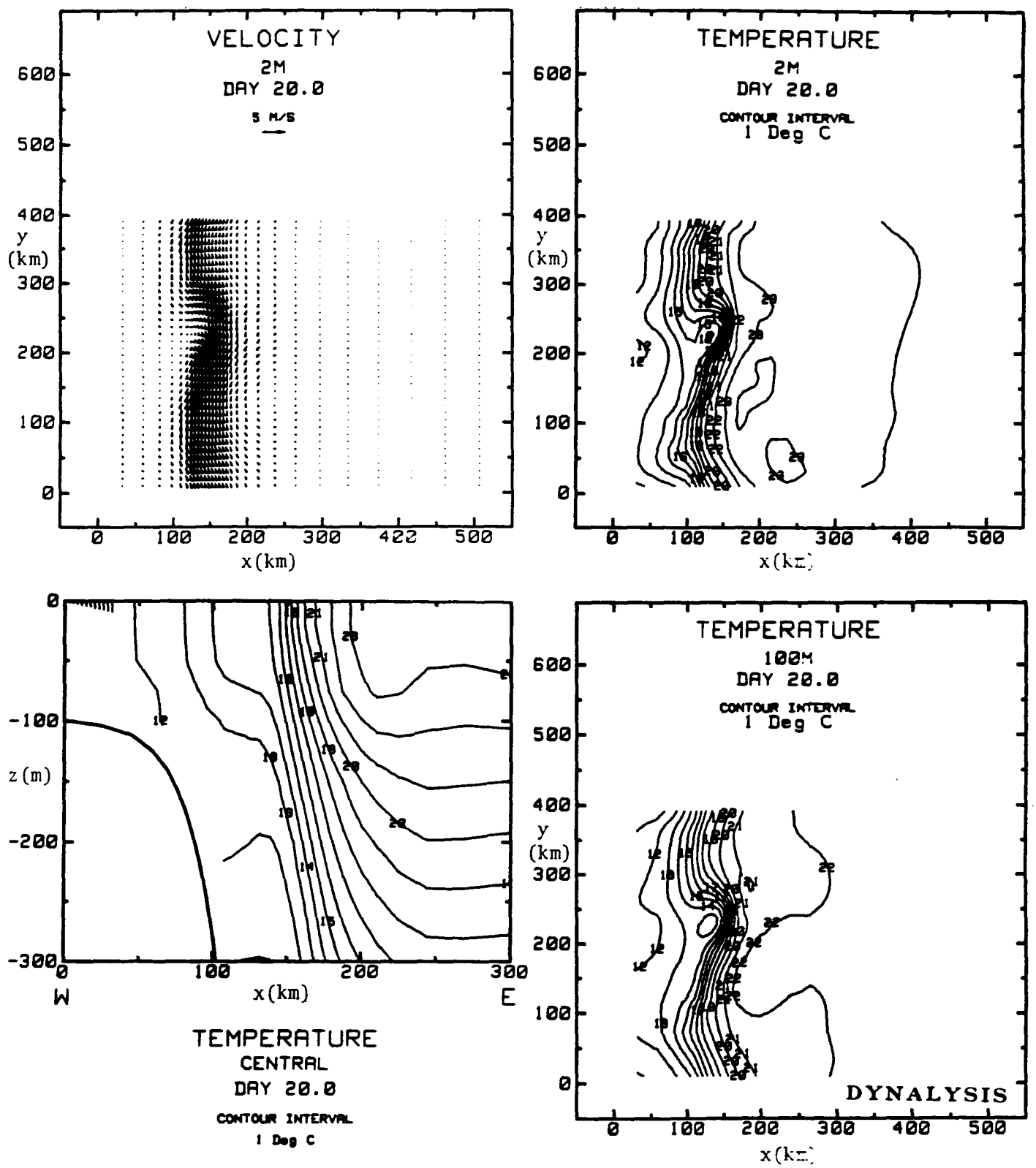

Figure 3.4.32 Calculated fields on day 20 for Gulf Stream lateral position modulation experiment with Δx = 25 km.

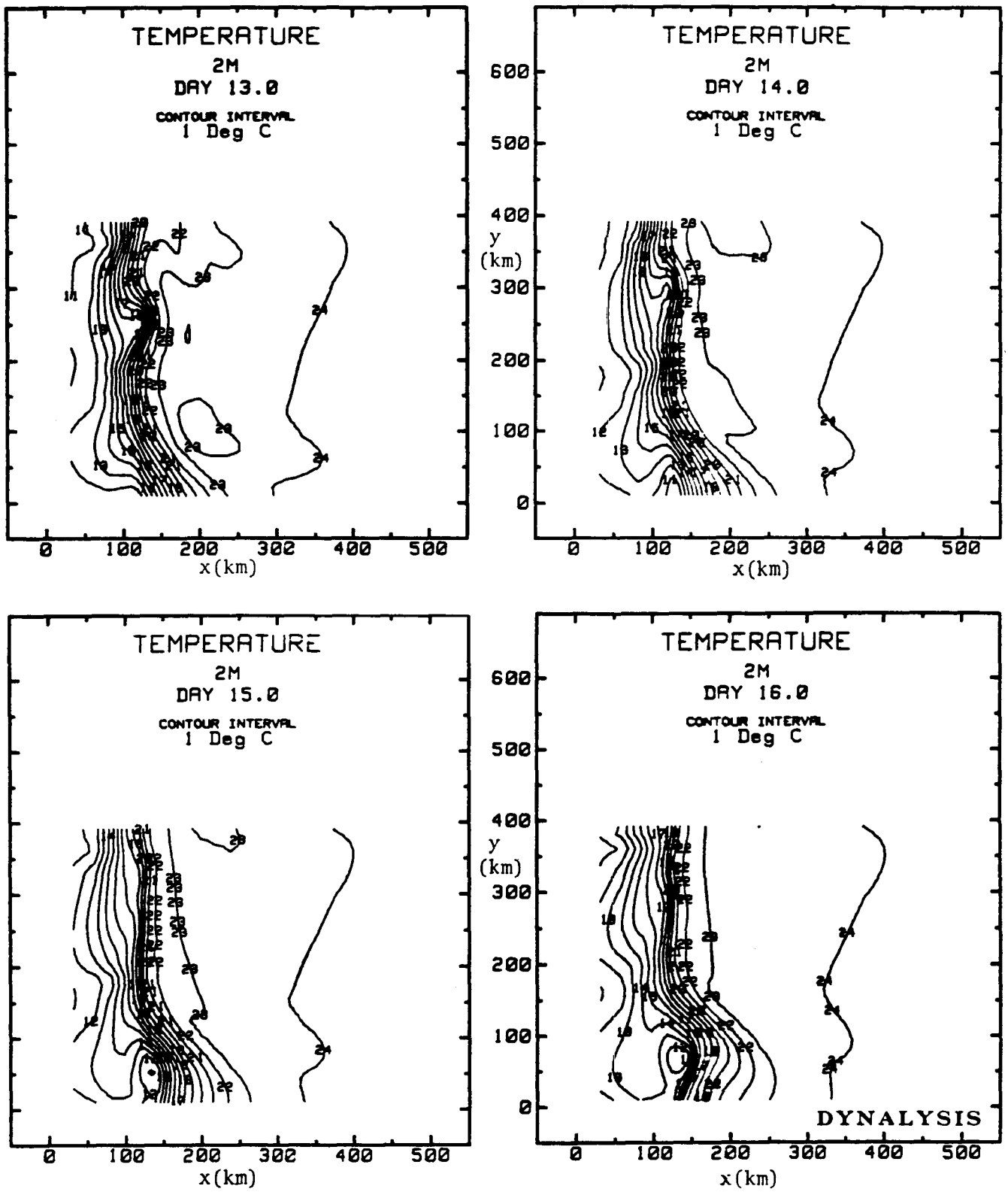

Figure 3.4.33 Calculated surface temperature fields for days 13 to 16 for Gulf Stream lateral position modulation experiment with Δx = 25 km but A_M doubled and A_H halved.

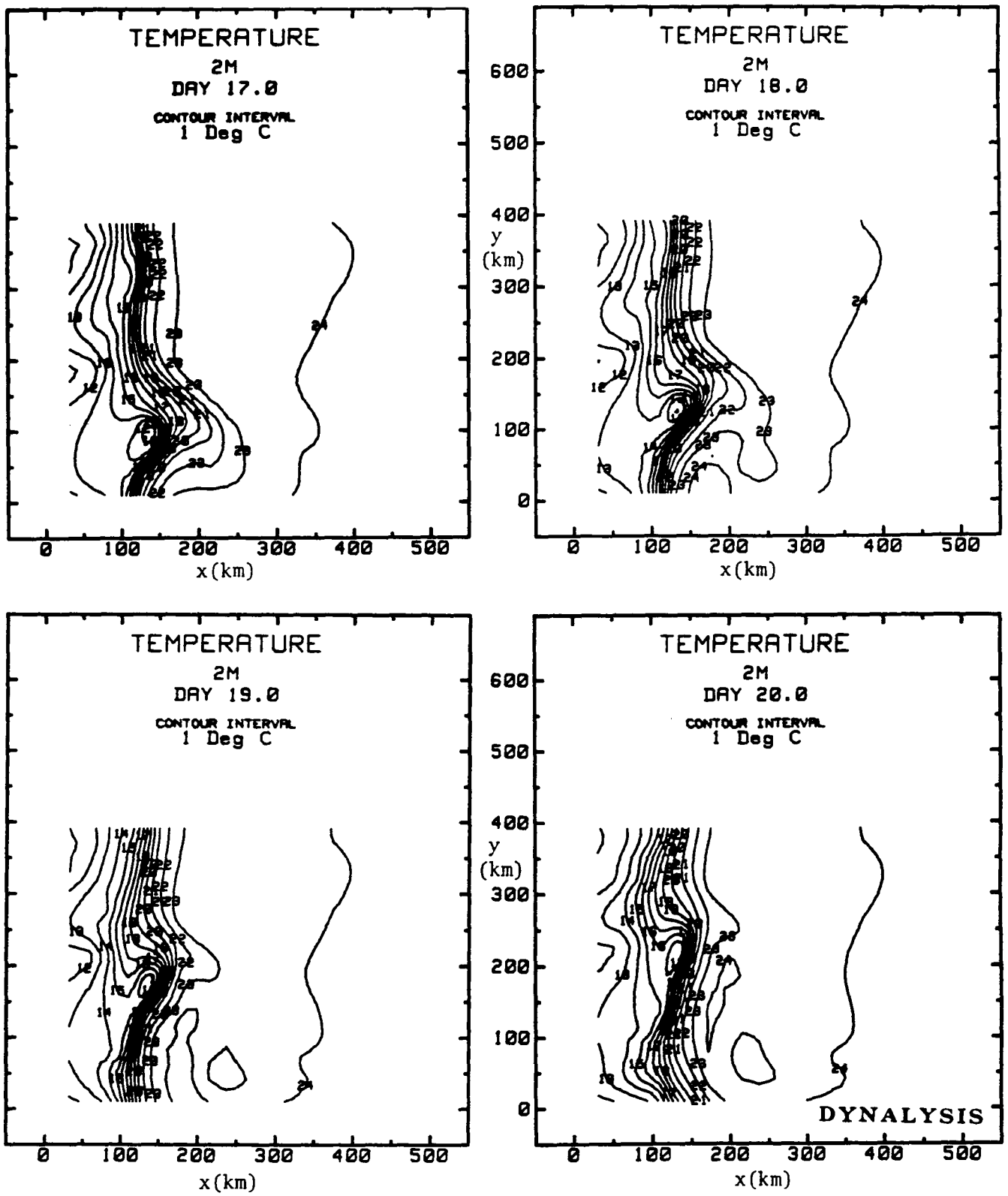

Figure 3.4.34 Calculated surface temperature fields for days 17 to 20 for Gulf Stream lateral position modulation experiment with Δx = 25 km but A_M doubled and A_H halved.

no doubt due to the increased momentum diffusion. Nevertheless, the changes brought about are negligibly small.

It is remarkable that a modulation of the lateral position of the Gulf Stream axis of sufficient amplitude can produce rather realistic cold dome meanders. The underlying physical mechanism is however not yet clear. Whether topographic modification of potential vorticity inherent in any lateral shift of the Gulf Stream is the responsible agent is also not clear. The dependence of the phenomenon on the parameters of the problem such as the extent of lateral shift, and the characteristics of the Gulf Stream fields employed remains to be explored. The mechanism for the decay of the cold core eddy (whether it is transfer of eddy kinetic energy to the mean flow) is also unexplored. Clearly the numerical experiments described in this report are just the beginning of a thorough numerical study into the phenomenon of Gulf Stream frontal meanders. The fact that a realistic cold dome meander has indeed been produced is in itself, however, a considerable achievement.

An immediate extension that comes to mind is another Gulf Stream axis modulation experiment in which the alongshore extent of the domain is doubled and the resolution in the vicinity of the Gulf Stream front as well as on the outer shelf refined to a value of perhaps 2.5 km. The latter would enable the concomitant horizontal viscosity to be lowered further and the warm filaments to be resolved better. The former would enable the complete cycle from initiation to decay of a cold dome frontal eddy to be simulated in the domain.

4. CONCLUDING REMARKS

The results of a program to understand and calculate the oceanic circulation on the East Coast of the United States including the South Atlantic Bight have been described in this report. The program is designed to provide the MMS with timely estimates of the currents for use in the assessment of potential environmental impacts of offshore activities associated with oil and gas exploration. The program, while seemingly focused towards the use of numerical models, has a heavy reliance on observational data. In this section the major accomplishments of the program are summarized.

A comprehensive physical oceanographic climatology of the continental shelf waters of the East Coast from the Florida Keys to Nova Scotia has been compiled and analyzed as part of this investigation. The most up-to-date hydrographic data base has been assembled from the National Oceanographic Data Center and Fleet Numerical Oceanography Center and local sources, including studies sponsored by the Minerals Management Service in the South Atlantic Bight. These data have been subjected to a comprehensive data analysis procedure to deduce the climatological distributions of various properties of the water masses on the East Coast. Marine Surface Observations for the region have been processed to produce climatological distributions of the fluxes of momentum and heat across the sea surface at a resolution never before achieved. The resulting high resolution, climatological distributions of oceanic properties and sea surface fluxes should be of considerable value in understanding the dynamics of these waters.

These hydrographic and wind stress data have been used as input to The Characteristic Tracing Model to infer climatological circulation prevailing in the coastal waters of the Eastern United States. The model, based on geostrophic-Ekman dynamics, incorporates the effect of the density gradients, wind stress at the sea surface and the bottom stresses, and based on simple transport information in the Straits of Florida deduces the circulation on the entire coastal waters of the East Coast. Velocities at the surface and at various levels in the water column, as well as the total transport in the water column and the sea surface elevation, are the products available from the model. These results are in general agreement with what is known about the circulation on the East Coast of the United States.

With respect to the South Atlantic Bight, it has now been possible to deduce the circulation in these waters based on the latest data available, including MMS and DOE sponsored programs. The present one-quarter degree resolution hydrography has permitted a better definition of baroclinicity so that the model results are improved. This, in concert with improved modelling strategy and a more complete dynamics, makes the results of the CTM , for the SAB in particular and the ECS in general, unique and valuable.

An important application for the CTM circulation obtained in this study is, of course, oil spill modelling. The version of the MMS OSRA model presently employed on the ECS uses as input these seasonally averaged climatological currents with the Ekman drift due to the effects of the climatological wind stress removed. Variations in the OSRA model winds are determined from a wind transition matrix constructed from historical wind data. An oil spill trajectory is the vector sum of the climatological surface currents and the surface drift component which is

related to the wind speed, rotated clockwise in relation to the wind direction to reflect the Coriolis effect.

While the diagnostic climatological currents of the Characteristic Tracing Model are compatible with the philosophy of the present oil spill model, it is evident that potentially significant effects are not included in the long term averaged current fields. First, it is clear that the temporal and spatial variability, on the shelf particularly in the vicinity of the Gulf Stream, may play an important role in pollutant transport. Second, the influence of winds on surface currents on the Shelf may not be negligible compared with the climatological currents, particularly in establishing slope currents.

Although to date the requirements of MMS oil spill modelling have been met with diagnostic currents, the research focus of this program has always been to provide time varying prognostic currents. In principle, given self consistent time dependent currents and winds, the trajectory of an oil spill could be calculated. Provided with such wind and current fields for a sufficiently long time period, the trajectories of a statistically significant number of spills could be computed and the results used to assess the risk to specific coastal regions. The refinement and testing of the GCM, then, is of major importance in order to be prepared to provide accurate and scientifically defensible current fields.

An earlier article [Blumberg and Mellor, 1983] describes prognostic model results obtained for this region using climatological lateral and surface boundary conditions. The present report describes the successful completion of the next logical step in the development process; the simulation of Gulf Stream frontal characteristics. The results indicate that the model contains the prerequisite physics to describe these complex mesoscale events.

Further process studies are necessary, however, to obtain a more complete understanding of the dynamics of shingles and eddies from the computational point of view. Experiments with a wider band of high resolution grid should be expected to improve the structure of the eddies close to the coast. This behavior is important in order to assess the impact of Gulf Stream variability on the coastal regions of the South Atlantic Bight. To the extent that these Gulf Stream frontal features become detached from the Stream itself, the resulting current anomalies could be several times the magnitude of the background currents. As shown in Vukovich et al [1984], the oil spill trajectory calculations using synoptic currents can vary markedly from those based on long term average currents.

In the same spirit, process studies would be valuable to aid in understanding the numerical simulation of warm core eddies which develop after the Gulf Stream departs from the coast. Since warm core eddies are observed to be advected back into the Mid-Atlantic Bight region from their genesis hundreds of kilometers offshore, their episodic influence on the coastal current would also be significant. If the domain were considerably longer in the streamwise direction, the evolution of these warm core eddies would be more completely simulated.

Some degree of skill assessment would also be valuable utilizing the extensive data base and knowledge being compiled by the ongoing MMS-sponsored Florida Atlantic Coast Transport Study (FACTS) and South Atlantic Bight (SAB) observations, and NOAA-ONR sponsored Subtropical Atlantic Climate Study (STACS). These observational studies will establish the currents in the Gulf Stream and cross-shelf transports more accurately. Accurate monitoring of the Gulf Stream volume transport will enable more accurate input of conditions on the southern boundary of the

model, which in turn will enable a more accurate simulation of the variability of, and induced on the shelf by, the Gulf Stream. The observational programs are designed [Maul, 1985] to provide synoptic coverage of Gulf Stream variability from the Straits of Florida to Onslow Bay for a period of 15 months. This unprecedented data base is excellently suited for driving and verifying a GCM designed to simulate the shelf and shelf-edge processes caused by such variability.

The climatological hydrographic and meteorological data base should also be updated to include more recent observations (for example FACTS casts) and perhaps used to update climatological circulation patterns derived from the CTM. Although these data will be reduced and averaged on a one-quarter degree square grid, linear interpolation to a variable resolution curvilinear GCM model grid is a simple and straightforward process. In regions with rapidly changing conditions, such as fronts, the quarter degree grid will smooth out these features to a certain extent. However, since this data is used only to initialize the model, the effects of smoothing are diminished as the GCM begins its calculation on the high resolution curvilinear grid.

Since Gulf Stream frontal variability is not restricted to the SAB and the Mid-Atlantic Bight (MAB) and since these regions in addition to the Gulf of Maine are of critical importance to MMS goals, similar modelling should be conducted in each of these MAB regions. Recent observational efforts (DOE sponsored Shelf Edge Exchange Processes [SEEP], MMS sponsored Mid-Atlantic Slope and Rise [MASAR], and the North Atlantic Slope and Canyon Study [NASACS] programs) have also added considerably to our knowledge of shelf and shelf break processes in the MAB and modelling would provide an excellent and unique opportunity to complement these efforts.

The orthogonal curvilinear GCM described in this report makes simulation and prediction of Gulf Stream frontal activity throughout the Eastern Continental Shelf economically feasible, because the requisite higher resolution all along the front can be provided without overwhelming the computer resources required. It is estimated that on a curvilinear grid (45 x 150) sufficient to cover the entire ECS that a year-long calculation could require 25 hours on a CYBER 205 with a 2.5 megaword memory. While not negligible, this amount of computer time is possible, whereas the task would be prohibitively expensive with a conventional rectilinear coordinate system GCM even with modern vector computers such as the CYBER 205 or the CRAY 2. Once a curvilinear coordinate system with requisite resolution to resolve the dynamical processes has been selected it can be used for all calculations. In fact, if long term calculations were performed and archived, the resulting computational data bank could be accessed to obtain answers to a broad range of environmental questions.

ACKNOWLEDGEMENTS

The authors are pleased to acknowledge the suggestions and comments of Alan F. Blumberg and David E. Amstutz during the early phases of this work. Discussions with Robert P. LaBelle and William Lang have also been very helpful in defining the objectives relating to oil spill modelling.

The large quantity of data employed has been assembled from a variety of sources. Particularly noteworthy are Larry P. Atkinson for his hydrographic data sets, Sigurd E. Larson and Craig S. Nelson for access to the FNOC MOODS data, Evans Waddell for the FACTS data and Chris Casagrande for Blake Plateau data. In addition to those cited, Thomas N. Lee, Otis B. Brown and Thomas Curtin have generously assisted in interpretation of the conditions prevailing in the region of study.

The encouragement and patience of James Lane and Jeffrey P. Petrino during the final stages of the program is greatly appreciated. Most of all the authors are indebted to Marianne L. LaRiche for her unstinting commitment to quality in all stages of the report preparation.

REFERENCES

Allen, J.S., R.C. Beardsley, J.O. Blanton, W.C. Boicourt, B. Butman, L.K. Coachman, A. Huyer, T.H. Kinder, T.C. Royer, J.D. Schumacher, R.L. Smith, W. Sturges and C.D. Winant, 1983. Physical oceanography of continental shelves. Rev. Geophys. Space Phys., 21, 1149-1181.

Anderson, D. and R.A. Corry, 1983. The seasonal variation of the transport of the Florida Current, the Antilles Current and the Windward Passage. Ocean Modelling, 51, 1-4.

Anderson, E.R., 1954. Energy-Budget Studies. Water-Loss Investigations: Vol. I - Lake Hefner Studies, U.S. Geological Survey Circ., No. 299: 71-88.

Angstrom, A, 1924. Solar and terrestrial radiation. Quart. J. Roy. Met. Soc., 50, 121-125.

Atkinson, L.P., T.N. Lee, J.O. Blanton and W.S. Chandler, 1983. Climatology of the Southeastern United States Continental Shelf Waters. J. Geophys. Res., 88, 4705-4718.

Bane, J. M., Jr., 1983. Initial observations of the subsurface structure and short-term variability of the seaward deflection of the Gulf Stream off Charleston, South Carolina. J. Geophys. Res., 88, 4673-4684.

Bane, J.M., Jr., D.A. Brooks and K.R. Lorenson, 1981. Synoptic observations of the three-dimensional structure and propagation of Gulf Stream meanders along the continental margin. J. Geophys. Res., 86, 6411-6425.

Beardsley, R.C. and W.C. Boicourt, 1981. On estuarine and continental-shelf circulation in the Middle Atlantic Bight. In Evolution of Physical Oceanography, (Scientific Surveys in honor of Henry Stommel), B.A. Warren and C. Wunsch, Eds., M.I.T. Press, 198-234.

Beardsley, R.C., W.C. Boicourt and D.V. Hansen, 1976. Physical oceanography of the Middle Atlantic Bight. In Middle Atlantic Continental Shelf and the New York Bight, M.G. Gross, Ed., American Society of Limnology and Oceanography, Special Symposia, 2, 20-34.

Beardsley, R.C. and C.N. Flagg, 1976. The water structure, mean currents, and shelf-water/slope-water front on the New England Continental Shelf. Memoires Soc. Roy. des Sciences de Liege, 10, 209-225.

Beardsley, R.C. and C.D. Winant, 1979. On the mean circulation in the Mid-Atlantic Bight. J. Phys. Oceanogr., 9, 612-619.

Bigelow, H.B., 1927. Physical oceanography of the Gulf of Maine. Bull. U.S. Bur. Fish., 40, 511-1027.

Bishop, J.M., 1980. A note on the seasonal transport on the Middle Atlantic Shelf. J. Geophys. Res., 85, 4933-4936.

Bishop, J.M. and J.E. Overland, 1977. Seasonal drift on the Middle Atlantic Shelf. Deep-Sea Res., 24, 161-169.

Blumberg, A. F. and H. J. Herring, 1983. Circulation modelling using a curvilinear coordinates. Dynalysis of Princeton Report No. 81, 62 pp.

Blumberg, A. F. and G. L. Mellor, 1981. A numerical calculation of the circulation in the South Atlantic Bight. Dynalysis of Princeton Report No. 71. 101 pp.

Blumberg, A. F. and G. L. Mellor, 1983. Diagnostic and Prognostic Numerical Circulation Studies of the South Atlantic Bight. J. Geophys. Res., 88, 4579-4592.

Blumberg, A.F., G.L. Mellor and S. Levitus, 1977. The Middle Atlantic Bight: A climatological atlas of oceanographic properties. New Jersey Marine Consortium Report No. NJ/P-SG-01-08-77.

Blumberg, A. F., H. J. Herring, L. H. Kantha and G. L. Mellor, 1983. California Shelf physical oceanography circulation model: first progress report, Dynalysis of Princeton Report No. 76, 210 pp.

Blumberg, A. F., L. H. Kantha, H. J. Herring and G. L. Mellor, 1984. California Shelf physical oceanography circulation model: final report, Dynalysis of Princeton Report No. 88, 404 pp.

Brooks, D. A., 1979. Fluctuations in the transport of the Florida Current at periods between tidal and two weeks. J. Phys. Oceanogr., 9, 1048-1053.

Brooks, D.A. and J.M. Bane, Jr., 1981. Gulf Stream fluctuations and meanders over the Onslow Bay upper continental slope. J. Phys. Oceanogr., 11, 247-256.

Brooks, D.A. and J.M. Bane, Jr., 1983. Gulf Stream meanders off North Carolina during winter and summer 1979. J. Geophys. Res., 88, 4633-4650.

Brooks, I., and P. P. Niiler, 1977. Energetics of the Florida Current. J. Mar. Res., 35, 163-191.

Brown, O., 1981. Private communication.

Brunt, D.,1939. Physical and Dynamical Meteorology, Cambridge University Press.

Budyko, M.I., 1958. Heat balance of the earth's surface, (Translation), U.S. Weather Bureau, Washington, D.C., MGA 13E-286, 11B-25.

Bumpus, D.F., 1973. A description of the circulation on the continental shelf of the East Coast of the United States. Progress in Oceanogr., 6, 111-157.

Bumpus, D.F., 1976. Review of the physical oceanography of Georges Bank. Int. Comm. Northwest Atl. Fish. Res. Bull., 12, 119-134.

Bumpus, D.F. and L.M. Lauzier, 1965. Surface circulation on the continental shelf of eastern North America between Newfoundland and Florida. Serial Atlas of the Marine Environment, Folio 7, Amer. Geogr. Soc., 8 pp.

Bunker, A.F., 1975. Energy exchange at the surface of the western north Atlantic Ocean. W.H.O.I. Technical Report WHOI-75-3, 107 pp.

Bunker, A.F., 1976. Computations of surface energy flux and annual air-sea interaction cycles of the North Atlantic Ocean. Mon. Wea. Rev., 104, 1122-1140.

Bunker, A.F., 1980. Trends of variables and energy fluxes over the Atlantic Ocean from 1948 to 1972. Mon. Wea. Rev., 108, 720-732.

Butman, B., R.C. Beardsley, B. Magnell, D. Frye, J.A. Vermersch, R. Schlitz, R. Limeburner, W.R. Wright, and M.A. Noble, 1982. Recent observations of the mean circulation on Georges Bank. J. Phys. Oceanogr., 12, 569-591.

Chao, S., and G. S. Janowitz, 1979. The effect of a localized topographical irregularity on the flow of a boundary current along the continental margin. J. Phys. Oceanogr., 9, 900-910.

Charnock, H., 1955. Wind stress on water surfaces. Quart. J. Roy. Met. Soc., 81, 639-640.

Clauser, F. H., 1954. Turbulent Boundary Layers in adverse pressure gradients. J. Aero. Sci., 21, 91-108.

Chew, F., 1981. Shingles, spin-off eddies and an hypothesis. Deep-Sea Res., 28A, 379-391.

Chew, F., J.M. Bane, Jr. and D.A. Brooks, 1985. On vertical motion, divergence and the thermal wind balance in cold-dome meanders. J. Geophys. Res., 90, 3173-3184.

Cressman, G. P., 1959. An operational objective analysis scheme. Mon. Wea. Rev., 87, 329-340.

Csanady, G.T., 1978. The arrested topographic wave. J. Phys. Oceanogr., 8, 47-62.

Dorfman, C.E. and R.H. Bourke, 1978. A temperature correction for Tuckers' ocean rainfall estimates. Quart. J. Roy. Met. Soc., 104, 765-773.

Etter, P.C, 1975. A climatic heat budget study of the Gulf of Mexico, M.S. Thesis, Texas A & M University, 98 pp.

Gill, A.E., 1982. Atmosphere-Ocean Dynamics. Academic Press, New York. 662 pp.

Greenberg, D.A., 1983. Modeling the mean barotropic circulation in the Bay of Fundy and Gulf of Maine. J. Phys. Oceanogr., 13, 886-904.

Haight, F.J., 1942. Coastal currents along the Atlantic coast of the United States. U.S. Dept. of Commerce, Coast and Geodetic Survey Special Publication No. 230, 73 pp.

Hansen, D.V., 1977. Circulation. MESA New York Bight Atlas Monograph 3, New York Sea Grant Institute, 23 pp.

Hastenrath, S. and P.J. Lamb, 1977. Climatic Atlas of the Tropical Atlantic and Eastern Pacific Oceans, University of Wisconsin Press, Madison, Wisconsin, 116 pp.

Hastenrath, S. and P.J. Lamb, 1978. Heat Budget Atlas of the Tropical Atlantic and Eastern Pacific Oceans, University of Wisconsin Press, Madison, Wisconsin, 90 pp.

Holland, W. R., 1973. Baroclinic and topographic influences on the transport in western boundary currents. Geophys. Fluid Dyn., 4, 187-210.

Holland, J. Z., 1972. Comparative Evaluation of some BOMEX measurements of sea surface evaporation, energy flux and stress. J. Phys. Oceanogr., 2, 476-486.

Hopkins, T.S., 1982. On the sea level forcing of the Mid-Atlantic Bight. J. Geophys. Res., 87, 1997-2006.

Kader, B. A., and A. M. Yaglom, 1972. Heat and mass transfer laws for fully turbulent wall flows. Int. J. Heat and Mass Transfer, 15, 2329-2351.

Kantha, L. H., 1980. A diagnostic characteristic-tracing scheme for deducing the climatological current distribution in the South Atlantic Bight. Dynalysis of Princeton Report No. 64, 75 pp.

Kantha, L. H., A. F. Blumberg, and G. L. Mellor, 1981. A diagnostic technique for deducing the climatological circulation as applied to the South Atlantic Bight. Dynalysis of Princeton Report No. 69, 124 pp.

Kantha, L. H., A. F. Blumberg, H. J. Herring and G. L. Mellor, 1981. The physical oceanographic and sea surface flux climatology of the South Atlantic Bight. Dynalysis of Princeton Report No. 70, 142 pp.

Kantha, L. H., G. L. Mellor, and A. F. Blumberg, 1981a. Diagnostic calculations of the circulation in the Middle and South Atlantic Bights. Ocean Modelling, 37, 5-8.

Kantha, L. H., G. L. Mellor, and A. F. Blumberg, 1982. A diagnostic calculation of the general circulation in the South Atlantic Bight. J. Phys. Oceanogr., 12, 805-819.

Kimball, H.H., 1928. Amount of solar radiation that reaches the earth on the land and on the sea, and methods by which it is measured. Mon. Wea. Rev., 56, 393-398.

Knauss, J. A., 1969. A note on the transport of the Gulf Stream. Deep-Sea Res., Supplement to Vol. 16: 117-123.

Lee, T. N., (Ed.), 1983. Oceanography of the southeast U. S. continental shelf and adjacent Gulf Stream., Collection of papers from J. Geophys. Res., 88, 4541-4738.

Lee, T. N., and L. P. Atkinson, 1983. Low-frequency current and temperature variability from Gulf Stream frontal eddies and atmospheric forcing along the Southeast U.S. Outer Continental Shelf. J. Geophys. Res., 88, 4541-4568.

Lee, T.N., L.P. Atkinson and R.V. Legeckis, 1981. Detailed observations of a Gulf Stream spin-off eddy on the Georgia continental shelf, April, 1977. Deep-Sea Res., 28, 347-378.

Lee, T. N., I. Brooks, and W. D ing, 1977. The Florida Current - its structure and variability. U. of Miami Technical Report/RSMAS 77003, 275 pp.

Levitus, S., 1982. Climatological atlas of the world ocean. NOAA professional paper 13. NOAA, U.S. Dept. of Commerce, Washington, D.C.

Li, L., M. Wimbush, D.R. Watts, A.J. Brinko and T.N. Lee, 1985. Gulf Stream and wind-induced variability on the Georgia Continental shelf, winter 1978. J. Geophys. Res., 90, 3199-3210.

Luther, M.E. and J.M. Bane, Jr., 1985. Mixed instabilities in the Gulf Stream over the continental slope. J. Phys. Oceanogr., 15, 3-23.

Maul, G.A., 1985. FACTS: The Florida Atlantic Coast transport study. EOS, 66, 434-435.

Mayer, D.A., D.V. Hansen and D.A. Ortman, 1979. Long-term current and temperature observations on the Middle Atlantic Shelf. J. Geophys. Res., 84, 1776-1792.

Mellor, G. L. and T. Yamada, 1982. Development of a turbulence closure model for geophysical fluid problems. Rev. Geophys. and Space Phys., 20, 851-875.

Millikan, C. B., 1938. A critical discussion of turbulent flows in channels and circular tubes. Proc. 5th International Congress of Applied Mechanics, 386 pp.

Mooers, C. N. K., and D. A. Brooks, 1977. Fluctuations in the Florida Current, summer 1970. Deep-Sea Res., 24, 399-425.

Moore, W. F., 1951. An experimental investigation of the boundary-layer development along a rough surface. Ph.D Dissertation, State University of Iowa.

Nelson, C. S., 1977. Wind stress and wind stress curl over the California current. U. S. Dept. Comm., NOAA Report NMFS SSRF-714, 87 pp.

Nelson, C.S. and D.M. Husby, 1983. Climatology of surface heat fluxes over the California current region. U.S. Dept. Comm., NOAA Report NMFS SSRF-763, 155 pp.

Neumann, G. and R. Hollman, 1961. On the albedo of the sea surface. Union Geod. Geophys. Intern. Monogr., 10, 72-83.

Niiler, P. P., and W. S. Richardson, 1973. Seasonal variability of the Florida Current. J. Mar. Res., 31, 144-167.

Nikuradse, J., 1933. Str mungsgesetze in Rauhen Rohren. Forsch. Arb. Ing.-Wes. 361.

Oey, L.-Y., G. L. Mellor and R. I. Hires, 1985. A three-dimensional simulation of the Hudson-Raritan estuary. Part I: Description of the model and model simulations. J. Phys. Oceanogr., 15, 1732-1745.

Olson, D. B., O. B. Brown, and S. R. Emmerson, 1983. Gulf Stream frontal statistics from Florida Straits to Cape Hatteras derived from satellite and historical data, J. Geophys. Res., 88, 4569-4577.

Orlanski, I., 1969. The influence of bottom topography on the stability of jets in a baroclinic fluid. J. Atmos. Sci., 26, 1216-1232.

Orlanski, I. and M.D. Cox, 1973. Baroclinic instability in ocean currents. Geophys. Fluid Dyn., 4, 297-332.

Payne, R. E.,1972. Albedo of the sea surface. J. Atmos. Sci., 29, 959-970.

Pietrafesa, L. J., 1983. Survey of a Gulf Stream frontal filament. Geophys. Res. Lett., 10(3), 203-206.

Pond, S., G. T. Phelps, J. E. Paquin, G. McBean, and R. W. Stewart, 1971. Measurements of the turbulent fluxes of momentum, moisture, and sensible heat over the ocean. J. Atmos. Sci., 28, 901-917.

Prandtl, L., and H. Schlichting, 1934. Das Widerstandgesetz Rauher Platten. Werft, Reederei Hafen, 15, 1-4.

Price, J.F., C.N.K. Mooers and J.C. Van Leer, 1978. Observation and simulation of storm-induced mixed-layer deepening. J. Phys. Oceanogr., 8, 582-599.

Rabiner, L. R., M. R. Sambur, and C. E. Schmidt, 1975. Applications of a nonlinear smoothing algorithm to speech processing. IEEE Transactions on Acoustics, Speech, and Signal Processing, ASSP-22, No. 6: 552-557.

Reed, R.K., 1976. On estimation of net long-wave radiation from the oceans. J. Geophys. Res., 81, 5793-5794.

Reed, R.K. and D. Halpern, 1975. Insolation and net long-wave radiation off the Oregon coast. J. Geophys. Res., 80, 839-844.

Richardson, W. S., W. J. Schmitz, Jr., and P. P. Niiler, 1969. The velocity structure of the Florida Current from the Straits of Florida to Cape Fear. Deep-Sea Res., 16, 225-231.

Saunders, P.M., 1977. Wind stress on the ocean over the eastern continental shelf of North America. J. Phys. Oceanogr., 7, 555-566.

Schmitz, W. J., Jr. and W. S. Richardson, 1968. On the transport of the Florida Current. Deep-Sea Res., 16, 679-693.

Schott, F., and H. Stommel, 1978. Beta spirals and absolute velocities in different oceans. Deep-Sea Res., 25, 961-1010.

Seban, R. A., and T. T. Shimazki, 1951. Temperature distributions for air flowing turbulently in a smooth heated pipe. Proc. General Discus. Heat Transfer, Inst. Mech. Engng. and ASME, London.

Sheppard, P.A., 1958. Transfer across the earth's surface and through the air above. Quart. J. Roy. Met. Soc., 84, 205-224.

Smith, P.C., 1983. The mean and seasonal circulations off southwest Nova Scotia. J. Phys. Oceanogr., 13, 1034-1054.

Stern, M.E., 1985. Lateral wave-breaking and "shingle" formation in large-scale shear flow. J. Phys. Oceanogr., 15, 1274-1283.

Sverdrup, H.U., M.W. Johnson and R.H. Fleming, 1942. The Oceans, Their Physics, Chemistry, and General Biology, Prentice Hall, Englewood Cliffs, New Jersey.

Tabata, S., 1964. Insolation in relation to cloud amount and sun's attitude. Studies in Oceanography (Ed. K. Yoshida), University of Tokyo Press, Tokyo.

Tucker, G.B., 1961. Precipitation over the North Atlantic. Quart. J. Roy. Met. Soc., 87, 147-158.

Vanwyckhouse, R. J., 1973. Synthetic bathymetric profiling system (SYNBAPS). Technical Report TR-233, U.S. Naval Oceanographic Office, Washington, D.C.

Vukovich, F. M., B. W. Crissman, L. J. Pietrafesa, G. S. Janowitz and R. H. Weisberg, 1984. Effects of wind and Gulf Stream events on the currents off the coast of North Carolina as it relates to to oil spill risk potential. Research Triangle Institute Report. Submitted to: Offshore Environmental Assessment Branch, Minerals Management Service, Reston, Virginia.

Weber, A.H. and J.O. Blanton, 1980. Monthly mean wind fields for the South Atlantic Bight. J. Phys. Oceanogr., 10, 1256-1263.

Wu, J., 1967. Wind stress and surface roughness at air-sea interface. Tech. Rep. 231-18, Hydronautics, Inc., Laurel, Maryland.

Wu, J., 1968. Froude number scaling of wind stress coefficients - a correlation for wind-stress determined at all fetches. Tech. Rep. 231-23, Hydronautics, Laurel, Maryland.